The Transport of Mass and Energy in Toroidal Fusion Machines



A thesis presented in partial
fulfillment of the requirements for the
Degree of Doctor of Philosophy
of the University of Oxford.

by
G.B. Deane.
Trinity College.

March 1989

Abstract

The Transport of Mass and Energy in Toroidal Fusion Machines

G. B. Deane

Trinity College

A thesis presented in partial fulfillment of the requirements for the Degree of Doctor of Philosophy of the University of Oxford. Submitted Hilary Term 1989.

To understand the physical mechanism underlying the cross-field transport of mass and energy in magnetoplasmas is a long-standing problem in fusion research. Woods (1987) has recently developed a second-order transport theory which has been used to explain a number of transport-related phenomena observed in tokamaks. Here, we apply second-order transport theory to the reverse field pinch (RFP) and a phenomenon observed in tokamaks known as 'snakes'.

Expressions for the mass and energy confinement times in the RFP, τ_p and τ_e, are deduced and agreement with experimental results from HBTX is found. For typical operating conditions the times $\tau_p \sim 0.1$ms and $\tau_e \sim 0.2$ms are observed in HBTX. Second-order transport theory predicts $\tau_p \sim 0.4$ms and $\tau_e \sim 0.4$ms for this machine. Scaling laws for β_p versus n_e, β_p versus I_φ and τ_e versus I_φ are compared with measurements from HBTX and agree well with observation.

Snakes are large density perturbations observed in JET after fuel pellet injection. Typical snakes in JET are remarkably stable and are found to have density decay times longer than predictions based on neoclassical theory (Stringer 1987). After their formation, snakes have even been observed to grow (Weller *et al.* 1987), which suggests the presence of an inward diffusion mechanism. There is also some evidence for a temperature depression in the snakes region. An explanation of the stability and energy balance in snakes based on second-order transport theory is proposed.

Preface

The purpose of this thesis is to investigate the transport of mass and energy in fusion machines within the framework of a theory developed by Professor L. C. Woods. This theory has already been applied to tokamaks (Woods 1987) and produced feasible explanations for many transport-related phenomena in these machines. Despite its considerable explanatory power when applied to tokamaks, Woods' theory has not gained widespread acceptance from the plasma physics community. Our concern here will not be with the acceptability or otherwise of the basis of Wood's theory. Rather, we will be interested in the ability of this transport mechanism to provide explanations for phenomena which lie outside the compass of currently acceptable theory.

In the spirit of Popper, we shall accept the theory as a hypothesis to be discarded should it fail to meet the demands of observation.

The structure of the thesis is as follows. Chapter 1 introduces the elements of basic plasma theory, toroidal confinement machines and cross field transport mechanisms. Chapter 2 contains those elements of Woods' theory necessary to derive transport coefficients for the RFP. Chapters 3 and 4 contain the bulk of the original work presented in this thesis. In Chapter 3 we derive expressions for the energy and mass confinement times for the RFP, and compare them with experiment. Chapter 4 presents an explanation for certain characteristics of a phenomenon observed in tokamaks known as a 'snake'. A summary of the analysis and results is made in Chapter 5.

I wish to express my gratitude to Professor L. C. Woods, whose patience, humour, and physical insight into the nature of plasmas made this work possible.

I am also pleased to acknowledge the support of the Esson Bequest, Trinity College, the Oxford University Graduate Studies Office and the Overseas Research Students Awards Scheme, all of whom provided financial assistance. Finally, I wish to thank my parents, my siblings and my fiancée for their unfailing support.

Contents

1 Introduction **1**

1.1 Fusion and Magnetic Confinement 1

1.1.1 Thermonuclear Fusion as an Energy Source 1

1.1.2 Ignition 1

1.1.3 Magnetic Confinement 2

1.2 Magnetoplasmas 3

1.2.1 Definition of a Magnetoplasma 3

1.2.2 A Mathematical Description of Magnetoplasmas 5

1.2.3 The One-fluid Description of Magnetoplasmas 7

1.2.4 The Two-fluid Description of Magnetoplasmas 10

1.3 Toroidal Confinement Machines 12

1.3.1 The Tokamak 12

1.3.2 The Reversed Field Pinch (RFP) 16

1.3.3 Energy Balance in Toroidal Confinement Machines 17

1.4 The Trapping of Charged Particles in Toroidal Confinement Machines 20

1.4.1 Magnetic Mirrors. 20

1.4.2 Particle Trapping in Tokamaks 21

1.4.3 Banana Orbits 22

1.5 Theories of Transport in Magnetoplasmas 23

1.5.1 Introduction 23

1.5.2 Neoclassical Transport 24

1.5.3 Theories of Anomalous Transport 25

1.5.4 Scale Transformations 26
1.5.5 Second-order Transport 26
1.6 Survey of Neoclassical Transport Theory 27
1.6.1 The Banana Regime 27
1.6.2 The Plateau Regime 29
1.6.3 Pfirsch-Schlüter Diffusion 29
1.6.4 The Ware Pinch Effect, Bootstrap Current, and Neoclassical Conductivity 31
1.6.5 The Kinetic Theory Basis of Neoclassical Theory 33

2 Second-Order Transport Theory **35**
2.1 The Physical Mechanism 35
2.1.1 Second-Order Transport in a Neutral Gas 35
2.1.2 Second-Order Transport in a Magnetoplasma 37
2.1.3 The Second-Order Transport Coefficients 38
2.1.4 The Validity of the Second-Order Transport Coefficients . 39
2.2 Second-Order Transport in Toroidal Confinement Machines . . . 40
2.2.1 The Second-Order Heat Flux in a Tokamak 40
2.2.2 The Second-Order Heat Flux in a RFP 42
2.2.3 The Second-Order Viscous Stress Tensor in the RFP . . . 44
2.3 The Scaling of the Thermal Diffusivity with Poloidal Beta: Comparison with Experiment 46
2.3.1 Woods' Scaling Law 46
2.3.2 The Empirical Scaling Law 48
2.3.3 A Comparison with Experiment 48
2.3.4 Contrast Between Second-Order Transport Theory and Neoclassical Theory 50

3 Second-Order Transport in RFPs **53**
3.1 A Description of the RFP 54
3.1.1 The RFP Magnetic Field Structure 54

3.1.2 The Time Evolution and Characteristics of an RFP Discharge 57
3.1.3 Relaxation, Dynamos and Anomalous Transport 58
3.1.4 Loop Voltage Relationships. 66
3.2 An Experimental Model for Currents, Number Densities, and Temperatures in the RFP 67
3.2.1 Current Density Profiles 68
3.2.2 Number Density and Temperature Profiles 73
3.3 The Particle Confinement Time 75
3.3.1 The Electron Source Distribution 77
3.3.2 The Plasma Radial Velocity 80
3.3.3 An Estimate of the Particle Confinement Time 87
3.4 The Energy Confinement Time 92
3.4.1 An Expression for the Energy Confinement Time 93
3.4.2 The Plasma Thermal Diffusivity 96
3.4.3 The Energy Confinement Time for Non Steady-State Conditions 101
3.5 Comparision with Experiment 106
3.5.1 The Particle Confinement Time 106
3.5.2 The Energy Confinement Time 107

4 Snakes in Tokamaks **113**
4.1 Observations of Snakes 113
4.1.1 Present Snake Theory 116
4.2 A Model for Snakes 117
4.2.1 Snake Variables and Geometry 117
4.3 The Stability of Snakes 125
4.3.1 The Steady-State Number Density Profile. 126
4.3.2 The Stability of the Steady-State Number Density Profile 127
4.4 The Temperature Depression in Snakes 128
4.4.1 Energy Balance in Snakes 129

4.4.2 The Energy Replacement Time 130
4.4.3 The Energy Confinement Time 133

5 Conclusions **136**
5.1 A Summary of the Research 136
5.1.1 The Strengths and Weakness of the Analysis 136
5.2 The Implications for Woods' Second-Order Transport Theory . . 137
5.2.1 The Transport of Mass and Energy in the RFP 137

A The Equilibrium Poloidal Magnetic Field in Toriodal Machines 139

List of Figures

1.1 The geometry assumed for tokamaks 13

1.2 How a collision can displace a trapped particle by a banana width (from Wesson 1987) 28

1.3 Variation of diffusion coefficient with collision frequency 32

2.1 The temperature profiles adopted for high β_p discharges (from Woods 1987) 47

3.1 Experimental and Bessel Function Model magnetic field profiles for HBTX (from Bodin 1984) 55

3.2 The F, θ diagram with points from three experiments (from Bodin 1980) 56

3.3 Experimental magnetic field profiles 69

3.4 Experimental current densities 69

3.5 Filtered and fitted magnetic field profiles 70

3.6 Filtered and fitted current density profiles 70

3.7 Poloidal beta versus density for HBTX (from Bodin 1987) 74

3.8 The dominant atomic and molecular processes associated with the recycling of hydrogen (from Harrison 1986). 78

3.9 A typical plot of the ion and electron source distributions. Parameters are: $n_{e0} = 1.0 \times 10^{19}\mathrm{m}^{-3}$ and $T_{e0} = 100\mathrm{eV}$. 79

3.10 S_e versus r (from Carolan *et al.* 1987) 81

3.11 Plot of n_e versus t for ZT-40M (from Wurden *et al.* 1987) 102

3.12 Plot of n_e versus t for ETA-BETA-II (from Innocente *et al.* 1987) 102

3.13 Plot of β_p versus n_e: Theory and Experiment 110
3.14 Plot of β_p versus I_φ: Theory and Experiment 111
3.15 Plot of T_e versus I_φ: Theory and Experiment 112
3.16 Plot of τ_E versus n_e: Theory and Experiment 112

4.1 Pellet ablation (10.035s) and snake oscillation seen by the vertical soft-X-ray camera (from Edwards *et al.* 1987) 114
4.2 Electron density and temperature profiles in JET with a snake present (from Weller *et al.* 1987) 115
4.3 The snake coordinate systems used 119

List of Tables

2.1 The functions ϕ_1 and ϕ_2 48

3.1 Values of A_p for central values of T_e and n_e calculated from HSLAB data 79

3.2 Values of A_p fitted to the HSLAB data 80

3.3 Values of F_E 90

3.4 Values of F_R 90

3.5 Values of F_π 91

3.6 Values of the ratio $(A_E F_E)/(A_\pi F_\pi)$ 92

3.7 Values of $F_\pi^\dagger$ 96

3.8 Values of the factor $\Gamma\mathcal{F}_E$ as a function of $x \equiv r/a$ 98

3.9 Values of $(a^2/2)\langle\mathcal{F}_E\rangle$ 100

3.10 Values of l_i and Γ 100

3.11 Values of A_p^* 104

3.12 The function $\mathcal{F}_p$ for $\theta = 1.6$ 108

4.1 Parameters of typical snakes in JET. Variables refer to the electron fluid: Δn = density perturbation in snake, n_b = background density, ΔT = temperature perturbation in snake, T_b = background temperature. 114

4.2 The function $F_\Omega(\zeta)$ 132

4.3 The function $F_W(\alpha, \zeta)$ 132

4.4 The function $F_Q(\alpha, \zeta)$ 134

Chapter 1

Introduction

1.1 Fusion and Magnetic Confinement

1.1.1 Thermonuclear Fusion as an Energy Source

One of the great goals of modern day science is to develop a machine that will harness the energy released when light atomic nuclei fuse. To induce fusion it is necessary to overcome the mutual electrostatic repulsion of interacting atomic nuclei. One method of doing this is to heat the nuclei until their thermal kinetic energies are sufficient to overcome the electrostatic potential barrier. Such a process is known as thermonuclear fusion.

Of the reactions between the light nuclei, the one the most favorable in cross-section and energy release is that between deuterium and tritium:

$$D_1^2 + T_1^3 \rightarrow He_2^4 + n + 17.6\text{MeV}. \tag{1.1}$$

1.1.2 Ignition

A deuterium-tritium (D-T) mixture at fusion temperatures is in a state of matter known as a plasma, a term defined in section 1.2.1. If a D-T plasma is maintained at a sufficient temperature and ion density, the energy released into the plasma by fusion reactions will exceed the energy losses due to radiation, conduction, convection and neutron flux. A plasma in such a state will sustain thermonuclear reactions without additional energy input and is described as being ignited.

For ignition to occur, the product $n_i\tau_E$ of plasma ion density and energy

confinement time must exceed a critical value for a given ion temperature. The plasma energy confinement time is the time taken for the energy loss processes to completely cool the plasma. The curve of $n_i\tau_E$ required for ignition versus the ion temperature T_i for a D-T plasma has a minimum at $T_i \sim 30$keV. At this temperature $n_i\tau_E \sim 1.5 \times 10^{20}\mathrm{m}^{-3}\mathrm{s}$. These are the values of T_i and $n_i\tau_E$ that must be reached to achieve ignition.

1.1.3 Magnetic Confinement

No material substance is capable of containing a plasma at fusion temperatures. It is possible, however, to confine fusion plasmas with magnetic fields. The fundamental physical effect responsible for confinement is the gyratory motion of charged particles in magnetic fields. The plasma ions and electrons gyrate in a plane perpendicular to the field, and the motion of charged particles across strong fields is inhibited.

Many fusion machines based on the concept of magnetic confinement have been built and they have all been beset with two major problems, these being plasma instability and poor confinement. Extensive investigations of the equations governing plasma behaviour in magnetic fields have shown that only certain magnetic configurations give rise to a stable plasma discharge. While there is still much research being done in this area, the basis for plasma stability is now well understood. This is not the case for the confinement of plasma mass and energy.

One of the greatest difficulties in designing a working fusion machine has been the lack of an explanation of how plasma and plasma energy are transported across magnetic fields. The subject is termed in a general fashion 'cross-field transport', and until recently there has been no single theoretical model that successfully explains many of the phenomena associated with energy transport in toroidal fusion machines.

It seem unlikely that an economic fusion reactor based on the concept of magnetic confinement will be built until the basic mechanisms of particle and

energy transport across magnetic fields are understood.

1.2 Magnetoplasmas

The results presented in this section are part of basic plasma theory and can be found in texts such as Boyd and Sanderson (1969), Chen (1984), Artzimovich (1965), Miyamoto (1976) and Woods (1987).

1.2.1 Definition of a Magnetoplasma

A plasma is a gas in which a sufficient number of atoms are ionised for its characteristics to be primarily determined by interactions between ions and electrons. A magnetoplasma is a plasma in which the trajectories of the charged particles are significantly affected by a macroscopic magnetic field. This field may be due to currents flowing in *or external to* the plasma. The effect of the magnetic field is to produce an anisotropy in the plasma. Charged particles are free to move along field lines, but constrained to gyrate about them.

There are certain length and time-scales which arise naturally when considering magnetoplasmas, and these are described below.

The Debye Length

In a neutral gas, particles move freely between collisions. That is to say that the forces of interaction between the particles operate over a short range and collisions occur abruptly when particles move closely together. In a plasma, particles interact via the long range coulomb force, the consequence being that a particle at any given time will be interacting with a large number of other particles simultaneously. The effective range of this interaction is the debye length, given by

$$\lambda_D = \left(\frac{\epsilon_0 k T_e}{n_e e^2} \right)^{\frac{1}{2}}, \tag{1.2}$$

where T_e and n_e are the electron temperature and density respectively, $-e$ is the charge of an electron, k is Boltzmann's constant and ϵ_0 is the permittivity of free

space. This is the length over which departures from local charge neutrality are screened from the rest of the plasma. On length scales less than λ_D the plasma cannot be guaranteed to be locally neutral.

The Cyclotron Frequency and the Larmor Radius

Consider the motion of an isolated, charged particle p of mass m and charge q moving with a velocity $\boldsymbol{c}_\perp$ perpendicular to a uniform magnetic field $\boldsymbol{B}$ in the absence of an electric field or gravity. The particle experiences a force $\boldsymbol{F}_p = q\boldsymbol{c}_\perp \times \boldsymbol{B}$ and as a consequence executes a circular orbit. Suppose the radius of the orbit is r_L. Then balancing centripetal acceleration of circular motion with $\boldsymbol{F}_p/m$, we obtain

$$\frac{c_\perp^2}{r_L} = q\frac{c_\perp B}{m}. \tag{1.3}$$

So

$$r_L = c_\perp \frac{m}{qB}. \tag{1.4}$$

The distance r_L is known as the Larmor radius. The frequency of gyration of the particle, denoted by ω_c, is given by

$$\omega_c = \frac{2\pi}{2\pi r_L/c_\perp} = \frac{qB}{m}. \tag{1.5}$$

The charged particles in a magnetoplasma are not isolated, and their trajectories are significantly affected by mutual interactions on time-scales of the order of the collision time τ, a term defined in the following section. Provided we restrict attention to time-scales much less than τ, the motion of charged particles can be considered unaffected by collisions, and thus (1.4) and (1.5) can be considered valid provided $2\pi/\omega_c \ll \tau$. This is the case for the magnetoplasmas of interest to us.

Suppose that a charged particle has a random thermal velocity $\boldsymbol{c}$ and the fluid of which the particle is a constituent has a velocity $\boldsymbol{v}$. Then provided $v \ll c$, we may equate $c_\perp$ in (1.4) and (1.5) with

$$c_\perp = |\boldsymbol{b} \times \boldsymbol{c}|. \tag{1.6}$$

Then assuming c to be isotropic, we obtain the estimate $c_\perp = (2kT/m)^{1/2}$, which follows from equating the average particle kinetic energy to its thermal energy kT.

1.2.2 A Mathematical Description of Magnetoplasmas

The most fundamental level of description of a magnetoplasma is a kinetic one, where each particle species comprising the plasma has its state defined by a distribution function $f_s(\boldsymbol{r}, \boldsymbol{\omega}_s, t)$. Here the variables $\boldsymbol{r}$ and $\boldsymbol{\omega}_s$ define a point in the 6-dimensional coordinate and velocity space, or 'phase space' for the particle species s. The product $f_s(\boldsymbol{r}, \boldsymbol{\omega}_s, t)\, d\boldsymbol{r}\, d\boldsymbol{\omega}_s$ is the probability of finding a particle in the volume element $d\boldsymbol{r}\, d\boldsymbol{\omega}_s$ centered on the point $(\boldsymbol{r}, \boldsymbol{\omega}_s)$ at time t. The evolution of f_s with time is described by a suitable kinetic equation. Exactly what constitutes a 'suitable' kinetic equation is determined by the assumptions inherent in the formulation of the time evolution equation, and how realistically these assumptions model a magnetoplasma. The basic form of any kinetic equation is based on the principle of conservation of number of particles. According to this principle, as we follow a group of particles through phase space the distribution function must satisfy

$$\frac{\partial f_s}{\partial t} + \boldsymbol{\omega}_s \cdot \frac{\partial f_s}{\partial \boldsymbol{r}} + \frac{d\boldsymbol{\omega}_s}{dt} \cdot \frac{\partial f_s}{\partial \boldsymbol{\omega}_s} = \mathcal{C}, \tag{1.7}$$

where the collision operator $\mathcal{C}$ is the rate of the number of change of particles in phase space due to collisions. The physics of the interactions between particles is contained in $\mathcal{C}$ and the applicability of a kinetic equation to a magnetoplasma depends on an appropriate choice for this term.

At the kinetic level of description there are various time-scales which form the basis of transport processes within the plasma. An account of these time-scales is part of standard plasma theory (eg. see Braginskii 1965) We shall present only the results which we require for our analysis.

The Collision Time

For coulomb collisions with an impact parameter limited to the debye length, the electron-ion collision frequency ν_{ei} is given by

$$\nu_{ei} = \frac{n_i}{w^3}\left(\frac{Z^2 e^4 \ln\Lambda}{4\pi\epsilon_0^2 m_e^2}\right), \tag{1.8}$$

where Z is the charge number of the ion species, w is the electron speed measured in the laboratory frame and $\ln\Lambda$ is the coulomb logarithm. For Λ we have

$$\Lambda = 12\pi\frac{n_e}{Z}\left(\frac{\epsilon_0 k T_e}{n_e e^2}\right)^{3/2}. \tag{1.9}$$

The collision time τ_e is an averaged value of ν_{ei}^{-1} given by

$$\tau_e = 3(2\pi)^{3/2}\frac{\epsilon_0^2}{e^4}\frac{m_e^{1/2}}{\ln\Lambda}\frac{(kT_e)^{3/2}}{Z^* n_e}, \tag{1.10}$$

where the factor Z^*, known as 'Z effective', arises when there are several types of ion present in the plasma. The factor $n_i Z^2 = n_e Z$ in the expression for the ion-electron collision frequency, equation (1.8) is replaced by $n_e Z^* = \sum_s n_s Z_s^2$, where the sum is over the ion species present.

The 90° Deflection Time

This is the time taken for collisions to deflect a particle through 90°. For electrons with a temperature T_e being scattered by ions at a similar temperature

$$\tau_D = 2\pi 3^{3/2}\frac{\epsilon_0}{e^4}\frac{m_e^{1/2}}{\ln\Lambda}\frac{(kT_e)^{\frac{3}{2}}}{Z n_e} \approx 0.69\tau_e. \tag{1.11}$$

The Time-Scales Associated with Momentum and Energy Transport

There are two time-scales, which we shall denote by τ_1 and τ_2, that arise when considering the viscous stress tensor and the heat flux vector. From first-order kinetic theory for a neutral gas, we have

$$\boldsymbol{\pi} = -2\mu\,\overset{\circ}{\nabla}\boldsymbol{v}, \qquad \mu = p\tau_1, \tag{1.12}$$

and

$$\boldsymbol{q} = -\kappa\nabla T, \qquad \kappa = \frac{5}{2}\frac{k}{m}p\tau_2, \tag{1.13}$$

where $\boldsymbol{\pi}$ is the viscous stress tensor, $\boldsymbol{q}$ is the heat flux vector and $\overset{\circ}{\nabla}\boldsymbol{v}$ is the deviator of the velocity gradient tensor, defined in section 1.2.3

The times τ_1 and τ_2 are related; for a monatomic gas the ratio τ_1/τ_2 is $2/3$. Values of τ_1 for the ion and electron fluids in a plasma, which we shall denote by τ_{1i} and τ_{1e} respectively, can be deduced from calculations made using the Fokker-Plank equation (Braginskii 1965). We have

$$\tau_{1i} = 0.96\tau_i, \qquad \tau_{1e} = 0.73\tau_e, \tag{1.14}$$

where τ_e is given by (1.10) and $\tau_i = (2m_i/m_e)^{1/2}(T_i/T_e)^{3/2}Z^{-2}\tau_e$.

Equation (1.7) for f_s cannot be solved until the collision operator C has been specified. Provided that the collision operator used is a correct description for the interactions between particles in a magnetoplasma, the kinetic equation will correctly model phenomena on all length and time-scales. If, however, we are interested in phenomena which occur on time-scales longer than the collision time τ_e, and length scales longer than a mean-free-path λ then a fluid description may be employed.

In the following two subsections we shall present the equations for the one-fluid and two-fluid models of magnetoplasmas. This is standard theory, covered in such texts as referenced at the beginning of this chapter. A good account of the fluid equations and the relationship between the one-fluid and two-fluid models is given by Woods (1987).

1.2.3 The One-fluid Description of Magnetoplasmas

The simplest fluid description of a magnetoplasma is given by the fluid conservation equations, the electromagnetic equations and constitutive equations for the current and heat flux. Collectively, these form the equations of magnetohydrodynamics (MHD).

The Electromagnetic Equations

These are Maxwell's equations with the displacement current dropped from Ampere's law and the assumption that there are no current sources (ie. $\nabla \cdot j = 0$). We have that

$$\nabla \times \boldsymbol{E} = -\frac{\partial \boldsymbol{B}}{\partial t}, \tag{1.15}$$

$$\nabla \cdot \boldsymbol{B} = 0, \tag{1.16}$$

$$\nabla \times \boldsymbol{B} = \mu_0 j, \tag{1.17}$$

$$\nabla \cdot j = 0. \tag{1.18}$$

Here $\boldsymbol{E}$ and $\boldsymbol{B}$ are the macroscopic electric and magnetic fields respectively. The constant μ_0 is the permittivity of the plasma, which is the same as that for free space, and j denotes the plasma current density. Equations (1.17) and (1.18) are approximations, that are valid provided that the macroscopic variables of the plasma change on time-scales much less than the plasma frequency, and length-scales much less than a debye length.

The Fluid Conservation Equations

The plasma mass density ρ, the fluid velocity $\boldsymbol{v}$ and the internal energy u are the three basic fluid variables. The equations of conservation of mass, momentum and energy that relate these variables are, respectively,

$$D\rho + \rho \nabla \cdot \boldsymbol{v} = 0, \tag{1.19}$$

$$\rho D\boldsymbol{v} + \nabla \cdot \boldsymbol{p} = j \times \boldsymbol{B} + \rho \boldsymbol{F}, \tag{1.20}$$

$$\rho Du + \rho p D\rho^{-1} = -\boldsymbol{\pi} : \nabla \boldsymbol{v} - \nabla \cdot \boldsymbol{q} + j \cdot (\boldsymbol{E} + \boldsymbol{v} \times \boldsymbol{B}) + \psi + \phi, \tag{1.21}$$

where $D \equiv \partial/\partial t + \boldsymbol{v} \cdot \nabla$ is the material time derivative, external body forces per unit mass are denoted by $\boldsymbol{F}$, and $\boldsymbol{\pi}$ is the viscous stress tensor, defined below. The final two terms in the energy equation, ψ and ϕ represent radiation losses and additional heating mechanisms, and $\boldsymbol{q}$ is the heat flux vector.

The Constitutive Relations

These are relations that depend on the material in which the electromagnetic fields occur. They are:

$$\boldsymbol{j} = \boldsymbol{\sigma} \cdot \boldsymbol{E}' + \boldsymbol{\beta} \cdot \nabla T, \tag{1.22}$$

$$\boldsymbol{q} = -T(\boldsymbol{\beta} + \frac{5k}{2e}\boldsymbol{\sigma}) \cdot \boldsymbol{E}' - \boldsymbol{\kappa} \cdot \nabla T, \tag{1.23}$$

$$\boldsymbol{p} = p\mathbf{1} + \boldsymbol{\pi}, \quad \boldsymbol{\pi} = -2\boldsymbol{\mu} : \overset{\circ}{\nabla}\boldsymbol{v} \tag{1.24}$$

where $\boldsymbol{E}' = \boldsymbol{E} + \boldsymbol{v} \times \boldsymbol{B} - \frac{1}{en_e}\boldsymbol{j} \times \boldsymbol{B} + \frac{1}{en_e}\nabla \cdot \boldsymbol{p}_e$, $\mathbf{1}$ is the unit tensor, T is the plasma temperature, $\boldsymbol{\mu}$ is the 4th-order viscosity tensor and $\overset{\circ}{\nabla}\boldsymbol{v}$ is the deviator of the velocity gradient tensor, defined by $\overset{\circ}{\nabla}\boldsymbol{v} \equiv (\nabla\boldsymbol{v} + \tilde{\nabla}\boldsymbol{v})/2 - \nabla \cdot \boldsymbol{v}\mathbf{1}/3$ where $\tilde{\nabla}\boldsymbol{v}$ is the transpose of $\nabla\boldsymbol{v}$. The second order tensors $\boldsymbol{\sigma}$, $\boldsymbol{\beta}$ and $\boldsymbol{\kappa}$ are the plasma conductivity, the thermoelectric term and the plasma thermal diffusivity respectively. These may be considered as phenomenological coefficients, or deduced from kinetic theory.

Each of the second-order tensors is of the form

$$\boldsymbol{\delta} = \delta_{||}\boldsymbol{bb} + \delta_{\wedge}\boldsymbol{b} \times \mathbf{1} + \delta_{\perp}(\mathbf{1} - \boldsymbol{bb}), \tag{1.25}$$

where $\boldsymbol{b}$ is a unit vector in the direction of the magnetic field. We have a particular interest in the thermal diffusivity, $\boldsymbol{\kappa}$, and examine this tensor carefully in Chapter 2. For the conductivity parallel to the magnetic field, we have (Spitzer and Härm 1953)

$$\sigma_{||} = \left(0.295 + \frac{0.39}{0.85 + Z^*}\right)^{-1} \frac{e^2 n_e \tau_e}{m_e}. \tag{1.26}$$

The coefficients 0.295, 0.39 and 0.85 in (1.26) have been given by Woods (1987) as a good fit to the values for $\sigma_{||}$ as a function of Z^* calculated by Spitzer and Härm.

For the strong magnetic fields of interest in this work, where $|\omega_{ce}\tau_e| \gg 1$, the perpendicular and transverse conductivities are given by

$$\sigma_{\perp} \approx \tfrac{1}{2}\sigma_{||}, \qquad \sigma_{\wedge} \approx 0, \tag{1.27}$$

and the thermoelectric coefficients are given by

$$\delta_{||} = 0.71\frac{k}{e}, \qquad \delta_{\wedge} \approx \delta_{\perp} \approx 0. \tag{1.28}$$

The equations of MHD will provide a good description of magnetoplasma phenomena if the macroscopic variables change on suitably long length and time-scales, and the ion and electron fluids have the same temperature. Let ϕ be one of the macroscopic variables of MHD such as ρ or $\boldsymbol{T}$. Then we require that

$$|\boldsymbol{bb} \cdot \nabla \ln \phi| \;>>\; \lambda, \tag{1.29}$$

$$|(\mathbf{1} - \boldsymbol{bb}) \cdot \nabla \ln \phi| \;>>\; \max\{r_L, (r_L \tau V)^{\frac{1}{2}}\}, \tag{1.30}$$

where $\boldsymbol{b}$ is a unit vector parallel to the magnetic field, V is the change in fluid velocity over the distance $(\mathbf{1} - \boldsymbol{bb}) \cdot \nabla \ln \phi$ and λ is the mean-free-path. With a strong magnetic field where $r_L << \lambda$ it is possible to have a fluid description on very much shorter length scales perpendicular to the magnetic field than parallel to it.

1.2.4 The Two-fluid Description of Magnetoplasmas

The equations of MHD provide an adequate description of a magnetoplasma in many cases, and are useful, for example, in the treatment of small amplitude waves and plasma stability. There are, however, problems where a multi-fluid description is a more suitable model. In particular a one-fluid model is unsuitable when the electron and ion fluids are not in thermal equilibrium, or when a phenomenon is known to be associated with just one of the plasma particle species.

The most general fluid description of a plasma considers each of the particle species present to form a separate fluid, the fluids interacting via collisions between different species. In regions where the plasma is in a state of partial ionization it is generally necessary to employ a three-fluid model to take account of the interactions between electrons, ions and neutral molecules. This is the case at the edge of tokamak and Reverse Field Pinch discharges where the ion

and electron temperatures are low and ionization is incomplete. In the work that follows we shall neglect the transfer of momentum and energy between the ions and electrons and the neutral gas, although the transfer of mass shall be considered. Because the transfer of mass can be modelled simply by including a source term in the conservation of mass equation, for our purposes a two-fluid description is adequate.

The two-fluid model consists of the fluid equations applied separately to ions and electrons, the electromagnetic equations, and constitutive relations for $\boldsymbol{p}$, $\boldsymbol{q}$ and the drag force between the ion and electron fluids, $\boldsymbol{R}$.

Let the subscript $s = i, e$ denotes ion or electron variables, then the conservation equations for the electron and ion fluids are

$$D_s\rho_s + \rho_s\nabla\cdot\boldsymbol{v}_s = 0, \tag{1.31}$$

$$\rho_s D_s\boldsymbol{v}_s + \nabla\cdot\boldsymbol{p}_s = q_s n_s(\boldsymbol{E} + \boldsymbol{v}_s\times\boldsymbol{B}) + \boldsymbol{R}_s, \tag{1.32}$$

$$\tfrac{3}{2}n_s k D_s T_s + p_s\nabla\cdot\boldsymbol{v}_s = -\nabla\cdot\boldsymbol{q}_s - \boldsymbol{\pi}_s:\nabla\boldsymbol{v}_s + \psi_s + \varphi_s + \xi_s + \phi_s, \tag{1.33}$$

where $D_s \equiv \partial/\partial t + \boldsymbol{v}_s\cdot\nabla$, ψ_s is the radiation source term, ξ_s is the work done on the s fluid species by the drag force $\boldsymbol{R}_s$ and ϕ_s accounts for non-ohmic heating mechanisms. The transfer of energy from one fluid to the other at different temperatures is accounted for by φ_s and so $\varphi_i = -\varphi_e$. We also have that $q_e = -e$ and $q_i = Ze$ where Z is the charge number of the ion species. The drag force between the two fluids is given by $\boldsymbol{R}_s$, and by Newton's third law $\boldsymbol{R}_i = -\boldsymbol{R}_e$.

Assuming that the work done by the drag force is distributed between the fluid species in a manner inversely proportional to their particle mass, it follows that

$$\xi_e = \boldsymbol{R}_i\cdot(\boldsymbol{v}_i - \boldsymbol{v}_e), \tag{1.34}$$

$$\xi_i = 0. \tag{1.35}$$

Constitutive relations are needed to specify $\boldsymbol{R}_e$, $\boldsymbol{q}_s$, $\boldsymbol{p}_s$, φ_s and the radiation source term ψ_s. Because we intend to neglect radiation effects and the energy

transfer between the ion and electron fluids, we shall not require relations for φ_s or ψ_s. For $\boldsymbol{R}_e$, $\boldsymbol{q}_i$, $\boldsymbol{q}_e$ and p_s we have (Braginskii 1965)

$$\boldsymbol{R}_e = en_e(-\boldsymbol{\delta}\cdot\nabla T_e + \boldsymbol{\eta}\cdot j) \tag{1.36}$$

$$\boldsymbol{q}_e = -\boldsymbol{\kappa}^e\cdot\nabla T_e - \boldsymbol{\delta}\cdot j \tag{1.37}$$

$$\boldsymbol{q}_i = -\boldsymbol{\kappa}^i\cdot\nabla T_i \tag{1.38}$$

$$p_s = n_s k T_s \tag{1.39}$$

where $\boldsymbol{\kappa}^e$, $\boldsymbol{\kappa}^i$ and $\boldsymbol{\delta}$ are second-order tensors of the general form given by (1.25) and the resistivity tensor $\boldsymbol{\eta}$ is the inverse of the conductivity tensor, i.e. $\boldsymbol{\eta}\cdot\boldsymbol{\sigma} = \mathbf{1}$.

Equations (1.36), (1.37) and (1.38) replace the equations (1.22) and (1.23) for j and $\boldsymbol{q}$ of the one-fluid model.

1.3 Toroidal Confinement Machines

1.3.1 The Tokamak

Of all the magnetic confinement fusion machines, the tokamak has been the most throughly investigated. The geometry of tokamaks varies from machine to machine. They all have the shape of a torus, but the cross-section of the torus is not always circular. The Joint European Torus (JET) has a D-shaped cross-section, for example.

An analysis of toroidal confinement machines made using the geometry shown in Figure 1.1 is usually sufficiently accurate to understand the physics of these machines. This is the geometry that we shall employ in subsequent calculations. The torus can be described in terms of the cylindrical coordinate system (R, Z, φ) or local coordinates (r, θ, φ). Because it is often assumed that the plasma is symmetric about and along the minor axis, local coordinates will usually be used, although toroidal geometry will be employed to calculate particle trapping effects.

Wesson (1987) has written a comprehensive account of tokamak physics; we shall introduce only those variables necessary for the work which follows. The

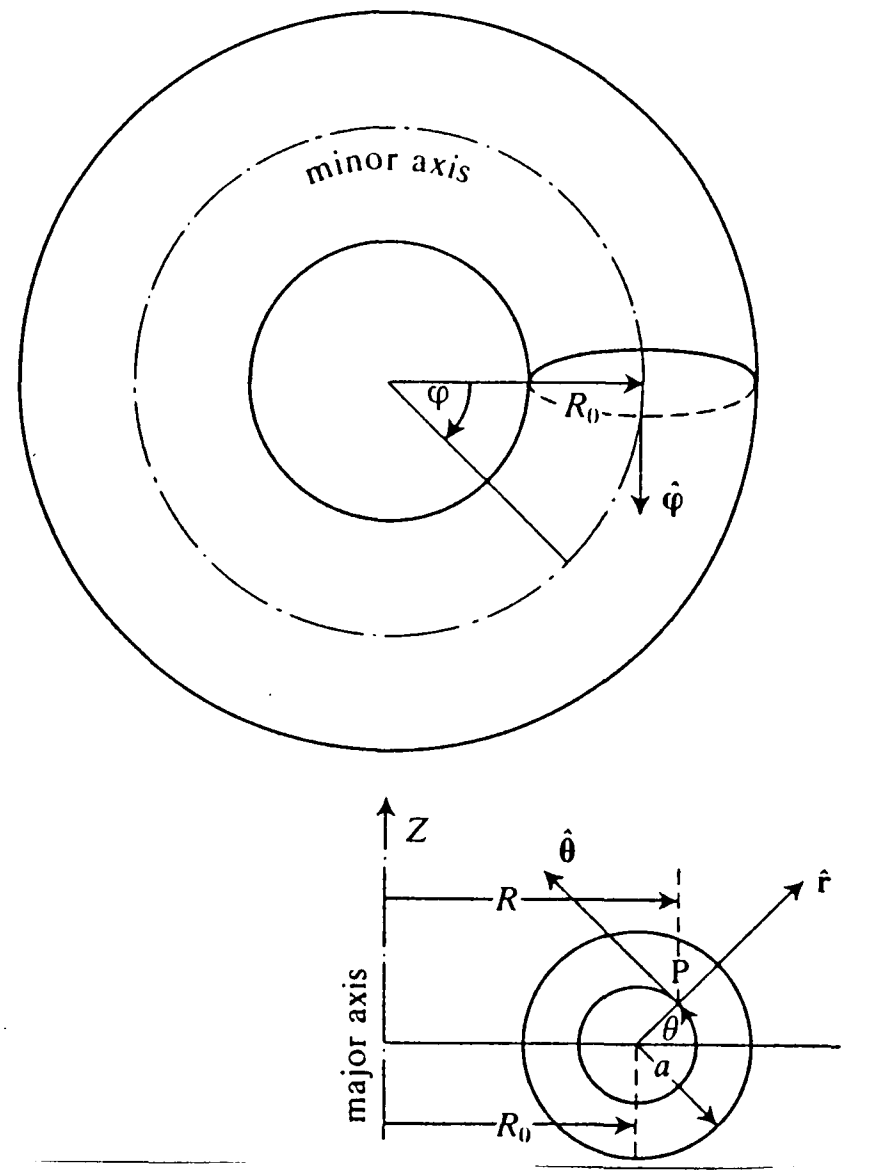

Figure 1.1: The geometry assumed for tokamaks

basic tokamak variables are described below.

The Magnetic Field

A tokamak has a strong toroidal field B_φ generated by field coils, and a weaker poloidal field $B_\theta(a)$ caused by a toroidal current flowing in the plasma. As a characterization of the magnetic field, a unit vector $\boldsymbol{b} \equiv \boldsymbol{B}/B$ parallel to $\boldsymbol{B}$ may be written as

$$\begin{aligned} \boldsymbol{b} &= \frac{1}{\sqrt{1+s^2}}(\hat{\boldsymbol{\varphi}} + s\hat{\boldsymbol{\theta}}) \\ &\simeq \hat{\boldsymbol{\varphi}} + s\hat{\boldsymbol{\theta}}, \end{aligned} \tag{1.40}$$

where $s \equiv B_\theta/B_\varphi$ and the unit vectors $\hat{\boldsymbol{\varphi}}$ and $\hat{\boldsymbol{\theta}}$ are defined in Figure 1.1.

The Safety Factor

The safety factor q is defined by

$$q = \frac{1}{2\pi}\oint \frac{B_\varphi}{RB_\theta}\, ds, \tag{1.41}$$

where the integral lies on a specified magnetic surface enclosing the minor axis. If the aspect ratio R_0/a of the tokamak is large then

$$q = \frac{rB_\varphi}{RB_\theta} = \frac{\epsilon}{s}, \qquad (\epsilon \equiv r/R). \tag{1.42}$$

As we shall shortly show, the safety factor is so named because of its importance in considerations of plasma stability.

One of the results obtained by considering the ideal MHD stability of cylindrical discharges (a good treatment is given by Miyamoto 1976) is that the plasma is stable to all modes of displacement if

$$\left(\frac{B_\theta}{B_\varphi}\right) < (kr)^2, \tag{1.43}$$

where B_θ is the external azimuthal magnetic field, B_φ is the longitudinal magnetic field, k is the longitudinal displacement wave number and r is the raduis of the plasma column. In a plasma of finite length L, k cannot be less than $2\pi/L$ and (1.43) can be written as

$$\left(\frac{B_\theta}{B_\varphi}\right) < \frac{2\pi r}{L}. \tag{1.44}$$

This is the Kruskal-Shafranov stability condition (Kruskal & Schwarzschild 1954, Shafranov 1957).

When (1.44) is applied to a toroidal system, k takes on values n/R, $n = 1, 2, 3, \cdots$ where R is the major axis of the torus, and the stability condition becomes

$$n^2\left(\frac{rB_\varphi}{RB_\theta}\right)^2 > 1, \tag{1.45}$$

As $q_a = rB_\varphi/RB_\theta$, all modes are stabilised if

$$q > 1. \tag{1.46}$$

Another important stability condition is the Mercier criterion (Laval *et al.* 1971), requires

$$\frac{rB_\varphi^2}{2\mu_0}\left(\frac{d\ln q}{dr}\right)^2 > \frac{dp}{dr}(q^2 - 1). \tag{1.47}$$

Unless (1.47) is satisfied, the plasma is subject to another ideal MHD instability, the 'interchange instability', induced by the plasma pressure gradient and magnetic field line curvature. Note that if $q > 1$ then $dp/dr < 0$ is always stable.

The Plasma Beta

Consider (1.17) and (1.20), neglecting the inertial term, viscosity and body forces. We have

$$\nabla \times \boldsymbol{B} = \mu_0 \boldsymbol{j} \qquad \text{and} \qquad \nabla p = \boldsymbol{j} \times \boldsymbol{B}. \tag{1.48}$$

It follows immediately that

$$\nabla p = \frac{1}{\mu_0}(\nabla \times \boldsymbol{B}) \times \boldsymbol{B}, \tag{1.49}$$

or

$$\nabla\left(p + \frac{B^2}{2\mu_0}\right) = \frac{1}{\mu_0}(\boldsymbol{B} \cdot \nabla)\boldsymbol{B}, \tag{1.50}$$

which follows from the vector identity $(\nabla \times \boldsymbol{B}) \times \boldsymbol{B} = (\boldsymbol{B} \cdot \nabla)\boldsymbol{B} - \nabla B^2/2$. The left-hand-side of (1.50) suggests that the magnetic field exerts a pressure $B^2/2\mu_0$, the gradient of which must balance the ∇p force for equilibrium when the right-hand-side of (1.50) is zero.

The plasma β is defined as the ratio of the plasma pressure and the magnetic field pressures. When β is small, from (1.50) we expect that the effect of plasma pressure will not significantly alter the equilibrium magnetic fields.

In toroidal geometry the poloidal and toroidal plasma beta are defined as

$$\beta_t = \frac{2\mu_0\langle p\rangle}{B_\varphi^2}, \qquad \beta_p = \frac{2\mu_0\langle p\rangle}{B_{\theta a}^2}, \tag{1.51}$$

respectively where $B_{\theta a}$ is the poloidal field at the limiter, and $\langle p\rangle = (2/a^2)\int_0^a pr\,dr$ is the volume-weighted average plasma pressure. These ratios of average plasma pressure to magnetic field pressure are important in considerations of plasma stability and fusion reactor economics.

We also note that if $\beta_p > 1$ then the toroidal magnetic field is less than the vacuum field and for this reason the discharge is termed "diamagnetic".

For the case of $\beta_p < 1$ the toroidal field is enhanced and the discharge termed "paramagnetic".

The Global Energy Confinement Time

The time taken for the whole of the energy of the plasma to be lost through convection and conduction is

$$\tau_E = \frac{W}{[r(\frac{5}{2}pv_r + Q_r)]_{r=a}}, \tag{1.52}$$

where v_r and Q_r are the plasma radial velocity and radial heat flux respectively and W is defined by

$$W \equiv \int_0^a \tfrac{3}{2}k(n_e T_e + n_i T_i) r \, dr. \tag{1.53}$$

As will be shown in section 1.3.3, energy balance within the plasma requires that

$$\frac{\partial \ln W}{\partial t} + \frac{1}{\tau_E} = \frac{1}{\tau_E^*} - \frac{1}{\tau_E^R}, \tag{1.54}$$

where

$$\tau_E^* = \frac{W}{\int_0^a j_\varphi E_\varphi r \, dr} \tag{1.55}$$

is the energy replacement time, and

$$\tau_E^R = \frac{W}{\int_0^a \psi r \, dr} \tag{1.56}$$

is the radiation loss time. In the presence of additional heating, the term $j_\varphi E_\varphi$ is augmented by the term ϕ appearing in (1.33).

Similar expressions can be derived for the plasma confinement time and the fluid momentum confinement time.

1.3.2 The Reversed Field Pinch (RFP)

The geometry of the RFP is the same as the tokamak; it is the magnetic field configuration of this machine that distinguishes it from the tokamak, and leads to quite different operating characteristics. The average poloidal and toroidal field strengths in the RFP are comparable, a significant contribution to the toroidal

field being due to poloidal currents flowing in the plasma. The magnetic field in a RFP evolves throughout the discharge. Variables used as a measure of the field state are the pinch ratio θ and the field reversal index F defined by

$$\theta \equiv \frac{B_{\theta a}}{\langle B_\varphi \rangle}, \tag{1.57}$$

$$F \equiv \frac{B_{\varphi a}}{\langle B_\varphi \rangle}, \tag{1.58}$$

where $\langle B_\varphi \rangle = (2/a^2) \int_0^a B_\varphi(r) r \, dr$ is the volume-weighted average value of B_φ.

Confinement times in RFP's are generally an order of magnitude smaller than tokamaks of comparable size.

1.3.3 Energy Balance in Toroidal Confinement Machines

A complete description of the energy balance in tokamaks and RFP's would include descriptions of the various heating and energy loss mechanisms in fusion plasmas. The former include ohmic heating by plasma currents, neutral beam injection and radio frequency electromagnetic wave heating. The major energy loss mechanisms are radiation, and the conduction and convection of energy and particles to the plasma limiter.

It is generally accepted (eg. Liewer 1985, Hugill 1983) that the main channel for energy loss in tokamaks is via electron thermal conduction. Exceptions to this observation occur when the plasma density is high and with some devices when the plasma is heated with neutral beams. In these cases it is observed that the ion heat flux exceeds the electron heat flux. The reason for this can be understood as follows. The flow of energy between the ion and electron fluids occurs on the equipartition time-scale, τ_{eq}. In relatively low density discharges $\tau_E < \tau_{eq}$ and the two fluids are thermally decoupled on the energy confinement time-scale. Thus for low density, ohmically heated discharges, where the bulk of the dissipated energy is deposited in the electron fluid, τ_E is determined by the loss of energy from the electron fluid. However, τ_E is observed to increase with increasing n while τ_{eq} has the opposite dependence. Thus as the density is increased, a point must eventually be reached for which ion thermal losses are

important. Ion thermal losses can also be expected to be important for discharges where a significant amount of energy is deposited in the ion fluid.

We shall restrict attention to ohmically heated discharges where the ion and electron fluids are thermally decoupled on the energy confinement time-scale.

We shall show in Chapter 3 that a reasonable account of the energy losses in a particular RFP (the HBTX machine) can be made by taking convection to be the dominant energy loss mechanism.

A derivation of an expression for the electron energy confinement time begins with the electron energy equation of the two-fluid model. After some algebra, (1.33) may be rewritten as

$$\frac{\partial}{\partial t}(\tfrac{3}{2}n_e k T_e) + \nabla\cdot(\tfrac{5}{2}n_e k T_e \boldsymbol{v}_e + \boldsymbol{Q}_e) = \boldsymbol{v}_e\cdot\nabla\cdot\boldsymbol{p}_e - \boldsymbol{\pi}_e : \nabla\boldsymbol{v}_e + \xi + \phi - \psi_e - Q_{ie}, \quad (1.59)$$

where ψ_e is the radiation term, Q_{ie} the transfer of energy from the electron fluid to the ion fluid, $\xi = \boldsymbol{R}_{ei}\cdot(\boldsymbol{v}_i - \boldsymbol{v}_e)$ is the ohmic dissipation in the electron fluid and ϕ is the energy due to additional sources such as neutral beam injection or radio frequency heating. We will restrict attention to ohmically heated discharges, and neglect ϕ in the sequel. Noting that the total electron thermal energy in the torus is proportional to

$$W_e \equiv \int_0^a \tfrac{3}{2} k n_e T_e r\, dr, \quad (1.60)$$

equation (1.59) may be rewritten as

$$\frac{\partial \ln W_e}{\partial t} + \frac{1}{\tau_{Ee}} = \frac{1}{\tau^*_{Ee}} - \frac{1}{\tau^R_{Ee}} - \frac{1}{\tau^i_{Ee}}, \quad (1.61)$$

where

$$\tau_{Ee} \equiv \frac{W_e}{[r(\frac{5}{2}pv_r + Q_{er})]_{r=a}}, \quad (1.62)$$

$$\tau^*_{Ee} \equiv \frac{W_e}{\int_0^a [\boldsymbol{v}_e\cdot\nabla\cdot\boldsymbol{p}_e - \boldsymbol{\pi}_e : \nabla\boldsymbol{v}_e + \boldsymbol{R}_{ei}\cdot(\boldsymbol{v}_i - \boldsymbol{v}_e)] r\, dr}, \quad (1.63)$$

$$\tau^R_{Ee} \equiv \frac{W_e}{\int_0^a \psi_e r\, dr}, \quad (1.64)$$

$$\tau^i_{Ee} \equiv \frac{W_e}{\int_0^a Q_{ie} r\, dr}. \quad (1.65)$$

The various times defined above are the electron energy confinement time τ_{Ee}, the electron energy replacement time τ^*_{Ee}, the electron radiation loss time τ^R_{Ee} and the electron-ion energy transfer time τ^i_{Ee}. In writing equation (1.61), we have assumed that the plasma has symmetry about the major and minor axes. The electron energy confinement time includes both convective and conductive losses. The three energy source terms appearing in the energy replacement time are the work done by the pressure gradient force, the viscous dissipation function and the ohmic dissipation term. This time may be expressed in a more standard form by substituting for the ohmic dissipation term $\boldsymbol{R}_{ei} \cdot (\boldsymbol{v}_i - \boldsymbol{v}_e)$. Neglecting the inertial term in equation (1.32) written for the electron fluid, we obtain

$$\boldsymbol{R}_{ei} = en_e(\boldsymbol{E} + \boldsymbol{v}_e \times \boldsymbol{B}) + \nabla \cdot \boldsymbol{p}_e, \tag{1.66}$$

so that

$$\boldsymbol{R}_{ei} \cdot (\boldsymbol{v}_i - \boldsymbol{v}_e) = \boldsymbol{j} \cdot \boldsymbol{E} - \boldsymbol{v} \cdot \nabla p, \tag{1.67}$$

where we have used the equilibrium condition $\boldsymbol{j} \times \boldsymbol{B} = \nabla p$(which follows from neglecting the inertial term in (1.20)) and neglected electron viscosity. To obtain (1.67) we have assumed that the radial component of $\boldsymbol{j}$ is zero and $\nabla \equiv \partial/\partial r$, both of which follow from assuming symmetry about the major and minor axes. Substituting equation (1.67) into the expression for τ^*_{Ee}, neglecting electron viscosity and a term of the form $\boldsymbol{v}_i \cdot \nabla p$, and setting $\boldsymbol{j} \cdot \boldsymbol{E} = j_\varphi E_\varphi$, yields

$$\tau^*_{Ee} = \frac{W_e}{\int_0^a j_\varphi E_\varphi r \, dr}. \tag{1.68}$$

Equation (1.68) is useful for the ohmically heated tokamak where electron viscosity can be ignored. As it will be shown in Chapter 3, in the RFP equation (1.67) is replaced by the constitutive equation for the drag force, which is (cf. (1.36))

$$\frac{\boldsymbol{R}_{ei}}{en_e} = -\boldsymbol{\delta} \cdot \nabla T_e + \boldsymbol{\eta} \cdot \boldsymbol{j}. \tag{1.69}$$

Neglecting the thermoelectric term, and using $\boldsymbol{v}_i - \boldsymbol{v}_e = \boldsymbol{j}/en_e$ we obtain for the ohmic dissipation term

$$\boldsymbol{R}_{ei} \cdot (\boldsymbol{v}_i - \boldsymbol{v}_e) = \boldsymbol{j} \cdot \boldsymbol{\eta} \cdot \boldsymbol{j}. \tag{1.70}$$

When substituted into equation (1.63) this yields

$$\tau_{Ee}^{*} = \frac{W_e}{\int_0^a (\boldsymbol{v}_e \cdot \nabla \cdot \boldsymbol{p}_e - \boldsymbol{\pi}_e : \nabla \boldsymbol{v}_e + \boldsymbol{j} \cdot \eta \cdot \boldsymbol{j}) r \, dr}. \tag{1.71}$$

1.4 The Trapping of Charged Particles in Toroidal Confinement Machines

A complete account of the motion of isolated charged particles in magnetic fields would be misplaced in this work. However, the concept of particle trapping in tokamaks and RFP's has an important role in the work to be presented, and an account of this phenomenon is called for.

1.4.1 Magnetic Mirrors.

In a uniform magnetic field, charged particles gyrate about field lines with an angular frequency

$$\omega_c = \frac{qB}{m} \tag{1.72}$$

known as the cyclotron frequency. The radius of the orbit, called the Larmor radius is

$$r_L = \frac{c_\perp}{|\omega_c|}, \tag{1.73}$$

where $c_\perp$ is the velocity of the particle perpendicular to the magnetic field measured in a frame convected with the fluid. In a non-uniform magnetic field which varies slowly on a length scale commensurate with the Larmor radius there are two constants of particle motion. These are the magnetic moment M and kinetic energy E of the gyrating particles given by

$$M = \frac{mc_\perp^2}{2B} = \text{constant}, \tag{1.74}$$

$$E = \tfrac{1}{2}mc^2 = \text{constant}, \tag{1.75}$$

where, if $\boldsymbol{c}$ is the particle velocity measured in a frame convected with the fluid, $c = |\boldsymbol{c}|$ and $c_\perp = |\boldsymbol{c} - \boldsymbol{bb} \cdot \boldsymbol{c}|$.

Now consider a particle moving in a magnetic field which varies from some minimum value B_0 to a maximum B_m. The peculiar velocity of the particle along the field lines $c_{||} = \boldsymbol{c} \cdot \boldsymbol{b}$ is related to E and M by

$$\begin{aligned} c_{||}^2 &= c^2 - c_\perp^2 \\ &= \frac{2}{m}(E - MB). \end{aligned} \tag{1.76}$$

As B increases, $c_\perp$ decreases and may become zero. The condition for this to occur is $E \leq qMB_m$, which is more conveniently expressed using the particle's pitch angle ϑ, defined by $\cos\vartheta \equiv c_\perp/c$ and the mirror ratio $R_m \equiv B_m/B_0$. Those particles at the point of B_0 with pitch angles satisfying

$$0 < \vartheta < \vartheta_c = \{\cos^{-1} R_m^{-1}\}^{\frac{1}{2}} \tag{1.77}$$

will be 'reflected' by the field before the point of B_m and are said to be trapped. Assuming that trapped particles are part of an equilibrium distribution it is possible to show that the fraction of trapped particles is

$$f_T = \sin\vartheta_c = (1 - R_m^{-1})^{1/2}. \tag{1.78}$$

1.4.2 Particle Trapping in Tokamaks

Particle trapping in tokamaks is a consequence of the toroidal geometry of these machines. The process can be understood by considering the structure of a magnetic field in toroidal geometry. Using the geometry of Figure 1.1, the divergence of $\boldsymbol{B}$ can be expressed

$$\nabla \cdot \boldsymbol{B} = \frac{1}{rR}\frac{\partial}{\partial r}(RrB_r) + \frac{1}{rR}\frac{\partial}{\partial\theta}(RB_\theta). \tag{1.79}$$

Using this, it can be shown that (see Appendix 1)

$$B_\theta(r,\theta) = \frac{B_{\theta 0}}{1 - \Lambda\epsilon\cos\theta}, \tag{1.80}$$

$$B_\varphi(r,\theta) = \frac{B_{\varphi 0}(r)}{1 + \epsilon\cos\theta}, \tag{1.81}$$

where

$$\Lambda = \beta_p - \beta_{p0} + l_i/2 - 1, \tag{1.82}$$

$$\beta_p(r) = \frac{2\mu_0}{B_{\theta 0}^2(r)} \frac{2}{r^2} \int_0^r p_0(r^*) r^* \, dr^*, \tag{1.83}$$

$$\beta_{p0} = \frac{2\mu_0 p_0(r)}{B_{\theta 0}^2(r)}, \tag{1.84}$$

$$l_i(r) = \frac{2\mu_0}{B_{\theta 0}^2(r)} \frac{2}{r^2} \int_0^r \frac{B_{\theta 0}^2(r^*)}{2\mu_0} r^* \, dr^*, \tag{1.85}$$

and $\epsilon \equiv r/R_0$, and the subscript 0 denotes the distribution in the limit $\epsilon = 0$.

For the discharges of interest to us, Λ in the RFP is usually < 0. Thus a consequence of equation (1.80) and equation (1.81) is that both B_θ and B_φ vary with the poloidal angle θ from a minimum at $\theta = 0$ to a maximum at $\theta = \pi$. If follows that there is the possibility of particles being trapped.

1.4.3 Banana Orbits

The path of a trapped particle in toroidal field geometry is called a banana orbit. As a particle bounces between reflection points it suffers a radial drift due to magnetic field line curvature. The resultant orbit has the shape of a banana, and hence the name 'banana orbit'. The time taken for a trapped particle to travel between the reflection points $\pm\theta_0$, known as the bounce time and denoted by $\tau_b(\theta_0)$, is given by (Kadomtsev and Pogutse 1967)

$$\tau_b(\theta_0) = \frac{2\sqrt{2}\, R_0 q}{c\sqrt{\epsilon}} K(\sin \tfrac{1}{2}\theta_0), \tag{1.86}$$

where K is the complete elliptic integral of the first kind.

The fraction of trapped particles at θ_0 is given by equation (1.78), where $R_m \equiv B_m/B_0$. From (1.80) and (1.81) we have that, correct to $O(\epsilon)$,

$$B_m^2 = \frac{B_{\varphi 0}^2}{1 - 2\epsilon \cos\theta_0} + \frac{B_{\theta 0}^2}{1 + 2\Lambda\epsilon \cos\theta_0}, \tag{1.87}$$

and

$$B_0^2 = \frac{B_{\varphi 0}^2}{1 + 2\epsilon} + \frac{B_{\theta 0}^2}{1 - 2\Lambda\epsilon}. \tag{1.88}$$

It follows from (1.87) and (1.88) that, correct to O(ϵ)

$$\begin{aligned} R_m &= \left(\frac{B_{\varphi 0}^2(1+2\epsilon\cos\theta_0)+B_{\theta 0}^2(1-2\Lambda\epsilon\cos\theta_0)}{B_{\varphi 0}^2(1-2\epsilon)+B_{\theta 0}^2(1+2\Lambda\epsilon)}\right)^{1/2} \\ &= \left(\frac{1+2\epsilon\Gamma\cos\theta_0}{1-2\epsilon\Gamma}\right)^{1/2} \qquad \left(\text{where } \Gamma \equiv \left|\frac{B_{\varphi 0}^2-\Lambda B_{\theta 0}^2}{B^2}\right|\right) \\ &= \frac{1+\epsilon\Gamma\cos\theta_0}{1-\epsilon\Gamma}. \end{aligned} \tag{1.89}$$

From (1.78) and the above, we find that

$$f_t = \left(\frac{2\epsilon\Gamma}{1+\epsilon\Gamma\cos\theta_0}\right)^{1/2}\sin\tfrac{1}{2}\theta_0. \tag{1.90}$$

It follows from (1.90) that the fraction of trapped particles being reflected in the poloidal angle range θ_0 to $\theta_0 + d\theta_0$ is

$$df_t(\theta_0) = \left(\frac{2\epsilon\Gamma}{1+\epsilon}\right)^{\frac{1}{2}}\tfrac{1}{2}\cos\tfrac{1}{2}\theta_0\, d\theta_0, \qquad (0<\theta_0<\pi). \tag{1.91}$$

The length of the banana orbit λ_b is the distance travelled by the particle between reflection points and is approximated by

$$\lambda_b(\theta_0) \simeq R_0 q\theta_0. \tag{1.92}$$

1.5 Theories of Transport in Magnetoplasmas

1.5.1 Introduction

The importance of cross-field transport in magnetic confinement machines was discussed in section 1.1.3. An understanding of the physics of transport processes is a crucial step in the realization of a fusion machine. It is not surprising, then, that since the inception of fusion research a considerable amount of effort has been directed towards understanding the physical mechanisms which drive energy and particles across magnetic fields. Despite this work, the generally accepted theories of cross-field transport have not been wholly successful in explaining the observations. Thus the term 'anomalous' transport has arisen to describe energy losses beyond those predicted by the accepted theory. The following sections give a brief account of the current theories of cross-field transport.

1.5.2 Neoclassical Transport

By "neoclassical" is meant that while the transport of mass and energy are determined (classically) from a kinetic equation for the velocity distribution function, in addition—unlike the classical theory of Chapman and Enskog—the geometry of the region plays an important role in determining the various diffusivities, especially when collisions are relatively rare. The geometry enters by creating a magnetic field structure that traps some particles in the banana orbits described in section 1.4.3. Since neo-classical theory is the leading theory of non-turbulent transport in tokamaks we shall discuss this theory in some detail in section 1.6 and present only the main results below.

The calculation of cross-field transport in toroidal magnetic confinement systems varies according to the collisionality of the plasma. The collisionality of a magnetoplasma with a toroidal magnetic field structure is defined in terms of the banana orbit bounce time τ_b and the 90° deflection time τ_D. The time taken on average for a trapped particle to be scattered out of its banana orbit is $\tau_{es} \sim \epsilon\tau_D$. If the collision time is such that $\tau_b < \tau_{es}$ then an average trapped particle completes at least one banana orbit before becoming detrapped and the particle species is said to be in the banana regime. When $\tau_b > \tau_{es}$, collisions dominate particle motions on time-scales of τ_b, and Pfirsch-Schlüter transport applies.

The Pfirsch-Schlüter diffusion coefficient is deduced by solving the equation of motion for the radial velocity in toroidal geometry. An account of Pfirsch-Schlüter diffusion is given in section 1.6.3. The result is

$$v_r = -\left(1 + \frac{2\eta_{\|}}{\eta_\perp} q^2\right) \frac{\eta_\perp p'}{B_{\varphi 0}^2} + \tfrac{3}{2}\eta_\perp \frac{n_e k T_e}{B_{\varphi 0}^2} - \frac{s E_\varphi}{B_\varphi}, \qquad \left(' \equiv \frac{\partial}{\partial r}\right). \tag{1.93}$$

The theory for the banana regime is somewhat more complicated and necessitates the use of a special form of kinetic theory. The particle and energy fluxes in this regime have been calculated by Rosenbluth, Hazeltine and Hilton (1972), and

are

$$\Gamma = \frac{q^2 r_{Le}^2 n}{\epsilon^{\frac{3}{2}} \tau_e T_e} \{-1.12(T_e + T_i)\frac{n'}{n} + 0.43T_e' + 0.19T_i'\} - \frac{2.44\epsilon^{\frac{1}{2}} n E_{||}}{B_\theta}, \quad (1.94)$$

$$Q_{er} = \frac{q^2 r_{Le}^2 p_e}{\epsilon^{\frac{3}{2}} \tau_e T_e} \{1.53(T_e + T_i)\frac{n'}{n} - 1.18T_e' - 0.27T_i'\} + \frac{1.75\epsilon^{\frac{1}{2}} p_e E_{||}}{B_\theta}, \quad (1.95)$$

$$Q_{ir} = -0.48(\frac{m_i T_e}{m_e T_i})^{\frac{1}{2}} \frac{q^2 r_{Le}^2 p_i}{\epsilon^{\frac{3}{2}} \tau_e} \frac{T_i'}{T_i}, \quad (1.96)$$

where $n = n_e = n_i$, $\Gamma = nv_r$, Q_{er} and Q_{ir} are the radial heat flux for the electron and ion fluids respectively and $E_{||} = \boldsymbol{E} \cdot \boldsymbol{B}/B$. Electron thermal losses exceed the predictions of neo-classical theory by up to two orders of magnitude (Wesson 1987). A similar circumstance is found for particle losses. Neoclassical predictions for ion thermal losses are generally closer to the observed values, but can still underestimate observation by an order of magnitude (Hugill 1983).

It is this discrepancy between the predictions of neoclassical theory and experimental results from toroidal confinement machines which has lead to the term 'anomalous' transport.

1.5.3 Theories of Anomalous Transport

It is generally accepted that the anomalous transport of electron fluid energy and mass is due to microturbulence generated by plasma instabilities. Much of the theoretical work on anomalous transport has centered on isolating the instability involved and calculating its effect on transport. The problems faced by researchers in this area are formidable. There are many instabilities and the appropriate equations of evolution are non-linear.

In a review paper of measurements of transport in tokamaks, Hugill (1983) makes the observation that electron thermal losses in tokamaks are still not understood. A more recent review paper by Liewer (1985) comparing measurements of microturbulence in tokamaks and theories of anomalous transport contains the conclusion that neither the source nor the role of broadband microturbulence in anomalous transport is understood. Woods (1987) has considered the implications of tokamak microturbulence for anomalous transport. He concludes that

the role of turbulence in transport is likely to be minor, and probably confined to the edge of the plasma. A general account of the theories of microturbulence and cross-field transport has been given by Wesson (1987).

1.5.4 Scale Transformations

A more general approach to finding scaling laws for cross-field transport is to require that the basic plasma equations remain invariant under scale transformations. Using this technique Connor and Taylor (1984) have determined the functional dependence of $B\tau_{Ee}$ on the dimensionless parameters $n_e a^2 T_e^{5/2} B^{-1}$, $BaT^{-1/2}$ and $n_e T_e B^{-2}$. By considering a particular microinstability, they derived energy confinement scaling laws for the tokamak and the RFP. The difficulties with this approach are twofold. First, the specific results of Connor and Taylor's application suggest that the confinement times of the RFP and the Tokamak should be similar. In fact the energy confinement times of RFP's are considerably smaller than tokamaks of similar dimensions and operating conditions. The second difficulty is more general, and it is that, while scale transformations may yield information about the set of equations under investigation, they do not offer insight into the physical mechanism underlying transport. If the original equations used to describe the plasma are not a good model then the results of the analysis will be flawed.

1.5.5 Second-order Transport

Woods (1987) has recently proposed a mechanism for the observed cross-field transport in magnetoplasmas which is quite different from the accepted theories of microturbulence. His theory is an extension of the classical first-order theory to second-order. An outline of the parts of his work that we shall be concerned with can be found in Chapter 2.

What we wish to emphasize here is the empirical evidence in support of second-order transport theory. Woods (1987 pp.411-503) has applied his theory to a wide range of phenomena in tokamaks with considerable success. The most

important of these is the accurate calculation of the electron energy confinement time in JET, without the introduction of empirical factors, and a scaling law for energy confinement very close to that obtained empirically. Woods has also obtained expressions for the particle and toroidal momentum confinement times and the sawtooth oscillation period which agree well with experiment as well as a number of other results which we will not detail here.

1.6 Survey of Neoclassical Transport Theory

A good review of neoclassical theory has been written by Galeev and Sadgeev (1979), who give clear physical interpretations of the diffusion coefficients in different regimes. A more comprehensive review can be found in Hinton and Hazeltine (1976). We shall present an account as it can be found in modern texts such as Miyamoto (1976) or Wesson (1987).

1.6.1 The Banana Regime

At a particle level of description, it is easy to see how banana orbits can enhance the cross-field transport of mass and energy. Figure 1.2 (from Wesson 1987, p.86) gives an impression of the collisional process in what is described as the banana regime.

Provided that the time τ_{es} for a particle p to escape from its banana orbit is comparable with or greater than its banana orbit bounce time τ_b, then p can move radially through a banana width in the time τ_{es}. Suppose that the average radial displacement of the trapped particles is Δr, then $\Delta r < w_b$, where w_b is the maximum banana width. The resulting diffusivity is estimated by taking $D = L^2/T$ where L is the displacement and T is the characteristic time for the diffusion process. Making the estimates $L \sim w_b$ and $T \sim \tau_{es}$ we obtain

$$D \sim f_T w_b^2/\tau_{es}, \tag{1.97}$$

where f_T is the fraction of trapped particles.

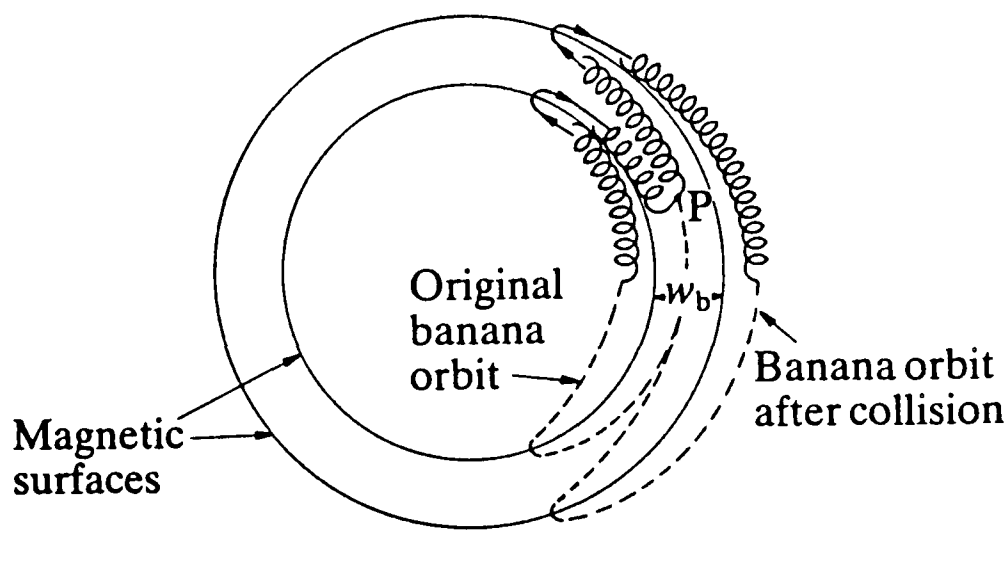

Figure 1.2: How a collision can displace a trapped particle by a banana width (from Wesson 1987)

In strong magnetic fields, without banana orbits, the maximum cross-field displacement of a particle is the Larmor radius r_L. Then if τ_D is the 90° deflection time resulting from collisions, the classical diffusivity is

$$D^c \sim r_L^2/\tau_D \tag{1.98}$$

The banana width is much larger than r_L, and τ_{es} is much smaller than τ_D, resulting in the neoclassical value of D being larger than D^c.

We require some time-scale estimates for the following analysis. These are:

$$\tau_{es} = \epsilon\tau_D, \quad \tau_b \sim Rq/C\epsilon^{1/2}, \quad v_d \sim Cr_L/R, \quad w_b \sim qr_L/\epsilon^{1/2}, \tag{1.99}$$

where v_d is the radial drift velocity due to the magnetic field gradient and C is the thermal speed $(2kT/m)^{1/2}$. These relations are well known, and can be found in Wesson (1987) or in Woods (1987, pp. 256, 228-230).

1.6.2 The Plateau Regime

In the region of collisionality where $\epsilon^{3/2} < \nu^* < 1$, the thermal diffusion coefficient is almost independent of ν^* (see figure 1.3) and is thus known as the "plateau region".

In the plateau region it is found that diffusion is determined mainly by those particles with a sufficiently low value of their parallel speed $w_{||}$ that they experience a small angle collision, $\Delta w_{||} \sim w_{||}$, during a single transit around the torus. As Coulomb collisions are diffuse in velocity space, the effective collision frequency for plateau region collisions is

$$\nu_{eff} = \nu(C/w_{||})^2. \tag{1.100}$$

Setting this equal to the reciprocal of the torus transit time, $Rq/w_{||}$, we obtain

$$w_{||} \sim C(\nu Rq/C)^{1/3}. \tag{1.101}$$

As $\epsilon^{3/2}C/Rq < \nu < C/Rq$ along the plateau, $w_{||}$ varies between $\epsilon^{1/2}C$ and C.

Because of the magnetic drift, a particle with the velocity $w_{||}$ drifts a radial distance $\Delta r \sim v_d Rq/w_{||}$ in one transit time. As it experiences one collision in this time, Δr is the characteristic displacement for the plateau diffusivity. The fraction of trapped particles with the speed $w_{||}$ is $\sim w_{||}/C$, and so

$$D^P \sim \frac{w_{||}}{C} v_d^2 \frac{Rq}{w_{||}} \sim \frac{Cqr_L^2}{R}. \tag{1.102}$$

1.6.3 Pfirsch-Schlüter Diffusion

When collisions dominate particle motions, a fluid model can be employed to describe a plasma. The original work on Pfirsch-Schlüter transport is found in Pfirsch and Schlüter (1962). The following treatment of Pfirsch-Schlüter diffusion is based on the accounts given by Miyamoto (1976), Wesson (1987) and Woods (1987), which all follow the same lines.

We begin with the expression for the electric field

$$\boldsymbol{E} = -\frac{\partial \phi}{\partial r}\hat{\boldsymbol{r}} - \frac{\partial \phi}{r \partial \theta} + E_\varphi \hat{\boldsymbol{\varphi}}, \tag{1.103}$$

and for the unit vector parallel to $\boldsymbol{b}$,

$$\boldsymbol{b} = \frac{1}{(1+s^2)^{1/2}}(\hat{\boldsymbol{\varphi}} + s\hat{\boldsymbol{\theta}}) \qquad (s \equiv B_\theta/B_\varphi). \tag{1.104}$$

The dot product of $\boldsymbol{b}$ with Ohm's law, (1.22), yields

$$\eta_{||}(j_\varphi + sj_\theta) = E_\varphi - \frac{s}{r}\frac{\partial\phi}{\partial\theta}. \tag{1.105}$$

Also, assuming that p depends only on r, the radial component of the equilibrium condition $j \times \boldsymbol{B} = \nabla p$ can be written

$$j_\theta - sj_\varphi = p'/B_\varphi. \tag{1.106}$$

For the subsequent calculations we will employ the Knorr field. Although the Knorr field does not strictly apply to toroidal machines (where it is not possible to assume that $B_r = 0$), it is a sufficiently accurate approximation for our purposes here. A more accurate derivation can be found in Kadomtsev (1966).

The Knorr field is characterised by $B_\varphi(r,\theta) = FB_{\varphi 0}(r)$, $B_\theta(r,\theta) = FB_{\theta 0}(r)$, $j_\theta(r,\theta) = Fj_{\theta 0}(r)$ and $E_\varphi(r,\theta) = FE_0(r)$ where $F^{-1} = 1 + \epsilon\cos\theta$ and E_0 is a constant. The second of these relations for B_θ holds only if we can assume that $B_r = 0$, otherwise we must adopt (1.80).

We proceed by taking the poloidal averages of (1.105) and (1.106), and solving for $j_{\theta 0}$. The expression for j_θ follows from $j_\theta = Fj_{\theta 0}$, and j_φ is obtained from (1.106). The expressions for j_θ and j_φ may be combined into

$$\eta_{||}(j_\varphi + sj_\theta) - E_\varphi = -\frac{\eta_{||}p'}{sB_{\varphi 0}}\left\{1 + \epsilon\cos\theta - \frac{(1-\epsilon^2)^{1/2}}{1+\epsilon\cos\theta}\right\}. \tag{1.107}$$

It follows from (1.103), (1.105), (1.107) and a neglect of terms of order s^2 that

$$\begin{aligned} \frac{\boldsymbol{b}\times\hat{\boldsymbol{r}}\cdot\boldsymbol{E}}{B} &= -\frac{1}{B_\varphi}\left(\frac{1}{r}\frac{\partial\phi}{\partial\theta} + sE_\varphi\right) \qquad (1.108)\\ &= -\frac{1}{B_{\varphi 0}}\left(sE_\varphi(1+\epsilon\cos\theta) + \frac{\eta_{||}p'}{s^2B_{\varphi 0}}[(1+\epsilon\cos\theta)^2 - (1-\epsilon^2)^{1/2}]\right). \end{aligned}$$

Neglecting the thermoelectric term from Ohm's law and solving for the radial fluid velocity, we obtain

$$\hat{\boldsymbol{r}}\cdot\boldsymbol{v} = \frac{\boldsymbol{b}\times\hat{\boldsymbol{r}}\cdot\boldsymbol{E}}{B} - \frac{\eta_\perp}{B}\hat{\boldsymbol{r}}\cdot\nabla p. \tag{1.109}$$

We can obtain the average particle flux nv_D from (1.109) by taking the poloidal average

$$nv_D = \frac{n}{2\pi}\int_0^{2\pi} \hat{\boldsymbol{r}} \cdot \boldsymbol{v}(1+\epsilon\cos\theta)\,\theta, \tag{1.110}$$

where the factor $1+\epsilon\cos\theta$ allows for the change in area of a surface element around the minor axis.

It follows from (1.54), (1.109), (1.109) and (1.110) that correct to first order in ϵ,

$$v_D = -(1+\frac{2\eta_{\|}}{\eta_\perp}q^2)\frac{\eta_\perp}{B_{\varphi 0}^2}p' - s\frac{E_\varphi}{B_\varphi}. \tag{1.111}$$

In summary, it is found that the diffusivity can be divided into three regions, depending on the value of the normalised frequency $\nu^* \equiv \tau_b/\tau_{es}$, or

$$\nu^* = Rq/C\tau_D, \qquad \Big(C \equiv (2kT/m)^{1/2}\Big). \tag{1.112}$$

We have

1. Banana Regime

$$D^B \sim \epsilon^{-3/2}q^2 r_L^2/\tau_D \sim D^c q^2 \epsilon^{-3/2} \qquad (0 < \nu^* < \epsilon^{3/2}). \tag{1.113}$$

2. Plateau Regime

$$D^P \sim Cqr_L^2/R \qquad (\epsilon^{3/2} < \nu^* < 1). \tag{1.114}$$

3. Pfirsch-Schlüter Regime

$$D^{FS} \sim D^c(1+2\frac{\eta_{\|}}{\eta_\perp}q^2) \qquad (1 < \nu^*). \tag{1.115}$$

These regions are illustrated in Figure 1.3 (from Wesson 1987, p.93).

The expression for D^B follows from (1.97), (1.99) and $f_t = (2\epsilon)^{1/2}$.

1.6.4 The Ware Pinch Effect, Bootstrap Current, and Neoclassical Conductivity

As well as enhancing classical diffusion, the trapping of charged particles in banana orbits produces three other effects in toroidal machines. These are (a)

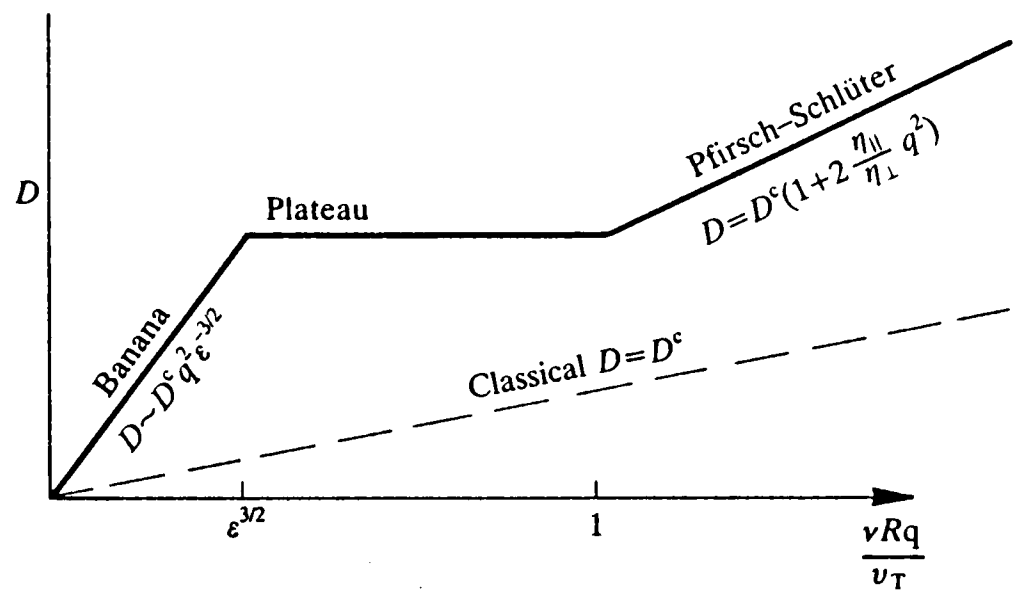

Figure 1.3: Variation of diffusion coefficient with collision frequency

an inward particle transport, known as the Ware pinch, (b) a parallel current driven by the radial density gradient known as the bootstrap current and (c) and a reduction in the toroidal conductivity.

The Ware Pinch

Ware (1970) has shown that conservation of canonical angular momentum requires that all trapped particles drift towrards the magnetic axis. In a complete account of neoclassical theory, the Ware pinch arises from the last term in (1.94),

$$\Gamma_w = -2.44\epsilon^{1/2} n E_{||}/B_\theta, \tag{1.116}$$

and follows from the fact that trapped particles have a guiding center drift $v_r = -E_\varphi/B_\theta$. As there are $n\epsilon^{1/2}$ trapped particles at a given radius, (1.116) follows from $\Gamma = n\epsilon^{1/2} v_r$.

The Bootstrap Current

Since the Ware pinch represents a radial flux driven by a toroidal electric field, the Onsagar symmetry relations require there to be a parallel current driven by

a density gradient. Such a current is predicted by neoclassical theory as a term of the form

$$j_b = -2.44\frac{\epsilon^{1/2}kn}{B_\theta}(T_e + T_i)\frac{n'}{n} \tag{1.117}$$

The term "bootstrap" arises since it seems that the radial diffusion of plasma is sufficient to generate a toroidal current which can remove the necessity for a driving electric field.

Neoclassical Conductivity

Neoclassical electrical conductivity arises from the fact that trapped particles are not free to move along the magnetic field in response to an applied electric field. Thus the current carried is reduced by the presence of trapped particles and the conductivity reduced. The original calculations were done by Hinton and Oberman 1967 for a Lorentz gas. To a good approximation (e.g. see Wesson 1987) we have, correct to order ϵ,

$$\frac{\sigma}{\sigma_{sp}} = 1 - \epsilon^{1/2} \tag{1.118}$$

1.6.5 The Kinetic Theory Basis of Neoclassical Theory

The starting point for an advanced treatment of neoclassical theory is the drift kinetic equation for the guiding centre distribution function $\tilde{f}$ (Hinton & Hazeltine 1976)

$$\frac{\partial \tilde{f}}{\partial t} + w_{||}\boldsymbol{b}\cdot\nabla\tilde{f} + \boldsymbol{u}_d\cdot\nabla\tilde{f} + \frac{e}{m}E_{||}\frac{\partial\tilde{f}}{\partial w_{||}} = \left(\frac{\partial\tilde{f}}{\partial t}\right)_{col}, \tag{1.119}$$

where $\boldsymbol{u}_d$ is the guiding centre drift velocity. This equation is based on the assumption that for the macroscopic variables of interest, ϕ say,

$$\eta \equiv \max\left\{|\omega_c^{-1}\frac{\partial}{\partial t}\ln\phi|,\ |r_L\nabla\ln\phi|\right\} \ll 1. \tag{1.120}$$

The drift kinetic equation is formulated so that the rapid gyratory motion of charged particles about field lines is averaged. For steady-state conditions, the expansion parameter η is the ratio of the Larmor radius to a macroscopic length scale. Second-order terms are not retained in the drift kinetic equation, and

because of the averaging about a Larmor radius, the classical diffusion term does not appear. However, it is generally accepted that the classical contribution to transport is unimportant when compared with neoclassical effects. This follows from the fact that the banana width is $q\epsilon^{-1/2}$ times larger than the Larmor radius plus the assumption that the first-order terms in classical theory are the dominant ones.

In the classical transport theory pursued by Woods, the expansion parameter is the Knudson number,

$$\epsilon \equiv \max\left\{ |\tau \frac{\partial}{\partial t} \ln \phi|,\ |\lambda \nabla \ln \phi| \right\} \ll 1, \tag{1.121}$$

where τ is the collision time and λ is the mean-free-path.

Woods (1987 pp. 91-92, pp. 331-333) discusses the Knudson number as an expansion parameter for the kinetic equation.

In the magnetoplasmas of interest in this thesis another basic parameter which arises is $\zeta = (\omega_c \tau)^{-1}$. Woods (private communication) has pointed out that this small parameter links the neoclassical expansion parameter and the Knudson number by

$$\eta = \epsilon\zeta. \tag{1.122}$$

This is a relation which we shall require when we compare neoclassical theory with second-order transport theory.

Chapter 2

Second-Order Transport Theory

In this chapter we will give an overview of Woods' second-order transport theory for magnetoplasmas and its application to toroidal confinement machines. We will present the physical mechanism which underlies the transport processes, and particularly that for the heat flux. A more formal treatment of this material may be found in *"Principles of Magnetoplasma Dynamics"* (Woods 1987).

The basic concepts are first illustrated in the context of neutral gas theory and then considered in the more complex case of a magnetoplasma.

The sections of this chapter presenting original work are those dealing with the second-order transport coefficients in the RFP, and the scaling of τ_E with β_p compared to experiment.

2.1 The Physical Mechanism

2.1.1 Second-Order Transport in a Neutral Gas

In neutral gas theory the kinetic equation is solved by expanding the velocity distribution function f as a power series (the Chapman-Enskog series) of the Knudsen number, ϵ:

$$f = f_0 + f_1 + f_2 + \cdots, \qquad f_n = O(\epsilon^n). \tag{2.1}$$

The Knudsen number is the ratio of a macroscopic time (or length) to a microscopic time-scale (or length-scale). For example, if ϕ is a macroscopic fluid

variable such as density or temperature then an appropriate expression for ϵ is

$$\epsilon = \tau \left| \frac{d \ln \phi}{dt} \right|, \tag{2.2}$$

where τ is a collision time.

Expansions similar to (2.1) are adopted for the heat flux vector $\boldsymbol{q}$ and the viscous stress tensor $\boldsymbol{\pi} = \boldsymbol{p} - p\mathbf{1}$, viz:

$$\boldsymbol{q} = \boldsymbol{q}_1 + \boldsymbol{q}_2 + \cdots, \quad \boldsymbol{\pi} = \boldsymbol{\pi}_1 + \boldsymbol{\pi}_2 + \cdots. \tag{2.3}$$

A first-order kinetic theory omits terms in (2.1) and (2.3) of higher order than ϵ, and for a monatomic gas yields

$$\boldsymbol{q}_1 = -\kappa \nabla T, \quad \boldsymbol{\pi}_1 = -2\mu \overset{\circ}{\nabla} \boldsymbol{v}, \tag{2.4}$$

where κ and μ are the (scalar) thermal conductivity and viscosity coefficients.

A second-order kinetic theory retains terms to order ϵ^2, and by 'second-order heat flux' and 'second-order viscosity', we mean the terms $\boldsymbol{q}_2$ and $\boldsymbol{\pi}_2$ of order ϵ^2 appearing in (2.3). These terms have been calculated by Burnett (1935), Grad (1949), Chapman and Cowling (1970) and, more recently, Woods (1987). The expressions obtained by Woods differ form those previously deduced in that they are frame indifferent. This point is discussed by Woods (1987, p.316). Woods obtains[1]

$$\boldsymbol{q}_2 = \frac{k}{m} p \tau_2^2 \{ \tfrac{15}{4}(3-s)\nabla \cdot \boldsymbol{v} \nabla T + \tfrac{48}{8}(D\nabla T - \Omega \times \nabla T) - 3\frac{T}{p}\nabla p \cdot \overset{\circ}{\boldsymbol{e}} + 3(\tfrac{55}{8} + s)\nabla T \cdot \overset{\circ}{\boldsymbol{e}} \}, \tag{2.5}$$

where $\overset{\circ}{\boldsymbol{e}} \equiv (\nabla \boldsymbol{v} + \tilde{\nabla} \boldsymbol{v})/2$, $s \equiv 1/2 + 2/(\nu - 1)$ (ν is the power law for the repulsive force between particles and $s = 5/2$ for a plasma), $D \equiv \partial/(\partial t) + \boldsymbol{v} \cdot \nabla$ is the material time derivative, $\Omega \equiv \frac{1}{2}\nabla \times \boldsymbol{v}$ is the fluid spin and τ_2 is the collision time associated with energy transport (see section 1.2.2). For the second-order viscous stress tensor, Woods obtains

[1]There is some question about whether or not the pressure term should be included in $\boldsymbol{q}_2$. However, this issue does not arise in the case of a magnetoplasma.

$$\boldsymbol{\pi}_2 = p\tau_1^2\{\tfrac{4}{3}(3-s)\overset{\circ}{\boldsymbol{e}}\nabla\cdot\boldsymbol{v} + 2(D\overset{\circ}{\boldsymbol{e}} - 2\overset{\circ}{\overline{\boldsymbol{\Omega}\times\overset{\circ}{\boldsymbol{e}}}}) + 3\frac{k}{m}\overset{\circ}{\overline{\nabla\nabla T}}$$

$$+3s\frac{k}{mT}\overset{\circ}{\overline{\nabla T\nabla T}} + 4\overset{\circ}{\overline{\overset{\circ}{\boldsymbol{e}}\cdot\overset{\circ}{\boldsymbol{e}}}}\}. \qquad (2.6)$$

Equations (2.5) and (2.6) are considerably more complicated than (2.4), and in most situations are of more academic than practical interest. For $\epsilon \ll 1$, $\boldsymbol{q}_2$ and $\boldsymbol{\pi}_2$ are only small corrections to the corresponding first order terms.

2.1.2 Second-Order Transport in a Magnetoplasma

The form of the heat flux vector and viscous stress tensor in the ion and electron fluids in a magnetoplasma is complicated by the anisotropy introduced by the presence of magnetic fields. The scalar thermal conductivity κ must be replaced by a tensor quantity $\boldsymbol{\kappa}$ (known as the thermal conductivity tensor) which has the form (Woods 1987 p.81)

$$\boldsymbol{\kappa} = \kappa_{||}\boldsymbol{bb} + \kappa_{\wedge}\boldsymbol{b}\times\mathbf{1} + \kappa_{\perp}(\mathbf{1}-\boldsymbol{bb}), \qquad (2.7)$$

where $\boldsymbol{b}$ is a unit vector parallel to the magnetic field, and the three terms on the right-hand side of this equation correspond to 'parallel', 'transverse' and 'perpendicular' components of $\boldsymbol{\kappa}$ respectively. The thermal conductivity tensor gives rise to a first-order heat flux of the form

$$\boldsymbol{q}_1 = -\boldsymbol{\kappa}\cdot\nabla T = \boldsymbol{q}_{||} + \boldsymbol{q}_{\wedge} + \boldsymbol{q}_{\perp}. \qquad (2.8)$$

With the field structure found in a tokamak, $\boldsymbol{q}_{||}$ and $\boldsymbol{q}_{\wedge}$ correspond to a heat flux parallel and perpendicular to $\boldsymbol{b}$ in a magnetic surface respectively, and $\boldsymbol{q}_{\perp}$ is the heat flux perpendicular to both $\boldsymbol{b}$ and a magnetic surface.

Woods (1987 p.81) has derived approximate expressions for $\kappa_{||}$, $\kappa_{\wedge}$ and $\kappa_{\perp}$ from elementary kinetic theory. These are

$$\kappa_{||} = \kappa, \quad \kappa_{\wedge} = -\kappa\frac{\tilde{\omega}}{1+\tilde{\omega}^2}, \quad \kappa_{\perp} = \kappa\frac{1}{1+\tilde{\omega}^2}, \qquad (\tilde{\omega}\equiv\omega_c\tau), \qquad (2.9)$$

where κ is the thermal conductivity in the absence of a magnetic field. These expressions are never more than a factor of two in error when compared with

the coefficients derived by Braginskii (1965) using the Fokker-Plank equation. In the magnetoplasmas of interest to us, $\xi \equiv 1/\tilde{\omega}$ is very small and is, in effect, another expansion parameter. From (2.8) and (2.9) we have that $\boldsymbol{q}_{||} = \mathrm{O}(\epsilon, 1)$, $\boldsymbol{q}_{\wedge} = \mathrm{O}(\epsilon, \xi)$ and $\boldsymbol{q}_{\perp} = \mathrm{O}(\epsilon, \xi^2)$. Thus, to order ϵ^2, $\boldsymbol{q}$ in, say, the electron fluid may be written as

$$\begin{aligned} \boldsymbol{q} =& \overset{(1)}{\underset{10^{-2}}{\mathrm{O}(\epsilon,1)}} + \overset{(2)}{\underset{10^{-9}}{\mathrm{O}(\epsilon,\xi)}} + \overset{(3)}{\underset{10^{-16}}{\mathrm{O}(\epsilon,\xi^2)}} + \overset{(4)}{\underset{10^{-4}}{\mathrm{O}(\epsilon^2,1)}} + \overset{(5)}{\underset{10^{-11}}{\mathrm{O}(\epsilon^2,\xi)}} + \overset{(6)}{\underset{10^{-18}}{\mathrm{O}(\epsilon^2,\xi^2)}} . \end{aligned} \tag{2.10}$$

The magnitudes in (2.10) come from setting $\epsilon \sim 10^{-2}$ and $\xi \sim 10^{-7}$, which are typical values for the electron fluid in tokamaks.

Only terms (3), (5), and (6) in (2.10) contribute to the radial heat flux, and of these it is term (5) which makes the dominant contribution. Thus in this formulation it is the radial component of the second-order term corresponding to $\boldsymbol{q}_{\wedge}$ which dominates the cross-field transport in tokamaks.

2.1.3 The Second-Order Transport Coefficients

Woods (1987) has formally derived expressions for $\boldsymbol{q}_2$ and $\boldsymbol{\pi}_2$ from kinetic theory, and what follows is a brief outline of his work. For full details, the reader is referred to his book '*Principles of Magnetoplasma Dynamics*', pp.313-333. Certain concepts used by Woods in applying his transport coefficients to tokamaks are discussed in section 2.2. These will be used when we consider second-order transport in the RFP.

The Second-Order Heat Flux

Woods obtains for the second-order heat flux

$$\boldsymbol{q}_2 = -\frac{5}{2}\frac{kp}{QB}\tau^* \boldsymbol{b}\times \overset{\circ}{\nabla}\boldsymbol{v} \cdot \nabla T, \tag{2.11}$$

where Q is the fluid species particle charge and $\tau^* = \tau_2$ in the absence of particle trapping effects. In deriving (2.11), Woods assumes steady, sheared flow and

neglects $\nabla \cdot \boldsymbol{v}$ terms. Terms of the type $\nabla \cdot \boldsymbol{v}$ are found to be small scalar modifications to the first-order terms, and can therefore be neglected. It is changes to the first-order terms that alter the direction of $\boldsymbol{q}_1$ which are of interest.

In toroidal confinement machines where particle trapping occurs, τ_2 is not the appropriate time-scale to use in (2.11). Separate physical arguments are required to determine this parameter. A discussion of this point can be found in section 2.2.

The Second-Order Viscous Stress Tensor

For the second-order viscous stress tensor, Woods obtains

$$\begin{aligned}\boldsymbol{\pi}_2 &= 4p\tau_1^2\Big\{\tfrac{1}{2}(3\boldsymbol{bb}-\mathbf{1})\boldsymbol{b}\cdot\boldsymbol{S}\cdot\boldsymbol{b}+\frac{1}{4\tilde{\omega}}(\mathbf{1}_\perp\cdot\boldsymbol{S}\times\boldsymbol{b}-\boldsymbol{b}\times\boldsymbol{S}\cdot\mathbf{1}_\perp)\\ &\quad+\frac{1}{4\tilde{\omega}}(\boldsymbol{bb}\cdot\boldsymbol{S}\times\boldsymbol{b}-\boldsymbol{b}\times\boldsymbol{S}\cdot\boldsymbol{bb})\Big\}+\text{terms } \mathrm{O}(\tilde{\omega}^{-2}),\end{aligned} \tag{2.12}$$

where $\mathbf{1}_\perp \equiv \mathbf{1} - \boldsymbol{bb}$ and

$$\boldsymbol{S} \equiv \overline{\nabla\boldsymbol{v}\cdot\overset{\circ}{\nabla\boldsymbol{v}}+\tfrac{1}{2}\boldsymbol{v}\cdot\nabla\overset{\circ}{\nabla\boldsymbol{v}}}^{\circ}\,. \tag{2.13}$$

In deriving (2.12), steady flow has been assumed and, for reasons already discussed, terms involving $\nabla \cdot \boldsymbol{v}$ have been neglected.

Equations (2.11) and (2.12) form the basis for the work which follows in Chapters 3 and 4.

The final point to be discussed in this section is the validity of the second-order terms.

2.1.4 The Validity of the Second-Order Transport Coefficients

Woods (1987) has given a complete account of when second-order terms dominate, and when equations (2.11) and (2.12) are valid. We do not intend to discuss this topic fully, but give only the most relevant restrictions on the validity of the theory.

The most fundamental requirement for (2.11) and (2.12) to hold is that $\tilde{\omega} \gg 1$. That is, a particle must, on average, complete many gyrations about a magnetic field line in one collision interval. Unless this condition holds, we are not entitled to omit terms $O(\tilde{\omega}^{-2})$ from the expansion of π as we shall do in subsequent sections. Woods has also used the condition $\tilde{\omega} \gg 1$ at an earlier stage in developing his kinetic theory.

Steady-state conditions have been assumed in the calculations which lead to (2.11) and (2.12).

In addition to these conditions, the usual conditions for the validity of the equations of MHD apply, (e.g. see Boyd and Sanderson 1969) and must be satisfied for the use of the transport coefficients to be meaningful.

2.2 Second-Order Transport in Toroidal Confinement Machines

As mentioned above, the calculations Woods has made to determine $\boldsymbol{q}_2$ require that special consideration be given to the time-scale τ^* in (2.11) when particle trapping occurs. The following discussion is concerned with how this time-scale can be determined in toroidal confinement machines.

2.2.1 The Second-Order Heat Flux in a Tokamak

The physical significance of τ^* in a toroidal confinement machine can be elucidated by considering the time-scale associated with the transport of energy in a neutral gas.

In a neutral gas, the heat flux vector, correct to first-order, is given by

$$\boldsymbol{q} = -\rho\chi\nabla u, \tag{2.14}$$

where χ is the thermal diffusivity, ρ is the gas density and $u = c_v T$ is the specific energy. For an ideal gas, the specific heat capacity at constant volume is $c_v = 3k/2m$, where k is Boltzmann's constant and m is the particle mass.

A calculation of χ can be made from kinetic theory, which yields

$$\chi = \lambda^2/\tau, \tag{2.15}$$

where λ is the mean-free-path and τ is (approximately) the collision time. Since the conduction of heat is a microscopic process, determined by particle interactions, it is not surprising that the thermal diffusivity can be expressed in terms of the microscopic length and time-scales λ and τ.

In the case of a magnetoplasma, the scalar diffusivity χ is replaced by a tensor tensor quantity $\boldsymbol{\chi}$ ($\boldsymbol{\chi} = \boldsymbol{\kappa}/\rho c_v$, cf. equation (2.7)); viz:

$$\boldsymbol{\chi} = \chi_{||}\boldsymbol{bb} - \chi_{\wedge}\boldsymbol{b} \times \mathbf{1} + \chi_{\perp}(\mathbf{1} - \boldsymbol{bb}), \tag{2.16}$$

where $\chi_{||} = \chi$, $\chi_{\wedge} = \tilde{\omega}\chi_{||}/(1+\tilde{\omega}^2)$ and $\chi_{\perp} = \chi_{||}/(1+\tilde{\omega}^2)$ and $\tilde{\omega} \equiv \omega_c\tau_c$. By analogy with (2.15), we expect that each of these diffusivities can be expressed in terms of microscopic length and time-scales.

If we examine $\chi_{\wedge}$—the term which, when carried to second-order, gives rise to a large radial heat flux (cf. (2.10))—we find that

$$\begin{aligned} \chi_{\wedge} &= \frac{\tilde{\omega}}{1+\tilde{\omega}^2}\chi_{||} \\ &\simeq \frac{\chi_{||}}{\tilde{\omega}}, \qquad \text{if } \tilde{\omega} \gg 1. \end{aligned} \tag{2.17}$$

The purpose of the following discussion is to determine what significance to apply to the term $\chi_{||}$ in (2.17). Woods (1987, p.233) has argued that in a torus untrapped particles do not contribute to $\chi_{||}$. It follows that $\chi_{||}$ is due to trapped particles only. We must therefore calculate the parallel thermal diffusivity of trapped particles. To do this, we replace λ, the mean-free-path of an untrapped particle parallel to the magnetic field, with λ_b, the corresponding length for a trapped particle. Since trapped particles execute banana orbits, we have the estimate that $\lambda_b = R_0 q \theta_0$, where θ_0 is the poloidal angle at which a particular particle is reflected and λ_b is the length of the banana orbit parallel to the magnetic field.

Woods further argues that the microscopic time-scale associated with the parallel diffusivity is $\tau_b/2$, where τ_b is the particle bounce time.

It follows that the parallel diffusivity associated with the $df_t(\theta_0)$ particles reflected between θ_0 and $\theta_0 + d\theta_0$ is

$$dD_{||} = \frac{2\lambda_b^2(\theta_0)}{\tau_b(\theta_0)} df_t(\theta_0). \tag{2.18}$$

As diffusivities must be summed, the total diffusivity is found by integrating (2.18) over the range of θ_0 for which trapping occurs. Using the relation $df_t(\theta_0) = (2\epsilon/(1+\epsilon))^{1/2}(1/2)\cos(\theta_0/2)\, d\theta_0$ (the factor $\Gamma \simeq 1$ for a tokamak) and making the substitution $\epsilon = r/R_0$, (2.18) can be integrated to yield

$$D_{||} = \frac{4rqc}{(1+\epsilon)^{1/2}} \int_0^{\pi/2} \frac{x^2 \cos x}{K(\sin x)}\, dx. \tag{2.19}$$

With the substitution $(1+\epsilon)^{1/2} \simeq 1$, equation (2.19) yields the approximation

$$D_{||} \simeq rqC, \tag{2.20}$$

where we have replaced c by its average value $2\sqrt{\pi}C$, and $C = (2kT/m)^{1/2}$.

In a torus, $\chi_{||}$ must be replaced by $D_{||}$, and it is not difficult to show that this amounts to setting

$$\tau^* = 2rq/C \tag{2.21}$$

in (2.11).

2.2.2 The Second-Order Heat Flux in a RFP

The physical arguments in the preceeding section used to develop an expression for τ^* in the tokamak are valid in the RFP, but some assumptions have been made in the analysis which are not. In particular, the ratio

$$s \equiv \frac{b_\theta}{b_\varphi} \tag{2.22}$$

is small in a circular tokamak, but is not in the RFP and can be O(1) in a non-circular small aspect ratio device such as JET. When applying his theory to the

tokamak, Woods used the approximation

$$\begin{aligned} \boldsymbol{b} &= h(\hat{\varphi} + s\hat{\theta}), \qquad h \equiv \frac{1}{(1+s^2)^{1/2}} \\ &\simeq \hat{\varphi} + s\hat{\theta}, \qquad \text{if } s \ll 1. \end{aligned} \tag{2.23}$$

As typically $s \sim 1/10$ near the limiter in a tokamak with cylindrical cross-section, it is reasonable to neglect terms $O(s^2)$.

In the RFP, b_φ tends to zero near the reversal surface and s is unbounded. This makes (2.23) an inappropriate expression for $\boldsymbol{b}$, and invalidates any approximations which neglect terms involving s^2. To avoid this difficulty, we shall use the expression

$$\boldsymbol{b} = b_\theta \hat{\boldsymbol{\theta}} + b_\varphi \hat{\varphi}, \tag{2.24}$$

where $b_\theta \equiv B_\theta/B$ and $b_\varphi \equiv B_\varphi/B$.

The phenomenon of particle trapping that Woods used to calculate $\chi_{||}$ in the tokamak also occurs in the RFP. However, the calculation which leads to an expression for τ_b assumes $s \ll 1$, and needs to be revised.

Particle Trapping in the RFP

The work which follows is a slight generalization of a result due to Kadomtsev and Pogutse (1967). We will not present all the calculations, but indicate where approximations invalid in the RFP have been made, and the result obtained if all significant terms are retained.

One of the approximations made in calculating τ_b in the tokamak is that the element of distance along a field line,

$$ds = \{(Rd\varphi)^2 + (rd\theta)^2 + (dr)^2\}^{1/2}, \tag{2.25}$$

is well approximated by $ds \simeq R_0 q d\theta$, where $q = rB_\varphi/RB_\theta$. This approximation is not valid for the RFP. A complete calculation of τ_b including the effects of a finite B_r has been made by Woods (private communication). He obtains the result

$$\tau_b(\theta_0) = \frac{2\sqrt{2}\{q^2 + \epsilon^2\}^{1/2} R_0}{c\sqrt{\Gamma\epsilon}} K(\sin \tfrac{1}{2}\theta_0), \tag{2.26}$$

We have not shown the calculations leading to this result as they are not essential to our argument. However, it can be seen that (2.26) can be derived immediately from (1.86) if we substitute $R_0\{q^2+\epsilon^2\}^{1/2}$ for $R_0 q$ and $\Gamma\epsilon$ for ϵ. A more careful analysis yields the same result.

The length of the banana orbit is approximated by

$$\lambda_b(\theta_0) = R_0\{q^2+\epsilon^2\}^{1/2}\theta_0. \tag{2.27}$$

Equations (2.26) and (2.27) give the correct expressions to be used for τ_b and λ_b when calculating $D_{||}$ in the RFP.

The Thermal Diffusivity due to Trapped Particles in the RFP

Substituting (2.26) and (2.27) into equation (2.18) for $dD_{||}$ and integrating over θ_0, we obtain

$$D_{||} = r\Gamma\{q^2+\epsilon^2\}^{1/2}C, \tag{2.28}$$

which reduces to (2.20) for the case of the tokamak where $q^2 \gg \epsilon^2$ and $\Gamma \simeq 1$. The resulting expression for τ^* is

$$\tau^* = \frac{2r\Gamma\{q^2+\epsilon^2\}^{1/2}}{C}. \tag{2.29}$$

Substituting (2.29) into equation (2.11) for $\boldsymbol{q}_2$, we obtain an expression for the second-order heat flux in the RFP, viz:

$$\boldsymbol{q}_2 = -\frac{5}{2}\frac{kp}{QB}\frac{2r\Gamma\{q^2+\epsilon^2\}^{1/2}}{C}\boldsymbol{b}\times\overset{\circ}{\nabla}\boldsymbol{v}\cdot\nabla T. \tag{2.30}$$

2.2.3 The Second-Order Viscous Stress Tensor in the RFP

According to Woods' theory, a calculation of $\boldsymbol{\pi}_2$ from (2.12) is not complicated by the same trapping effects as the thermal diffusivity. This is due to the fact that the microscopic time-scale appearing in (2.12) is associated with collisions and not the geometry of the confining magnetic field.

If we assume that the radial fluid velocity of the ions and electrons may be neglected compared with the toroidal and poloidal components, and that we have

symmetry about the minor and major axes, then we obtain

$$\nabla \boldsymbol{v} = v'_\theta \hat{\boldsymbol{r}}\hat{\boldsymbol{\theta}} - \frac{v_\theta}{r}\hat{\boldsymbol{\theta}}\hat{\boldsymbol{r}} + v_\varphi \hat{\boldsymbol{r}}\hat{\boldsymbol{\varphi}}, \tag{2.31}$$

where here and in the sequel, a dash denotes the radial derivative. From the definition $\overset{\circ}{\nabla}\boldsymbol{v} \equiv (\nabla \boldsymbol{v} + \tilde{\nabla}\boldsymbol{v})/2 - \nabla \cdot \boldsymbol{v}\mathbf{1}/3$ we find that

$$\overset{\circ}{\nabla}\boldsymbol{v} = \frac{1}{2}r\left(\frac{v_\theta}{r}\right)'(\hat{\boldsymbol{r}}\hat{\boldsymbol{\theta}} + \hat{\boldsymbol{\theta}}\hat{\boldsymbol{r}}) + \frac{1}{2}v'_\varphi(\hat{\boldsymbol{r}}\hat{\boldsymbol{\varphi}} + \hat{\boldsymbol{\varphi}}\hat{\boldsymbol{r}}), \qquad \left(' = \frac{\partial}{\partial r}\right). \tag{2.32}$$

Substitution of (2.31) and (2.32) into the definition of $\boldsymbol{S}$, (2.13), yields after some calculation

$$\boldsymbol{S} = \Theta \hat{\boldsymbol{r}}\hat{\boldsymbol{r}} + \Xi(\hat{\boldsymbol{\theta}}\hat{\boldsymbol{\varphi}} + \hat{\boldsymbol{\varphi}}\hat{\boldsymbol{\theta}}), \tag{2.33}$$

where

$$\Theta \equiv \frac{1}{2}\left\{r^2\left[\left(\frac{v_\theta}{r}\right)'\right]^2 + \left[v'_\varphi\right]^2\right\}, \tag{2.34}$$

and

$$\Xi \equiv \frac{1}{4}r\left(\frac{v_\theta}{r}\right)' v'_\varphi. \tag{2.35}$$

Writing $\boldsymbol{b} = b_\theta\hat{\boldsymbol{\theta}} + b_\varphi\hat{\boldsymbol{\varphi}}$ and substituting (2.33) into equation (2.12) for $\boldsymbol{\pi}_2$ we obtain, after some algebra and neglecting terms $O(\tilde{\omega}^{-2})$,

$$\begin{aligned}\boldsymbol{\pi}_2 \;=\; & 8p\tau_1^2\Big\{b_\theta b_\varphi \Xi\Big[-\hat{\boldsymbol{r}}\hat{\boldsymbol{r}} + (2b_\theta^2 - b_\varphi^2)\hat{\boldsymbol{\theta}}\hat{\boldsymbol{\theta}} + 3b_\theta b_\varphi(\hat{\boldsymbol{\theta}}\hat{\boldsymbol{\varphi}} + \hat{\boldsymbol{\varphi}}\hat{\boldsymbol{\theta}}) + (2b_\varphi^2 - b_\theta^2)\hat{\boldsymbol{\varphi}}\hat{\boldsymbol{\varphi}}\Big] \\ & + \frac{1}{4\tilde{\omega}}\Big[\{\Theta b_\theta + 2\Xi b_\varphi(2b_\varphi^2 - b_\theta^2)\}(\hat{\boldsymbol{r}}\hat{\boldsymbol{\varphi}} + \hat{\boldsymbol{\varphi}}\hat{\boldsymbol{r}}) \\ & + \{-\Theta b_\varphi - 2\Xi b_\theta(2b_\theta^2 - b_\varphi^2)\}(\hat{\boldsymbol{r}}\hat{\boldsymbol{\theta}} + \hat{\boldsymbol{\theta}}\hat{\boldsymbol{r}})\Big]\Big\}.\end{aligned} \tag{2.36}$$

As it is the divergence of the viscous stress tensor that we shall be using in the work which follows, an expression for $\nabla \cdot \boldsymbol{\pi}_2$ can be found below.

Only those terms involving $(\hat{\boldsymbol{r}}\hat{\boldsymbol{\varphi}} + \hat{\boldsymbol{\varphi}}\hat{\boldsymbol{r}})$ and $(\hat{\boldsymbol{r}}\hat{\boldsymbol{\theta}} + \hat{\boldsymbol{\theta}}\hat{\boldsymbol{r}})$, i.e. those terms of $O(\tilde{\omega}^{-1})$ in (2.36) give $\hat{\boldsymbol{\theta}}$ and $\hat{\boldsymbol{\varphi}}$ components upon taking the divergence of the pressure tensor. As we shall not be concerned with the radial component of $\nabla \cdot \boldsymbol{\pi}_2$ in subsequent calculations, only the terms of $O(\tilde{\omega}^{-1})$ are found in (2.37) below. Taking the divergence of (2.36) and neglecting radial components, we find that

$$\nabla \cdot \boldsymbol{\pi}_2 = -\frac{2}{r^2}\left\{r^2\frac{p\tau_1^2}{\tilde{\omega}}\left[\Theta b_\varphi + 2\Xi b_\theta(2b_\theta^2 - b_\varphi^2)\right]\right\}'\hat{\boldsymbol{\theta}} + \frac{1}{r}\left\{r\frac{p\tau_1^2}{\tilde{\omega}}\left[\Theta b_\theta + 2\Xi b_\varphi(2b_\varphi^2 - b_\theta^2)\right]\right\}'\hat{\boldsymbol{\varphi}}. \tag{2.37}$$

This expression may be compared with that obtained by Woods (1987 p.461) by making the substitutions $b_\theta = s$, $b_\varphi = 1$ and neglecting terms $O(s^2)$.[2]

Equation (2.37) is valid for all values of b_θ and b_φ, and we will make use of this expression in Chapter 3 when calculating the plasma radial velocity in the RFP.

2.3 The Scaling of the Thermal Diffusivity with Poloidal Beta: Comparison with Experiment

Woods (1987) has made a thorough comparison of second-order transport theory applied to the tokamak with experiment. In particular, he has examined the electron radial heat flux $q_{er} = \hat{r} \cdot \boldsymbol{q}_2$. Although we do not intend to elaborate Woods' work on q_{er} in the tokamak, in this section we will pursue a prediction made by him concerning the scaling of χ_e in tokamaks with β_p. The results are of some interest as Woods' work was done before the experimental results were available.

2.3.1 Woods' Scaling Law

Woods (1987 p.445) finds the electron thermal diffusivity in a tokamak to be given by

$$\chi_e = \frac{5m_e r q C_e}{6e^2 n_e B_\varphi^2}\Big\{\mu_0 j_\varphi \frac{2}{r^2}\int_0^r [j_\varphi(r^*) - j_\varphi(r)]r^*\, dr^* - r n_e\Big(\frac{p_t'}{r n_e}\Big)'\Big\}, \qquad (2.38)$$

where $p_t = k(n_e T_e + n_i T_i)$ is the total plasma pressure and $C_e = (2kT_e/m_e)^{1/2}$. This result for χ_e can be derived from (2.11), and applies in a toroidal magnetoplasma with circular cross-section in which $\omega_{ce} \gg 1$ and $B \simeq B_\varphi$. In order to evaluate χ_e from (2.38) we need profiles for T_e and n_e. The toroidal current density can be estimated from the approximation $j_\varphi = \eta_{||}^{-1} E_\varphi$.

Woods has determined a family of temperature profiles representative of those found in high β_p tokamak discharges. These profiles are characterised by a single

[2]We note that equation (19.1) of the reference contains two minor errors. The $\hat{\theta}$ term and the term $O(s)$ in the $\hat{\varphi}$ term are a factor of 1/2 too small.

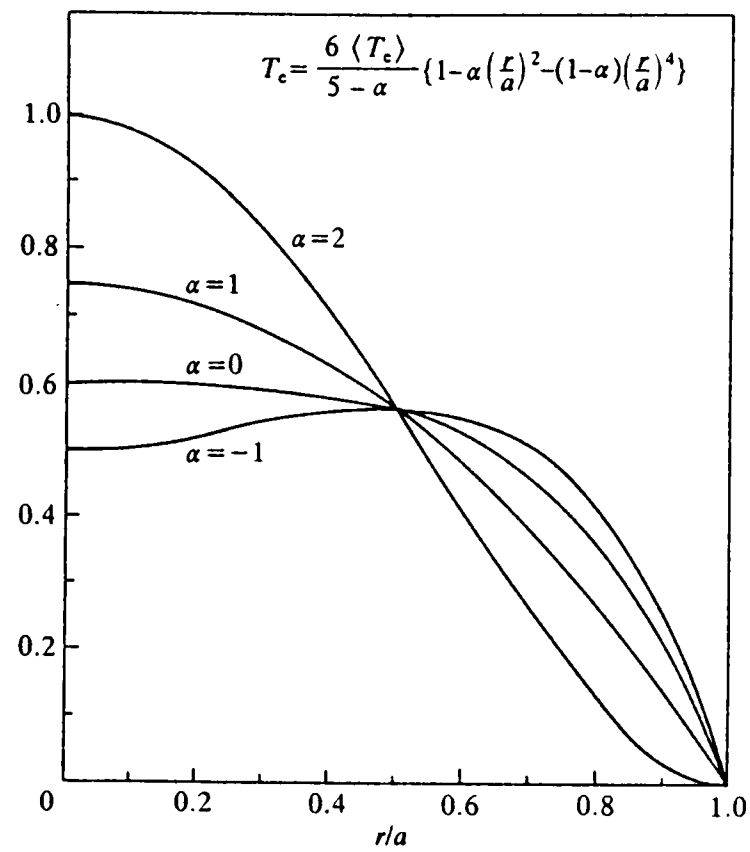

Figure 2.1: The temperature profiles adopted for high β_p discharges (from Woods 1987)

dimensionless parameter α, and are expressed as

$$T_e = \frac{6\langle T_e\rangle}{5-\alpha}\{1-\alpha(r/a)^2-(1-\alpha)(r/a)^4\}, \qquad (-1 \le \alpha \le 2), \tag{2.39}$$

where $\langle\,\rangle$ denotes the volume-weighted average and a is the minor radius of the torus. These profiles have the merit that they all have the same average values; only the shape of the profiles varies from hollow to peaked on the axis as α varies from -1 to 2 (see Figure 2.1).

For simplicity, Woods adopted the parabolic distribution

$$n_e = n_{e0}(1-(r/a)^2) \tag{2.40}$$

for the number density profile.

Employing (2.39), (2.40) and (2.38), Woods has calculated that

$$\langle Q_{er}\rangle = \frac{(2m_e)^{\frac{1}{2}}}{\mu_0 e^2}\frac{\langle kT_e\rangle^{\frac{1}{2}}}{R^2 q_a}\{\phi_1(\alpha)+\beta_p\phi_2(\alpha)\}, \qquad (-1 \le \alpha \le 2), \tag{2.41}$$

where $q_a = q(a)$, and the functions $\phi_1(\alpha)$ and $\phi_2(\alpha)$ are specified in Table 2.1. We shall use equation (2.41) for $\langle Q_{er}\rangle$ to make a comparison between Woods' theory

	α						
	-1.0	-0.5	0	0.5	1.0	1.5	2.0
ϕ_1	1.04	1.11	1.18	1.28	1.41	1.63	2.04
ϕ_2	4.40	3.50	2.48	1.31	0	-1.40	-2.80

Table 2.1: The functions ϕ_1 and ϕ_2

and an empirical scaling law for the electron thermal conductivity determined by Haas and Thyagaraja (1986).

2.3.2 The Empirical Scaling Law

In a recent paper Haas and Thyagaraja (1986) have reported a phenomenological interpretation of transport limits and slow-time evolution in tokamaks. One of their conclusions is that the electron thermal diffusivity appears to be an increasing function of the poloidal beta. This observation is made for those discharges with strong auxiliary heating and possibly with ohmic heating at higher values of β_p. Haas and Thyagaraja were able to produce results in agreement with observations from ISX-B and ASDEX discharges by assuming an electron thermal conductivity of the form

$$\kappa_{\perp e} = K(1 + A\beta_p), \tag{2.42}$$

where A and K are constants.

It is apparent from this investigation that a separate β_p-term is required in the expression for χ_e to give agreement with the experimental results analysed by Haas and Thyagaraja.

2.3.3 A Comparison with Experiment

A direct comparison between Woods' expression for χ_e, (2.38) and the empirical law for $\kappa_{\perp e}$ given by (2.42) is not possible. This is because in determining the constants A and K, Haas and Thyagaraja assume that the product $n_e\chi_e$ is constant across the minor radius, whereas the expression given by Woods for χ_e is more general, and varies according to the radial location. We can avoid this difficulty by comparing the $\chi_{\perp e}$ found by Haas and Thyagaraja with the

volume-weighted average heat flux rather than the thermal diffusivity.

To see why this is so, we introduce a new variable χ_e^*. Let χ_e^* have the properties that $n_e\chi_e^*$ is constant across the minor radius, and χ_e^* yields the same volume-weighted average heat flux as χ_e. Since $Q_{er} = \frac{3}{2}kn_e\chi_e T_e'$, χ_e^* must satisfy

$$-\frac{3}{2}kn_e\chi_e^*\frac{2}{a^2}\int_0^a T_e' r\,dr = \langle Q_{er}\rangle = -\frac{3}{2}k\frac{2}{a^2}\int_0^a n_e\chi_e T_e' r\,dr. \qquad (2.43)$$

An examination of (2.43) shows that if we are going to assume that the product $n_e\chi_e^*$ is constant across the minor radius, as Haas and Thyagaraja have done, then any scaling laws deduced for this product should be compared with scaling laws for $\langle Q_{er}\rangle$, not $n_e\chi_e$ directly.

When fitting their calculations to results from ISX-B and ASDEX discharges, Haas and Thyagaraja assumed

$$\kappa_\perp = 5\times 10^{17}\left(1 + B_i\frac{8\pi n_0 T_0}{B_\theta^2(a)}\right), \qquad B_i \text{ constant}, i = 1,2, \qquad (2.44)$$

and

$$n_e\chi_e = 3\times 10^{17}\left(\frac{T(r,t)}{T(0,t)}\right)^{-1/2}\left\{1 + 1.5\frac{8\pi n_0 T_0}{B_\theta^2(a)}\right\}, \qquad (2.45)$$

where B_i has the values $B_1 = 4$ and $B_2 = 1$. If we adopt parabolic number density and temperature profiles, and Haas and Thyagarajas' definition of β_p, equations (2.44) and (2.45) may be rewritten as

$$\kappa_\perp = 5\times 10^{17}(1 + A_i^{HT}\beta_p), \qquad A_i^{HT} = \text{constant}, \; i = 1,2, \qquad (2.46)$$

and

$$n_e\chi_e = 3\times 10^{17}\left(\frac{T(r,t)}{T(0,t)}\right)^{-1/2}\{1 + A_3^{HT}\beta_p\}, \qquad A_3^{HT} = \text{constant}, \qquad (2.47)$$

where the constants A_i^{HT}, $i = 1,2$ have the values $A_1 = 12$, $A_2 = 3$ and $A_3 = 4.5$.

The β_p factor predicted by Woods which corresponds to the empirical constants A_i^{HT} is $A^W \equiv \phi_2(\alpha)/\phi_1(\alpha)$ (cf. equation (2.41)). We can estimate A^W by noting the range of α over which equation (2.41) is valid and the values of ϕ_1 and ϕ_2 listed in Table 2.1. For L-mode discharges, (we use the term here as defined

by Woods) α is restricted to the range $-1 \leq \alpha \leq 1$ (Woods 1987 p.455). From Table 2.1 we see that

$$0 \leq A^W \leq 4.2, \qquad (-1 \leq \alpha \leq 1), \tag{2.48}$$

where the largest value of A^W corresponds to the most hollow temperature profile (α small).

We note that α has been observed to be as high as 2 in L-mode discharges (Robinson, private communication). In this case ϕ_2 is negative and Woods' theory predicts that $\langle Q_{er} \rangle$ should decrease with increasing β_p, contrary to the observations of Haas and Thyagaraja.

Comparing A_i^{TH} and A^W we see that there is fair agreement between Woods' predicted β_p-dependence of χ_e and the phenomenological relations found by Haas and Thyagaraja. The agreement is satisfactory considering the difficulty of determining exact coefficients from experimental data. The essential point is that Woods' prediction of a two-term expression for χ_e involving a β_p term has some experimental support.

2.3.4 Contrast Between Second-Order Transport Theory and Neoclassical Theory

The term "neoclassical" is applied to toroidal transport in two distinct senses. First when collisions are sufficiently rare for particles to execute banana orbits, the transport is non-local in character, and the toroidal geometry enters into the transport coefficients via the safety factor q and the ratio r/R. The other sense in which the term is used is for the collision-dominated situation described by the Pfirsch-Schlüter equations. Although the transport is determined locally, i.e. the usual expressions for resistivity and viscosity in collision-dominated plasmas apply, when the local equations are averaged over the poloidal variable, this has the effect of modifying the transport coefficients, and bringing in the geometrical elements q and r/R. Here our concern is with the first sense in which tokamak transport is termed "neoclassical". It is an approximation based on the expan-

sion parameter η defined in (1.120). On the other hand the classical theory of transport in a magnetoplasma, or at least that version described by Chapman and Cowlings' text (1970), is based on the Knudson number ϵ, which means that it applies only to collision-dominated situations.

The first approximation in neoclassical theory yields a kinetic equation for the gyro-averaged distribution function $\tilde{f}$, known as the drift kinetic equation. In turn this equation leads to the usual transport relations, as explained in the standard review of Hinton and Hazeltine (1976) and of Galeev and Sagdeev (1979). In the first approximation, the gyro-averaging removes any transport occurring as a result of Larmor orbits. For example the components

$$q_\wedge = \frac{\kappa\tilde{\omega}}{1+\tilde{\omega}^2}\boldsymbol{b}\times\nabla T, \qquad q_\perp = -\frac{\kappa}{1+\tilde{\omega}^2}(\mathbf{1}-\boldsymbol{bb})\cdot\nabla T, \tag{2.49}$$

appearing in (2.8), are not obtained in this approximation, although they do arise in first-order classical theory.

Second-order classical theory has been developed for neutral gases (e.g. see Chapman and Cowling 1970, chapter 515). This theory is based on the Boltzmann collision integral, and as the Fokker-Planck collision operator can be deduced from the collision integral, provided that magnetic fields can be neglected, a second-order theory for the Fokker-Planck equation could in principle be developed.

Magnetic fields complicate the situation somewhat. A second-order theory for the Fokker-Planck equation, in the presence of a strong field, would not lead to the terms given by Woods. He believes that the kinetic equation itself is in error, if pressed to second-order. As he explains in section 4.11 of his text, the kinetic equation can be viewed as being a Taylor expansion taken over distances of a mean free path. But when the particles are gyrating in small orbits about the magnetic field, such an expansion is not valid. It is necessary to take changes along paths lying *parallel* to the guiding centre motion to obtain a valid expansion, so in this respect Woods' second-order theory has something in common with neoclassical first-order theory. In any case it gives rise to a non-

standard kinetic equation, and hence to results unobtainable from any present form of neoclassical theory.

The precise relation between neoclassical theory and Woods' second-order theory, and whether or not the one could be extended to include the other, are questions that cannot be answered at present. Research on this topic is presently being undertaken at Oxford.

Chapter 3

Second-Order Transport in RFPs

The RFP belongs, like the tokamak, to the class of fusion machines known as Z pinches. Investigation of the pinch effect dates back to Bennett (1934) and toroidal pinch machines have been studied since the late nineteen forties. One of the most famous of these early pinch machines was the RFP ZETA at Harwell, England. It was not until the early nineteen sixties that the tokamak approach of a large externally imposed toroidal magnetic field was developed in the USSR. During the late nineteen sixties tokamaks demonstrated better confinement and stability properties than machines operated as RFP's. The temperature and confinement times of the T3 tokamak in 1968 were $\sim$ 1keV and 10ms respectively, which were good compared with the corresponding ZETA values of $\sim$ 150eV and a few milli-seconds (Bodin, 1980). Because of the difference in performance between the two approaches, the tokamak programme was pursued actively during the nineteen seventies and eighties while only a few RFP's were built in this period.

Four of the largest RFP's in operation now are HBTX ($a = 0.25$m, $R_0 = 0.8$m) at Culham, England, Repute-1 ($a = 0.2$m, $R_0 = 0.82$m) at the University of Tokyo, Japan, ZT-40 ($a = 0.114$m, $R_0 = 0.2$m) at Los Alamos, USA and ETA-BETA-II ($a = 0.125$m, $R_0 = 0.65$m) at Padova, Italy.

At the present time there are no texts dealing solely with the RFP. However, Bodin and Newton (1980) have written a comprehensive review paper on the physics of the RFP.

For the most part in this chapter we will adopt a case study approach using HBTX as a typical machine. The most compelling reason for doing this is the lack of a data set drawn from a number of machines.

3.1 A Description of the RFP

The main difference between the tokamak and the RFP lies in their magnetic field structures. The tokamak has a strong toroidal field component arising mainly from field coils external to the plasma. In the RFP the poloidal and toroidal field components are of similar magnitude and both components have significant contributions arising from currents flowing in the plasma discharge. The poloidal field never changes sign, but the toroidal field decreases monotonically from a maximum on the minor axis to a negative value at the limiter. It is this characteristic reversal of B_φ at the plasma edge which led to the name 'Reverse Field Pinch'.

3.1.1 The RFP Magnetic Field Structure

Unless helical field windings are used, the poloidal field in the RFP is determined solely by the toroidal current flowing in the plasma. Assuming that there is no radial field, equation (1.17) yields for the poloidal field

$$B_\theta(r) = \frac{\mu_0}{r}\int_0^r j_\varphi\, r^*\, dr^*. \tag{3.1}$$

The toroidal field is the result of contributions from poloidal plasma currents, poloidal currents in the conducting shell enclosing the plasma, and currents in the external field windings. Let the toroidal field at the limiter be $B_{\varphi a}$, then from Ampère's law

$$B_{\varphi a} = B_e + \frac{\mu_0 I_s}{2\pi R_0}, \tag{3.2}$$

where I_s is the poloidal current flowing in the shell, B_e is the field due to the external field windings, and we have neglected toroidal effects. It follows from (1.17) that

$$B_\varphi(r) = B_e + \frac{\mu_0 I_s}{2\pi R_0} + \mu_0\int_r^a j_\theta\, dr^*. \tag{3.3}$$

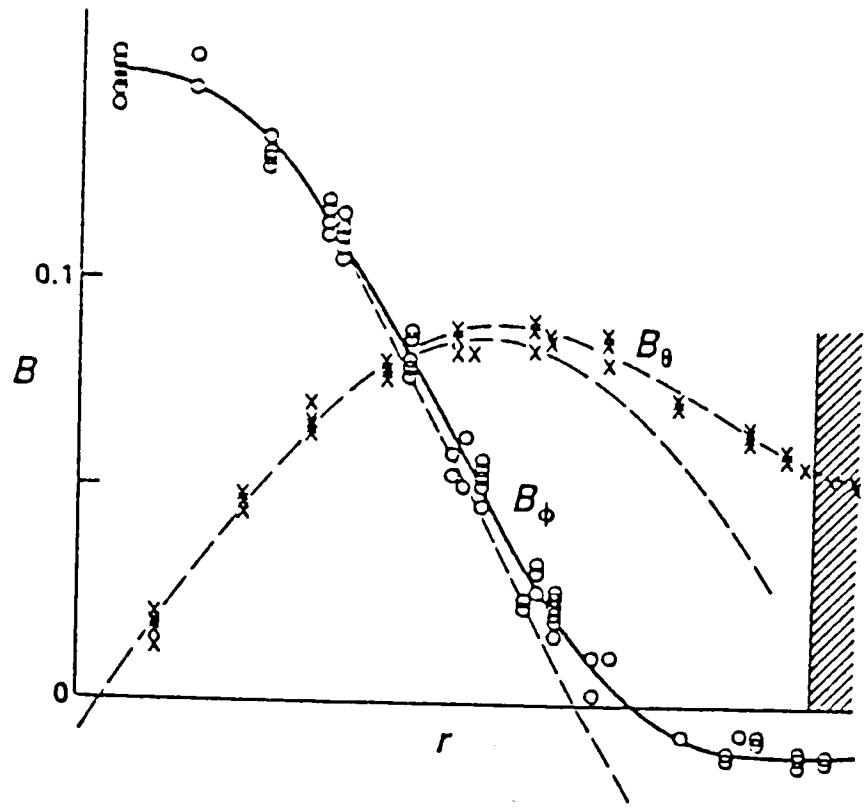

Figure 3.1: Experimental and Bessel Function Model magnetic field profiles for HBTX (from Bodin 1984)

If we now make the assumption that the shell is flux conserving, we must have that

$$\frac{\mu_0 I_s}{2\pi R_0}\frac{a^2}{2} = -\mu_0 \int_0^a \int_r^a j_\theta \, dr^* \, r dr, \tag{3.4}$$

or

$$B_\varphi(r) = B_e - \frac{\mu_0 a^2}{2} \int_0^a \int_r^a j_\theta dr^* \, r \, dr + \mu_0 \int_r^a j_\theta \, dr^*. \tag{3.5}$$

Since we may choose both B_e and j_θ to be positive, it is clear from (3.5) that a necessary condition for field reversal is that the field contribution due to currents flowing in the shell exceed B_e in magnitude and be of the opposite sign. The constant flux surface where $B_\varphi = 0$ is known as the reversal surface and is located in the outer region of the discharge. Typical magnetic field profiles are shown in Figure 3.1. The fields are characterised by the pinch ratio θ and field reversal index F defined by

$$\theta \equiv \frac{B_\theta(a)}{\langle B_\varphi \rangle}, \tag{3.6}$$

$$F \equiv \frac{B_\varphi(a)}{\langle B_\varphi \rangle}, \tag{3.7}$$

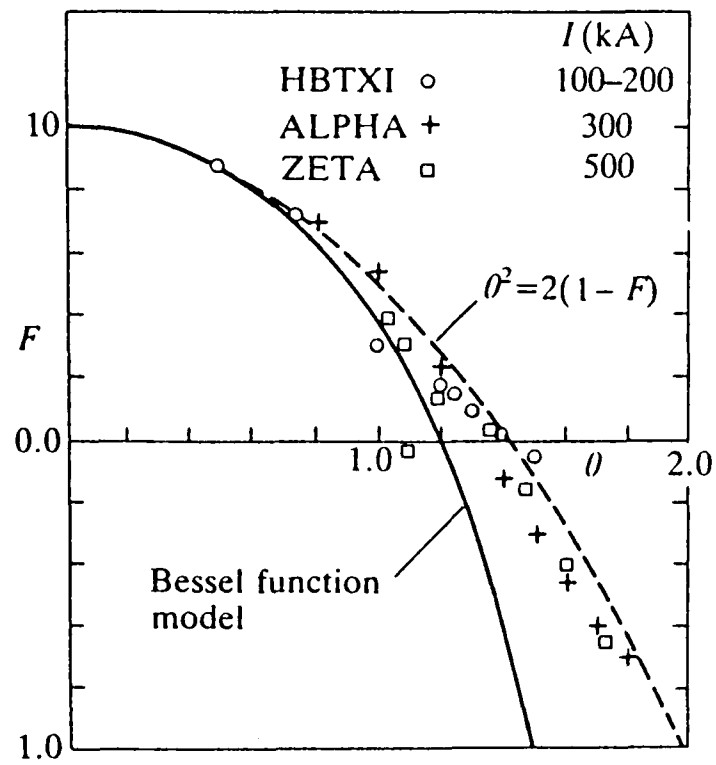

Figure 3.2: The F, θ diagram with points from three experiments (from Bodin 1980)

where

$$\langle B_\varphi \rangle \equiv \frac{2}{a^2} \int_0^a B_\varphi r \, dr, \tag{3.8}$$

is the volume-weighted average value of B_φ. An examination of (3.1) shows that $B_\theta(a) = \mu_0 I_\varphi / 2\pi a$ where I_φ is the total current flowing in the toroidal direction. Hence (3.6) can be rewritten as

$$\theta = \frac{\mu_0 I_\varphi}{2\pi a \langle B_\varphi \rangle}. \tag{3.9}$$

A number of experimental observations have shown that F and θ are quite well represented by the relation

$$\theta^2 = 2(1 - F). \tag{3.10}$$

Woods (1987) has deduced (3.10) from arguments related to magnetic field and plasma pressure equilibrium, but the close fit of this curve to points from experiment is sufficient justification for its use. The curve defined by (3.10) and points from three experiments are plotted in Figure 3.2.

3.1.2 The Time Evolution and Characteristics of an RFP Discharge

The evolution of an RFP discharge occurs in two phases. The initial phase is a rapid re-organization of the plasma known as 'relaxation'. If the toroidal current is sufficiently large, then by (3.10) the relaxation process leaves the toroidal field reversed at the limiter. The time-scale for relaxation to occur, τ_r, depends on how the discharge is initiated. In 'fast' experiments, I_φ is switched on quickly, θ varies rapidly and F attains its equilibrium value according to (3.10) in a time of the order of micro-seconds. In HBTX the relaxation time for fast experiments is $\tau_r \approx 6\mu s$. In 'slow' experiments the plasma follows the F-θ curve as I_φ is increased slowly compared with the time-scales of fast experiments. The discharge initiation is accompanied by a rapid expulsion of plasma known as 'pumpout'.

Once relaxation has occurred, the discharge enters a sustainment phase and it has been hypothesized (Bodin, 1980) that the field configuration can be maintained for as long as the toriodal current is driven. It is certainly observed that the propensity of the field to decay by resistive diffusion is balanced by some mechanism that drives the poloidal current and sustains the field structure. This mechanism is referred to as a 'dynamo'. The dynamo operates only for as long as the toroidal current is driven, so the duration of an RFP discharge varies according to the current drive capabilities of the particular machine concerned. However, RFP discharge times in general are of the order of milli-seconds, the longest pulse time published to date being 35ms (Wurden, *et al.* 1987).

RFP discharges are characterised by high energy and particle losses throughout the sustainment phase in addition to the plasma losses involved during the initial relaxation. These losses are typically an order of magnitude larger than those found in tokamaks of comparable dimensions. In an experiment reported by Robinson and Todd the CLEO device ($R = 0.9$m, $a = 0.14$m) was operated in a number of configurations including both as an RFP and a tokamak. In this experiment the tokamak energy confinement time was some 20 times greater

than that for the RFP.

3.1.3 Relaxation, Dynamos and Anomalous Transport

The three main problems of RFP research are these. (1) What mechanism causes the rapid plasma reorganization to the equilibrium state defined by (3.10)? (2) How are poloidal currents driven at the reversal surface, r_s, where $B_\varphi = 0$? (The simplest form of Ohm's law,

$$j = \sigma \cdot (E + v_e \times B + \frac{1}{en_e}\nabla p_e), \tag{3.11}$$

yields $j_\theta(r_s) = 0$ for a cylindrically symmetric system). (3) What is the transport mechanism that yields loss rates orders of magnitude larger than those predicted by neo-classical theory?

The aim of the following sections is to present and discuss the theories underlying these questions that are widely accepted by the plasma physics community.

Plasma Relaxation

Applying concepts originally developed by Woltjer (1958) in an astrophysical context to laboratory plasmas, Taylor (1974) has developed a model of 'plasma relaxation' suitable for RFPs. Woltjer demonstrated that in a closed system free of dissipation, a magnetic field of the form

$$\nabla \times B = \alpha B \qquad (\alpha = \text{constant}) \tag{3.12}$$

has the lowest possible state of magnetic energy. Taylor has applied this principle with the addition of dissipation to the RFP to deduce (3.12) subject to the constraint that the total magnetic helicity of the system is conserved.

The helicity, K, of a magnetic field is defined as follows. Let A be the magnetic vector potential so that $B = \nabla \times A$. Then the magnetic helicity K_0 in a volume V_0 is defined by

$$K_0 \equiv \int_{V_0} A \cdot \nabla \times A \, d\tau, \tag{3.13}$$

where $d\tau$ is a volume element of V_0. Some care is needed in defining K_0 in the multiply connected region of a torus (Taylor, 1986).

A priori, Taylor's conjecture that only the total helicity of the torus is conserved seems difficult to justify. However, were this not done, the final state of the discharge would depend on an infinity of conditions defined by the initial state of the plasma; which is a constraint contrary to observation. To avoid this situation, a relaxation mechanism is postulated that redistributes helicity between flux tubes but conserves helicity within the plasma shell on the relaxation time-scale. This hypothesis may be investigated by computing $\partial K_0/\partial t$ as follows. We note that

$$\begin{aligned}
\frac{\partial K_0}{\partial t} &= \frac{\partial}{\partial t}\int_{V_0} \boldsymbol{A}\cdot\nabla\times\boldsymbol{A}\,d\tau \\
&= \int_{V_0}\left[\frac{\partial \boldsymbol{A}}{\partial t}\cdot\nabla\times\boldsymbol{A}+\boldsymbol{A}\cdot\nabla\times\frac{\partial \boldsymbol{A}}{\partial t}\right]d\tau \\
&= \int_{V_0}\left[2\frac{\partial \boldsymbol{A}}{\partial t}\cdot\nabla\times\boldsymbol{A}-\nabla\cdot(\boldsymbol{A}\times\frac{\partial \boldsymbol{A}}{\partial t})\right]d\tau \\
&= 2\int_{V_0}\frac{\partial \boldsymbol{A}}{\partial t}\cdot\nabla\times\boldsymbol{A}\,d\tau-\oint_{\delta V}\boldsymbol{A}\times\frac{\partial \boldsymbol{A}}{\partial t}\cdot\hat{\boldsymbol{n}}\,d\Sigma, \qquad (3.14)
\end{aligned}$$

where $\hat{\boldsymbol{n}}\,d\Sigma$ is a surface element of δV, the boundary of V_0 and we have used the identity $\nabla\cdot(\boldsymbol{A}\times\partial\boldsymbol{A}/\partial t)=-\boldsymbol{A}\cdot\nabla\times\partial\boldsymbol{A}/\partial t+(\partial\boldsymbol{A}/\partial t)\cdot\nabla\times\boldsymbol{A}$. If we now substitute $\nabla\times\boldsymbol{E}=-\partial\boldsymbol{B}/\partial t=-\nabla\times\partial\boldsymbol{A}/\partial t$ into (3.14) we obtain

$$\frac{\partial K_0}{\partial t}=-2\int_{V_0}\boldsymbol{E}\cdot\boldsymbol{B}\,d\tau+\oint_{\delta V}\boldsymbol{A}\times\boldsymbol{E}\cdot\hat{\boldsymbol{n}}\,d\Sigma. \qquad (3.15)$$

Since $\boldsymbol{E}\times\hat{\boldsymbol{n}}$ must be continuous through the boundary and $\boldsymbol{E}\times\hat{\boldsymbol{n}}=0$ on δV, assuming this to be a perfect conductor on relaxation time-scales, the surface term $\oint_{\delta V}\boldsymbol{A}\times\boldsymbol{E}\cdot\hat{\boldsymbol{n}}\,d\Sigma$ in (3.15) vanishes. Thus $\partial K_0/\partial t$ can be expressed as

$$\frac{\partial K_0}{\partial t}=-2\int_{V_0}\boldsymbol{E}\cdot\boldsymbol{B}\,d\tau. \qquad (3.16)$$

A more careful derivation of $\partial K/\partial t$ which allows for the presence of a tangential electric field at the plasma boundary has been made by Bevir and Gimblett (1985), following work done by Bevie and Gray (1981). The result is

$$\frac{\partial K_u}{\partial t}=2\psi_\varphi V_\varphi-2\int_V\boldsymbol{E}\cdot\boldsymbol{B}\,d\tau, \qquad (3.17)$$

where $K_u \equiv \int_V \boldsymbol{A}\cdot\boldsymbol{B}\,d\tau - \psi_\varphi\psi_\theta$ is a helicity independent of the value of $\boldsymbol{A}$ outside the torus, ψ_φ and ψ_θ are the toroidal and poloidal fluxes respectively and V_φ is the toroidal loop voltage.

If we now substitute for $\boldsymbol{E}$ in (3.16) using Ohm's law, we obtain

$$\begin{aligned}\frac{\partial K_0}{\partial t} &= -2\int_{V_0}(\boldsymbol{\eta}\cdot\boldsymbol{j} - \frac{1}{en_e}\nabla\cdot\boldsymbol{p}_e)\cdot\boldsymbol{B}\,d\tau \\ &= -2\int_{V_0}\eta\boldsymbol{j}\cdot\boldsymbol{B}\,d\tau, \end{aligned} \tag{3.18}$$

neglecting electron viscosity and the plasma fluid velocity, and assuming $B_r = 0$, $\nabla p_e = \hat{r}\,\partial p_e/\partial r$, and $\boldsymbol{\eta} = \eta\mathbf{1}$.

The magnetic energy in the volume V_0 is given by

$$W_m = \int_{V_0}\frac{\boldsymbol{B}\cdot\boldsymbol{B}}{2\mu_0}\,d\tau. \tag{3.19}$$

Thus an expression for change in the magnetic energy, W_m, is

$$\begin{aligned}\frac{\partial W_m}{\partial t} &= \frac{1}{\mu_0}\int_{V_0}\boldsymbol{B}\cdot\frac{\partial\boldsymbol{B}}{\partial t}\,d\tau \\ &= -\frac{1}{\mu_0}\int_{V_0}\boldsymbol{B}\cdot\nabla\times\boldsymbol{E}\,d\tau \\ &= -\frac{1}{\mu_0}\int_{V_0}\Big[\nabla\cdot(\boldsymbol{B}\times\boldsymbol{E}) - \boldsymbol{E}\cdot\nabla\times\boldsymbol{B}\Big]\,d\tau \\ &= -\int_{V_0}\boldsymbol{E}\cdot\boldsymbol{j}\,d\tau. \end{aligned} \tag{3.20}$$

For the same reason as given above, we have set the term $\int_{V_0}\nabla\cdot(\boldsymbol{B}\times\boldsymbol{E})\,d\tau = \int_{\partial V_0}\boldsymbol{B}\times\boldsymbol{E}\cdot\hat{\boldsymbol{n}}\,d\Sigma = 0$. As before, we can eliminate $\boldsymbol{E}$ using Ohm's law to obtain

$$\begin{aligned}\frac{\partial W_m}{\partial t} &= -\int_{V_0}(\boldsymbol{\eta}\cdot\boldsymbol{j} - \frac{1}{en_e}\nabla\cdot\boldsymbol{p}_e)\cdot\boldsymbol{j}\,d\tau \\ &= -\int_{V_0}\eta j^2\,d\tau, \end{aligned} \tag{3.21}$$

provided the assumptions made in deriving (3.18) are valid.

As with $\partial K_u/\partial t$, Bevir and Gimblett (1985) have made a more general analysis of $\partial W_m/\partial t$ and obtained the result

$$\frac{\partial W_m}{\partial t} = I_\varphi V_\varphi - I_\theta V_\theta - \int_V \boldsymbol{E}\cdot\boldsymbol{j}\,d\tau, \tag{3.22}$$

where I_φ and I_θ are the total toroidal and poloidal currents respectively.

According to (3.18) and (3.21) (i.e. in the absence of the current and voltage driving terms of (3.17) and (3.22)) both magnetic energy and helicity decay on resistive time-scales. It appears then, that the initial hypothesis of helicity conservation on relaxation time-scales, i.e. the time-scale on which W_m changes, is invalid. However, Taylor recovers the situation by an appeal to small-scale fluctuations.

From (3.16) and (3.20) we see that changes in helicity are essentially determined by $\boldsymbol{E} \cdot \boldsymbol{B}$ while changes in magnetic energy are determined by $\boldsymbol{E} \cdot \boldsymbol{j}$. If we assume that $\boldsymbol{E}$ and $\boldsymbol{j}$ are primarily determined by fluctuations in the magnetic field having a scale length k (Taylor 1986) then

$$\frac{\partial K}{\partial t} \approx -2\eta \Sigma k B_k^2, \tag{3.23}$$

and

$$\frac{\partial W}{\partial t} \approx -\eta \Sigma k^2 B_k^2. \tag{3.24}$$

For scale lengths $k \sim \eta^{-1/2}$, energy dissipation occurs on time-scales of the order $\eta^{-1/2}$ faster than helicity dissipation.

There have been various refinements made to Taylor's theory. Reiman (1981) has extended the analysis to a toroidal plasma of arbitrary aspect ratio and cross-section, and included the energy contribution of wall currents neglected by Taylor. Turner and Christiansen (1981) have included the effects of finite plasma pressure, and there has been some discussion on the choice of conserving only the total helicity (see Taylor's 1986 review).

There are two points of a general nature that can be made concerning this theory. The first is that while the theory is not concerned with the specifics of the relaxation process, the length-scale argument given by Taylor does suggest that the process is driven by small scale turbulence. Computer simulations of the turbulent relaxation process (e.g. Aydemir *et al.* 1985, Aydemir and Barnes 1984) have been able to demonstrate the mechanism and the relaxation time-scale to lower energy states for various models.

The second point is somewhat more philosophical and concerns the origin of equation (3.12) for $\boldsymbol{B}$.

Taylor has deduced (3.12), which is

$$\nabla \times \boldsymbol{B} = \alpha \boldsymbol{B} \qquad (\alpha = \text{constant}), \tag{3.25}$$

from an energy minimization principle. Supposing this principle to be correct, we expect the physical system described by (3.12) to be always in the state corresponding to the lowest energy solution of this equation. In the case of the RFP this has the consequence that for $0 \leq \theta \leq 1.6$ the magnetic field configuration is expected to be axisymmetric, but for $\theta > 1.6$ the field should be observed to distort helically (Taylor 1986). The experimental evidence for the support of this conclusion in the RFP is not definitive. For example, the helically distorted state has been observed in HBTX (Bodin 1984) but not in CLEO (Robinson and Todd). There is clearer experimental evidence for (3.12) in the Multipinch (La Hayne *et al.* 1986)

Equation (3.12) models the magnetic field state in RFPs quite well after the plasma has undergone relaxation, at least in the inner part of the discharge.

Relaxation Mechanisms

It is generally accepted that plasma instabilities in some form drive plasma relaxation. There are two problems in explaining the process of spontaneous self-reversal. These are that the mechanism must operate on a sufficiently short time-scale, and that it must drive plasma currents not found in the accepted form of Ohm's law.

In his 1980 review Bodin cites two main mechanisms for reversal. The first of these is an $m = 1$ helical kink instability. This instability can redistribute the plasma magnetic field to generate the poloidal flux observed, but it does not leave the plasma in an axisymmetric state which is contrary to observation, for at least $\theta \leq 1.6$. The helical kink also belongs to the class of ideal instabilities, and does not involve the dissipation of energy. Some dissipative mechanism is

required to reduce the magnetic energy of the plasma on the relaxation time-scale, and thus the kink instability cannot explain relaxation on its own but must be accompanied by dissipative turbulence.

Dissipative turbulence is the second relaxation mechanism cited by Bodin, and is also supposed to be associated with the dynamo effect.

Dynamo Mechanisms

The concept of flux regeneration and the observation of magnetic fields persisting for many times the resistive diffusion time is found in geophysical and astrophysical contexts, as well as being observed in laboratory plasmas. A general account of this subject, known as 'dynamo theory', has been given by Moffatt (1978).

There have been a number of dynamo mechanisms postulated for the RFP. The Gimblett-Watkins dynamo (1976) is an adaptation of a model of the geophysical dynamo. The essential element is a modification of Ohm's law to the form

$$\eta j = \boldsymbol{E} + \alpha \boldsymbol{B} - \beta j, \tag{3.26}$$

where the α term arises from vorticity in the plasma motion, and β is a term arising from turbulent plasma motions, corresponding to an enhanced resistivity.

Rusbridge (1977) has also proposed a dynamo mechanism, known as the 'tangled discharge model'. The essential element of this model is that currents flow in flux tubes which wander randomly throughout the discharge. This leads to current densities driven by a global form of Ohm's law. It is thus postulated that poloidal currents at the reversal surface can be driven by electric fields occurring elsewhere in the plasma.

There are other models of the dynamo (e.g. a plasma-dynamo driven by particle transport (Jacobsen 1984) and a kinetic mechanism based on electron momentum transport in stochastic fields (Moses 1984)) but none of the postulated mechanisms have been positively identified by observation.

In a recent paper on toroidal pinches (Robinson 1987) it is stated "The nature of the process involved in generating the field configuration and the associated

plasma losses are not yet well understood, and are clearly critical in determining the confinement properties of the system."

Cross-field Transport Mechanisms.

Anomalous transport is one of the key problems in RFP research. Apart from the theory developed by Woods (1987)—which is classical in nature—the general approach is as follows. An instability is chosen as a candidate for transport enhancement, its growth rate and saturation level are calculated and the effect of the resultant electric and magnetic field fluctuations on transport is assessed.

It is generally agreed that resistive fluid turbulence is the most likely source of anomalous transport (Bodin 1987). Hender and Robinson (1982) and An *et al.* (1986) have studied the effects of particular instabilities on the confinement properties of RFPs. In a more general, but qualitative, approach Connor and Taylor (1984) have considered the effect of resistive fluid turbulence on the invariance properties of the equations of MHD under scale transformations.

An expression for the energy confinement time of RFPs that is often quoted (e.g. Bodin 1987, Ortolani 1987) is,

$$\tau_E = \frac{3}{8}\mu_0 R_0 \beta_p \frac{I_\varphi}{V_L}, \tag{3.27}$$

where V_L is the loop voltage measured outside the torus. This equation can be deduced as follows. Assume that steady-state conditions prevail, so that we may equate the energy replacement time and the energy confinement time, neglecting radiation losses (cf. (1.54)). Then if we suppose the energy replacement time to be

$$\tau_E^* = \frac{W_T}{I_\varphi V_L}, \tag{3.28}$$

where W_T is the total thermal energy in the torus, it follows that

$$\begin{aligned} \tau_E = \tau_E^* &= \frac{W_T}{I_\varphi V_L} \\ &= \frac{2\pi R \pi a^2 \frac{3}{2}\langle p \rangle}{V_L} \\ &= \frac{3}{8}\mu_0 R \beta_p \frac{I_\varphi}{V_L}, \end{aligned} \tag{3.29}$$

since $\beta_p = 2\mu_0\langle p\rangle/B_{\theta a}$ and $B_{\theta a} = \mu_0 I_\varphi/2\pi a$. Here $\langle p\rangle$ is the volume-weighted average pressure and $B_{\theta a}$ is the value of the poloidal field at the limiter. The two points to note here are: (1) that it is actually the energy replacement time which is being calculated; the two times are equal only if steady state conditions prevail, and (2) equation (3.28) needs justification.

At first sight it seems reasonable that the total ohmic energy being dissipated in the plasma is given by $I_\varphi V_L$ but, as we shall show, this is not a good approximation for the RFP.

From (1.63) and neglecting viscosity and the difference between τ_E^* and τ_{Ee}^* we obtain

$$\tau_{Ee}^* = \frac{W_T}{4\pi^2 R_0 P}, \tag{3.30}$$

where

$$P \equiv \int_0^a (\boldsymbol{R}_{ei}\cdot(\boldsymbol{v}_i - \boldsymbol{v}_e) + v_e\nabla p_e)\, r\,dr. \tag{3.31}$$

From (1.36) and neglecting the thermoelectric term

$$\frac{\boldsymbol{R}_{ei}}{en_e} = \eta\cdot j. \tag{3.32}$$

Since $j = en_e(\boldsymbol{v}_i - \boldsymbol{v}_e)$, (3.31) may be rewritten with the help of (3.32) as

$$P = \int_0^a (j\cdot\eta\cdot j + v_e\nabla p_e)\, r\,dr. \tag{3.33}$$

In equation (3.33), P is proportional to the ohmic dissipation per unit length of torus. In order for (3.28) to be justified, we must have that $4\pi^2 R_0 P = I_\varphi V_L$ (cf. (3.30) and (3.28)) or $P = (V_L/2\pi R_0)\int_0^a j_\varphi\, r\,dr$. Assuming that $E_\varphi = V_L/2\pi R_0$, we obtain

$$P = \int_0^a E_\varphi j_\varphi\, r\,dr. \tag{3.34}$$

We can reconcile (3.34) and (3.33) by assuming that

$$j_\varphi E_\varphi = j\cdot\eta\cdot j + v_e\nabla p_e, \tag{3.35}$$

but this is a dubious result. In fact, equation (3.28) for τ_E^* neglects the contribution to ohmic dissipation due to the pressure gradient term and the anisotropic

nature of the resistivity tensor. In the tokamak, where $j_\theta \ll j_\varphi$ and $v_e \nabla p_e \ll j \cdot \eta \cdot j$, this is a reasonable approximation. In the RFP $j_\theta \sim j_\varphi$ and should not be neglected.

3.1.4 Loop Voltage Relationships.

The current understanding in RFP research is that the plasma loop voltage can be expressed in terms of energy and helicity balances. If we take V_L^E to be the 'energy balance' loop voltage and V_L^K to be the 'helicity balance' loop voltage then

$$V_L^E I_\varphi = \int_{V_0} \boldsymbol{E} \cdot \boldsymbol{j} \, d\tau, \tag{3.36}$$

$$V_L^K \Phi_\varphi = \int_{V_0} \boldsymbol{E} \cdot \boldsymbol{B} \, d\tau, \tag{3.37}$$

where

$$\Phi_\varphi = 2\pi \int_0^a B_\varphi r \, dr \tag{3.38}$$

is the toroidal flux and V_0 is the volume of the torus. Provided energy is dissipated at a rate $\int_{V_0} \boldsymbol{E} \cdot \boldsymbol{j} \, d\tau$ and generated at a rate $V_L^E I_\varphi$, equation (3.36) describes the condition for steady-state energy balance. Similarly, if helicity is generated at a rate of $2V_L^K \Phi_\varphi$, (Taylor, 1986) and from (3.18), dissipated at the rate $2\int_{V_0} \boldsymbol{E} \cdot \boldsymbol{B} \, d\tau$, it follows that equation (3.37) is the steady-state helicity balance condition, subject to the constraint that (3.18) is valid.

The validity of (3.18) depends on a surface term of the form $\int_{\partial V} \boldsymbol{A} \times \boldsymbol{E} \cdot \hat{\boldsymbol{n}} \, d\Sigma$ vanishing, where $\boldsymbol{A}$ is the magnetic vector potential (cf. (3.15)). This assumption is certainly justified on time-scales very much less than the magnetic diffusion time of the conducting shell enclosing the plasma. On these time-scales the shell can be considered perfectly conducting and $\boldsymbol{E} \times \hat{\boldsymbol{n}} = 0$. However, equation (3.18) is applied on a time-scale commensurate with the shell-time constant, which is difficult to justify.

Given equation (3.36), it is usual to equate the product $V_L I_\varphi$ with the ohmic dissipation within the plasma, $\int_{V_0} \eta j^2 \, d\tau$. From (1.22) we have that, neglecting

viscosity and the thermoelectric term,

$$\boldsymbol{E}\cdot\boldsymbol{j}=\boldsymbol{j}\cdot\boldsymbol{\eta}\cdot\boldsymbol{j}-\boldsymbol{j}\cdot\Big(\boldsymbol{v}\times\boldsymbol{B}-\frac{\boldsymbol{j}\times\boldsymbol{B}}{en_e}+\frac{\nabla p_e}{en_e}\Big). \tag{3.39}$$

Assuming the equilibrium condition $\boldsymbol{j}\times\boldsymbol{B}=\nabla p$ and noting that by symmetry we may assume $\nabla p=\hat{r}\,\partial p/\partial r$ and $j_r=0$, we may rewrite (3.39) as

$$\boldsymbol{E}\cdot\boldsymbol{j}=\boldsymbol{j}\cdot\boldsymbol{\eta}\cdot\boldsymbol{j}+\boldsymbol{v}\cdot\nabla p. \tag{3.40}$$

Substituting (3.40) into (3.41) we obtain

$$V_L^E I_\varphi=\int_{V_0}[\boldsymbol{j}\cdot\boldsymbol{\eta}\cdot\boldsymbol{j}+\boldsymbol{v}\cdot\nabla p]\,d\tau, \tag{3.41}$$

and it should be noted that the neglect of the anisotropic nature of the resistivity tensor and the pressure gradient term can lead to substantial errors.

In fact it is well known that calculations of both V_L^E and V_L^K do not agree well with the measured loop voltage V_L. Bodin (1987) states that in HBTX typically $V_L\sim 20V$ compared with $V_L^K\sim 10V$, where V_L^K has been evaluated by making the substitution $\boldsymbol{E}=\eta j$ in (3.37) to obtain

$$V_L^K\Phi_\varphi=\int_{V_0}\eta j\cdot\boldsymbol{B}\,d\tau. \tag{3.42}$$

3.2 An Experimental Model for Currents, Number Densities, and Temperatures in the RFP

As seen in the preceeding sections, turbulence plays a major role in most theories dealing with transport, relaxation and flux-regeneration in the RFP. The aim of the following work is to apply Woods' theory, which is classical in nature and successful in explaining a variety of phenomena in tokamaks, to the RFP. Ideally, this application should result in a self-consistent derivation from the two-fluid model equations of the current, number density and temperature profiles found in RFP's. However, an examination of equations (2.30) and (2.36) show that there is little hope of such work proceeding analytically.

Accordingly, our aim here is to demonstrate feasibility. To do this we will develop an empirical model for the radial variation of plasma parameters observed

in the RFP. The substitution of these profiles into the appropriate transport coefficients should be able to account for the observed RFP energy and particle confinement times, granted that Woods' theory is on the correct lines.

3.2.1 Current Density Profiles

A model for the current densities in the RFP frequently adopted is the Bessel function model (BFM). This model comes from a solution of the field equation describing the minimum magnetic energy of the plasma assuming that it is force-free, viz. $\nabla \times \boldsymbol{B} = \alpha \boldsymbol{B}$ (α = constant). The minimum energy solution of this equation in cylindrical geometry is

$$B_\varphi = B_0 J_0(\alpha r), \quad B_\theta = B_0 J_1(\alpha r), \quad B_r = 0; \quad (\alpha \equiv 2\theta/a), \tag{3.43}$$

where θ is the pinch parameter, defined by (3.6). The curve of the F, θ relation predicted by this solution lies somewhat to the left of the empirical curve, a defect attributable to the neglect of plasma pressure and the fact that in RFP discharges α is observed to be a function of the radius. There is a second difficulty with (3.43). From (1.17) a solution of $\nabla \times \boldsymbol{B} = \alpha \boldsymbol{B}$ will have the property that $\mu_0 j = \alpha \boldsymbol{B}$. Observed current and magnetic field profiles, however, have this property in the inner regions of the plasma only. In the outer portion of the plasma j_θ and j_φ decrease, becoming zero at the walls.

Rather than adopt the BFM to calculate current densities, or more elaborate forms of this model, we prefer to use profiles deduced from observation. In the following analysis we will neglect toroidal effects. With $a/R = 1/3$ for HBTX this assumption involves some approximation, but the degree of accuracy obtained by using cylindrical coordinates is sufficient for our purposes here.

Bodin (1984) has published magnetic profiles obtained for HBTX (see Figure 3.1). From these profiles and Ampères's law in differential form it is possible to calculate the poloidal and toroidal current densities. The appropriate equations in cylindrical geometry are

$$j_\theta = -\frac{1}{\mu_0}\frac{\partial B_\varphi}{\partial r}, \quad j_\varphi = \frac{1}{\mu_0}\frac{1}{r}\frac{\partial (r B_\theta)}{\partial r}. \tag{3.44}$$

Experimental Profiles

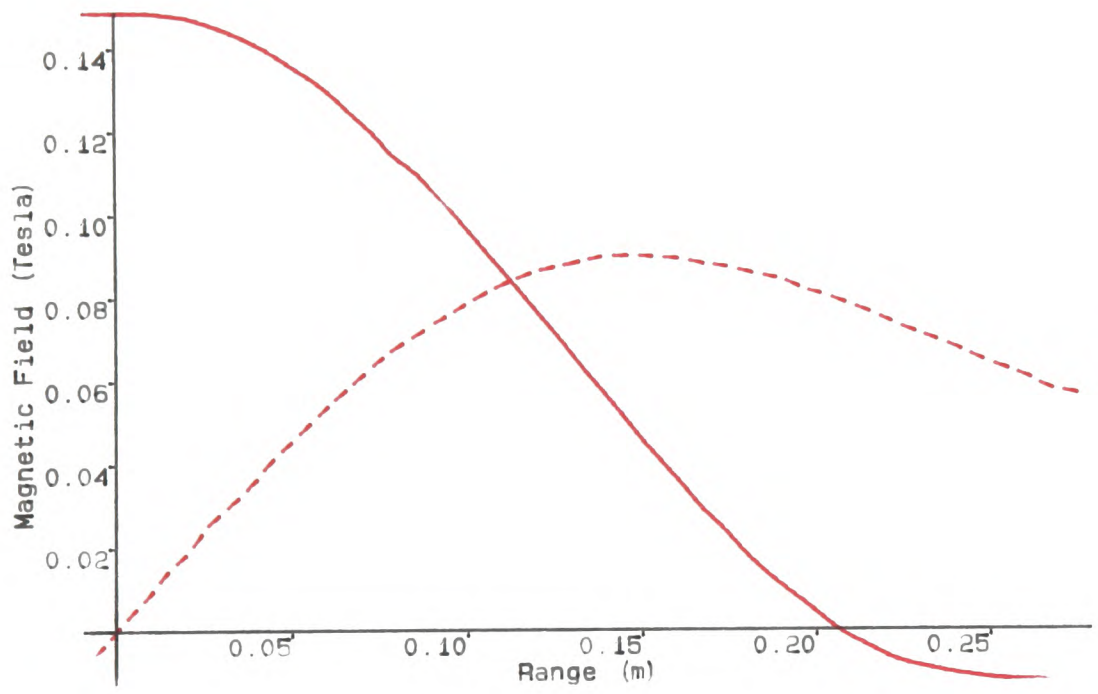

Figure 3.3: Magnetic field profiles

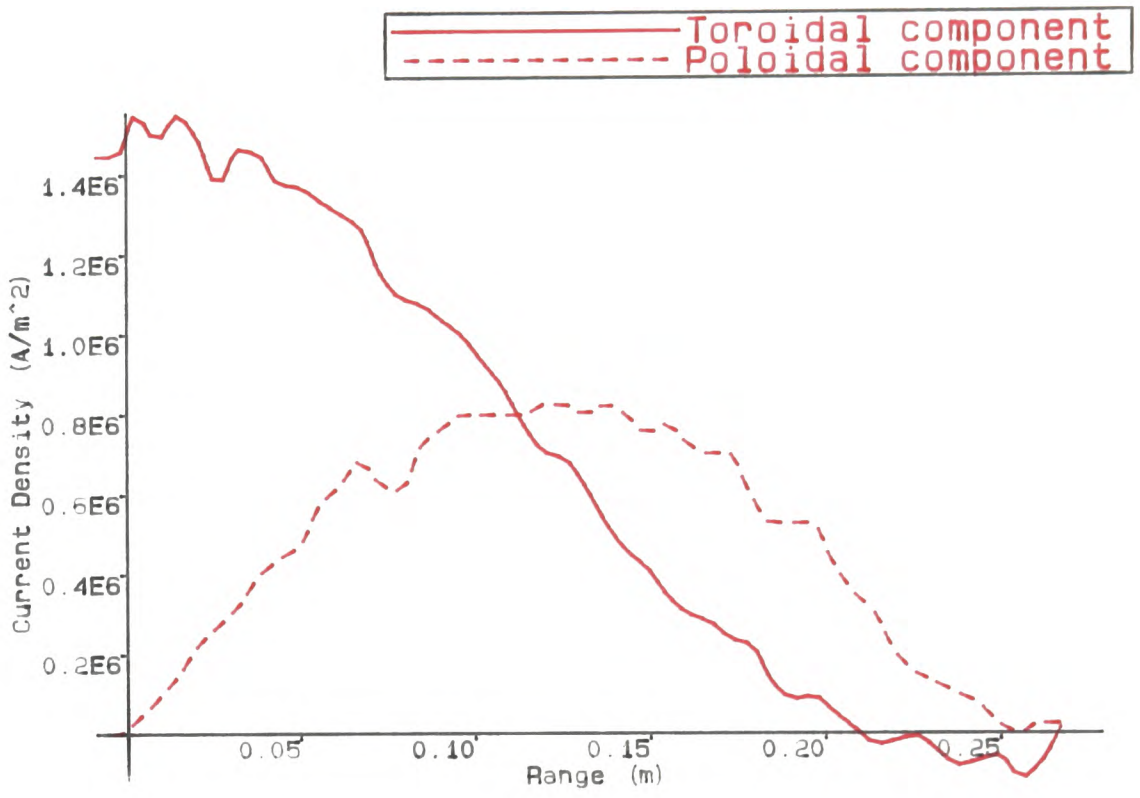

Figure 3.4: Current density profiles

Filtered and Fitted Profiles

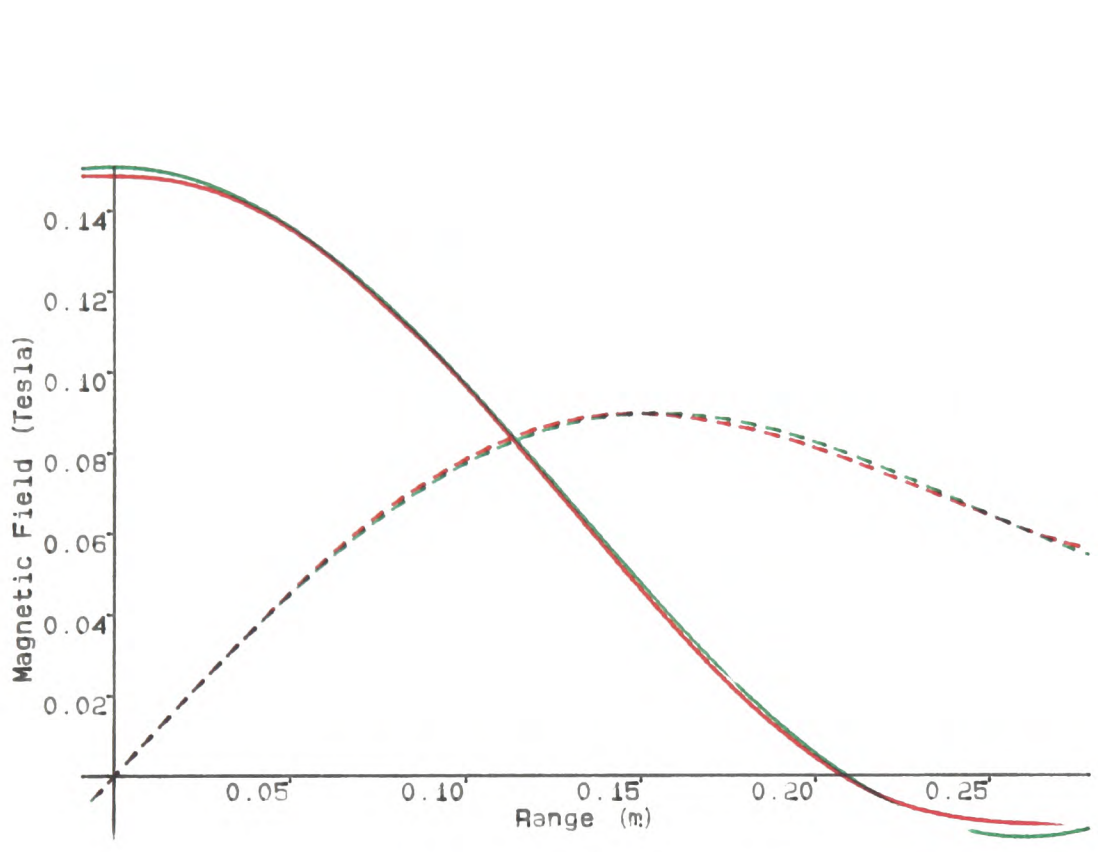

Figure 3.5: Magnetic field profiles

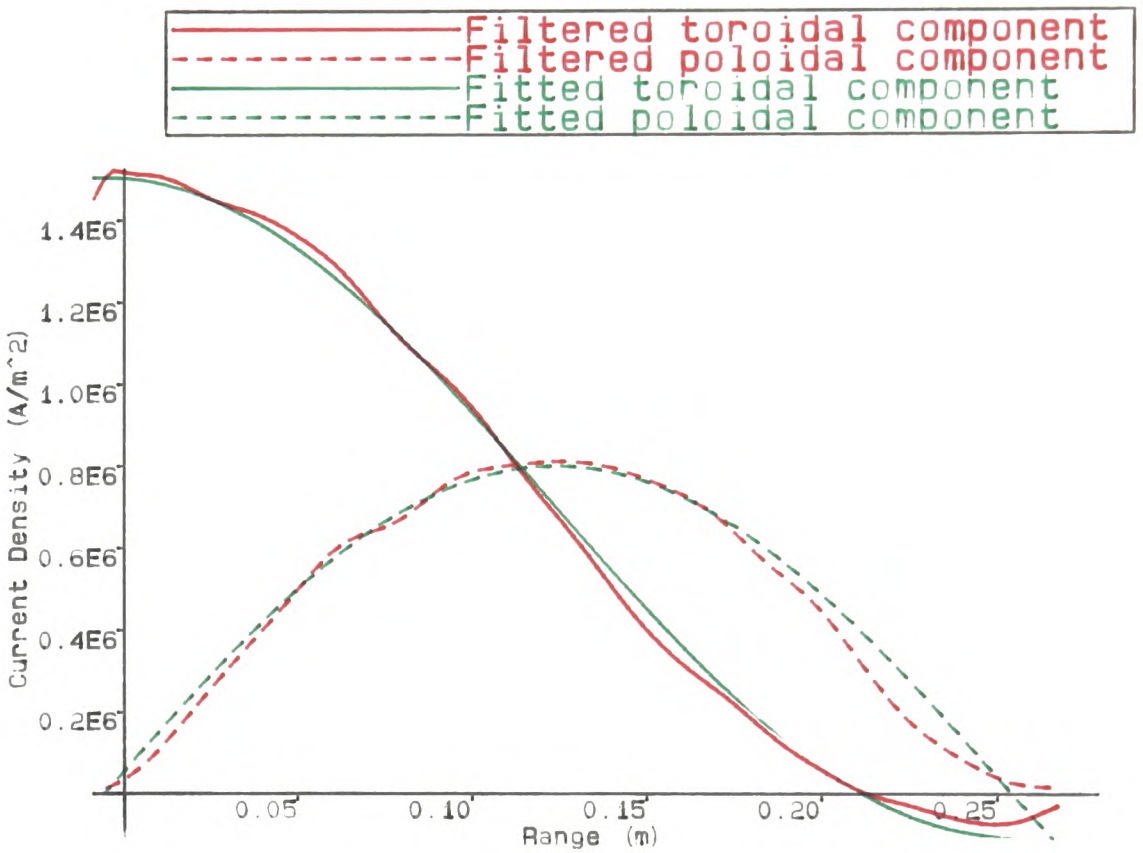

Figure 3.6: Current density profiles

The experimental profiles in Figure 3.1 were measured at 50 points in approximately 5mm increments over the range $0 \leq r \leq 0.26$m; the resulting data is plotted in Figure 3.3. There are carbon tile limiters at $r = 0.25$m and a liner at $r = 0.26$m in HBTX. Since the presence of the limiters restricts the plasma to values of radius less than 0.25m, we have taken the minor radius of the machine to be 0.25m and will not consider points beyond this value. Estimates for the j_θ and j_φ profiles were made using the formulae

$$\mu_0 j_\theta(x_i) = \frac{B_\varphi(x_{i+1}) - B_\varphi(x_{i-1})}{2\Delta x}, \qquad (1 \leq i < N), \tag{3.45}$$

and

$$-\mu_0 j_\varphi(x_i) = \frac{1}{x_i}\frac{x_{i+1}B_\theta(x_{i+1}) - x_{i-1}B_\theta(x_{i-1})}{2\Delta x}, \qquad (1 \leq i < N), \tag{3.46}$$

where $N+1$ is the number of points measured, $x_i = ia/N$ is the radius of the ith point and $\Delta x = a/N$ is the radius increment. The results of this calculation are shown in Figure 3.4.

As estimates of derivatives are sensitive to noise, the experimental profiles in Figure 3.4 have an undesirable random element to them. To remove this, the B_φ and B_θ magnetic field data were filtered by using the formula

$$B(x_i) = \frac{1}{4}B(x_{i+1}) + \frac{1}{2}B(x_i) + \frac{1}{4}B(x_{i-1}), \qquad (1 \leq i < N). \tag{3.47}$$

The magnetic field and current density profiles produced by running the experimental magnetic field profiles through this filter four times are shown in Figures 3.5 and 3.6.

We can see from Figure 3.6 that the experimental current density profiles are reasonably well approximated by

$$j_\theta = J_\theta \sin(\pi r/a), \tag{3.48}$$

$$j_\varphi = J_\varphi\big(\alpha_j + \cos(\pi r/a)\big), \tag{3.49}$$

where J_θ, J_φ and α_j are constants chosen so as to yield agreement with observation.

The current density profiles given by (3.48) and (3.49) with $J_\theta = 8.0 \times 10^5 \mathrm{Am}^{-2}$, $J_\varphi = 8.05 \times 10^5 \mathrm{Am}^{-2}$ and $\alpha_j = 0.87$ are plotted in Figure 3.6.

Given the fitted current density profiles, it is possible to obtain analytic expressions for B_θ and B_φ using equations (3.1) and (3.5). This serves the dual purpose of checking that (3.48) and (3.49) reproduce the observed magnetic field profiles, and of providing expressions for these profiles.

Substituting (3.48) and (3.49) into (3.1) and (3.5) we obtain

$$B_\theta = \frac{a\mu_0}{\pi} J_\varphi \{ \frac{\pi \alpha_j}{2a} r + \sin(\pi r/a) + (\frac{a}{\pi}) \frac{1}{r} [\cos(\pi r/a) - 1] \}, \qquad (3.50)$$

$$B_\varphi = B_e + \frac{a\mu_0 J_\theta}{\pi} \{ (2/\pi)^2 + \cos(\pi r/a) \}. \qquad (3.51)$$

These profiles are plotted in Figures 3.5 for a value of $B_e = 0.034\mathrm{T}$. Since there is good agreement between the fitted and observed fields, the profiles given by equations (3.48) to (3.51) will be adopted as being typical of those found in HBTX.

It is convenient to express J_φ in terms of I_φ, the total toroidal current. From (3.1) and (3.50) we have

$$\begin{aligned} I_\varphi &= \frac{2\pi a B_\theta(a)}{\mu_0} \\ &= \pi a^2 J_\varphi \{ \alpha_j - 4/\pi^2 \}. \end{aligned} \qquad (3.52)$$

The total toriodal current corresponding to $J_\varphi = 8.05 \times 10^5 \mathrm{Am}^{-2}$ and $\alpha_j = 0.87$ is 73kA. Assuming that the approximate relation $\theta^2 = 2(1 - F)$ holds, we can also establish a relationship between J_φ and J_θ. Substituting (3.50) and (3.51) with $r = a$ into (3.10) and noting that by flux conservation $\langle B_\varphi \rangle = B_e$, we obtain

$$J_\theta = \frac{\pi}{8} \frac{\mu_0 a}{B_e} J_\varphi^2 \frac{\{\alpha_j - 4/\pi^2\}^2}{\{1 - 4/\pi^2\}}. \qquad (3.53)$$

For the above values of J_φ and α_j, and $B_e = 0.034\mathrm{T}$, we obtain $J_\theta = 8.5 \times 10^5 \mathrm{Am}^{-2}$ which suggests that the magnetic field profiles shown in Figure 3.3 characterize a plasma discharge which lies close to the F, θ curve defined by equation (3.10).

The above analysis for the current and magnetic field profiles neglects toroidal effects. As we noted earlier, this is an approximation made to simplify a leading order calculation.

The values of J_θ, J_φ and B_e corresponding to the curves in Figures 3.4 and 3.5 were deduced from the magnetic field profiles, but in general it is more convenient to calculate values for these parameters from expressions relating J_θ, J_φ and B_e to the toroidal current I_φ, the pinch ratio θ and field reversal index F.

Given values of I_φ and θ, we can calculate

$$J_\varphi = \frac{I_\varphi}{\pi a^2}\{\alpha_j - 4/\pi^2\}^{-1}, \tag{3.54}$$

$$J_\theta = \frac{\pi}{8}\frac{\mu_0 a}{B_e}\left(\frac{I_\varphi}{\pi a^2}\right)^2\{1 - 4/\pi^2\}^{-1}, \tag{3.55}$$

$$B_e = \frac{\mu_0 I_\varphi}{2\pi a\theta}. \tag{3.56}$$

Equation (3.54) follows from (3.52), while equation (3.55) follows from (3.9) and the fact that $\langle B_\varphi \rangle = B_e$. Equation (3.55) follows from (3.53) and (3.52) and equation (3.56) is derived from (3.6) and (3.52).

In practice I_φ and B_e are the externally controlled parameters in RFP discharges, but B_e is seldom quoted in experimental papers, and must be inferred from equation (3.56).

3.2.2 Number Density and Temperature Profiles

In addition to current and magnetic field profiles we shall require expressions for the electron number density and temperature profiles. Alper *et al.* (1986) have established such profiles for HBTX. These are

$$n_e(r) = (n_{e0} - n_{ea})\{1 - (r/a)^2\}^{\alpha_n} + n_{ea}, \tag{3.57}$$

$$T_e(r) = (T_{e0} - T_{ea})\{1 - (r/a)^2\}^{\alpha_t} + T_{ea}, \tag{3.58}$$

where the subscripts 0 and a indicate a central value and a value at the limiter respectively, and α_n and α_t are phenomenological parameters chosen to give a fit with experimental data. Typical values are $\alpha_n \sim 0.5$ and $\alpha_t \sim 0.25$, making the profiles quite flat in the central regions and steep at the plasma edge.

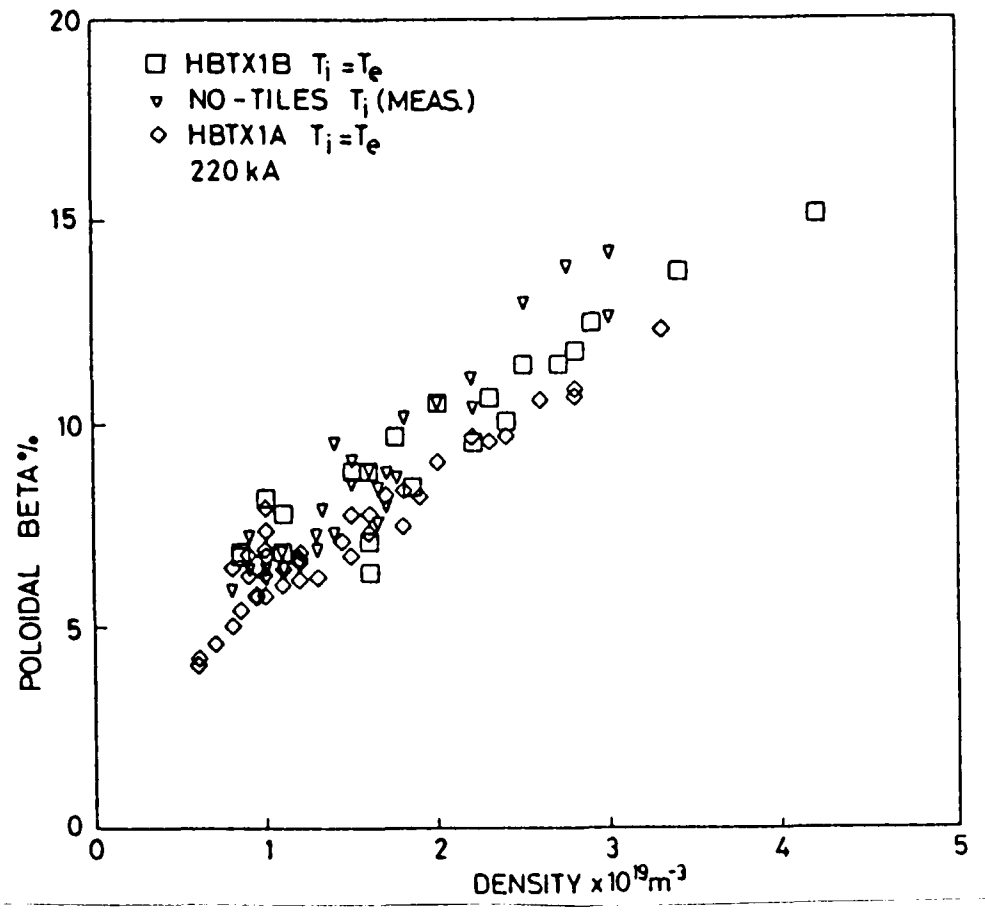

Figure 3.7: Poloidal beta versus density for HBTX (from Bodin 1987)

Values for n_{ea} and T_{ea} are difficult to estimate and are seldom published. It is, however, reasonable to assume that $n_{ea} \leq 0.1 n_{e0}$ and $T_{ea} \leq 0.1 T_{e0}$. As the inclusion or not of these values in the following calculations makes little numerical difference, we shall assume them to be zero.

In HBTX there is an observed relationship between the poloidal beta and number density for a fixed current (Bodin 1987). From the data plotted in Figure 3.7 we find that to a good approximation

$$\beta_p = 0.025 + 0.033 \frac{\langle n_e \rangle}{10^{19}}, \qquad (1 \leq \frac{\langle n_e \rangle}{10^{19}} \leq 3.5). \tag{3.59}$$

From the definition of β_p and the assumed profiles for n_e and T_e, we obtain

$$\beta_p = \frac{8\pi^2 a^2 2k n_{e0} T_{e0}}{(1 + \alpha_n + \alpha_t)\mu_0 I_\varphi^2}, \tag{3.60}$$

where we have assumed that $\langle p \rangle = 2k n_{e0} T_{e0}/(1 + \alpha_n + \alpha_t)$. Substituting (3.59) into (3.60), we obtain the phenomenological expression for T_{e0}:

$$T_{e0} = \frac{(1 + \alpha_n + \alpha_t)\mu_0 I_\varphi^2}{4\pi^2 a^2 k n_{e0}} \left\{ \frac{1 + \alpha_n}{40} + \frac{n_{e0}}{3 \times 10^{20}} \right\}, \quad (1 \leq \frac{\langle n_e \rangle}{10^{19}} \leq 3.5), \tag{3.61}$$

where, as in Figure 3.7, $I_\varphi \sim 220$kA.

3.3 The Particle Confinement Time

During the initial phase of a RFP discharge a large outflow of plasma known as 'pump-out' occurs. Once the reversed field configuration has been formed, the plasma density becomes relatively constant. In HBTX the density is normally controlled by wall preconditioning where the carbon tile limiters are preloaded with gas during a previous discharge (Bodin 1987). During the main part of the discharge, recycling occurs at the wall where plasma is cooled and neutralised. Neutral gas particles formed at the wall are unimpeded by the magnetic field and diffuse into the plasma until they become ionised. Thus a radial plasma flow can be maintained with a steady-state number density profile.

Since the condition $\nabla \cdot \boldsymbol{j} = 0$ (cf. (1.18)) implies that there are no radial currents in an axisymmetric discharge, and $\boldsymbol{j} = en_e(\boldsymbol{v}_i - \boldsymbol{v}_e)$ it follows that the radial velocity of the ion and electron fluids is the same, and the radial flow is said to be ambipolar. As we shall shortly show, the constraint imposed by ambipolar flow yields a relationship between the ion and electron particle confinement times. This being the case, we will restrict attention to a calculation of τ_{pe}, the electron confinement time.

An expression for τ_{pe} is derived as follows. From the electron fluid mass equation expressed in cylindrical geometry

$$\frac{\partial n_e}{\partial t} + \frac{1}{r}\frac{\partial}{\partial r}(r n_e v_r) = S_e(r), \tag{3.62}$$

where $S_e(r)$ is the electron source term, we obtain

$$\frac{\partial \ln N}{\partial t} + \frac{1}{\tau_{pe}} = \frac{1}{\tau_{pe}^*}, \tag{3.63}$$

where

$$N \equiv \int_0^a n_e r \, dr, \tag{3.64}$$

$$\tau_{pe} \equiv \frac{N}{[r n_e v_r]_{r=a}}, \tag{3.65}$$

$$\tau_{pe}^* \equiv \frac{N}{\int_0^a S_e r \, dr}. \tag{3.66}$$

The times defined by (3.65) and (3.66) are the electron particle confinement time and the electron particle replacement time. From (3.63) we can see that these two times are the same only when $\partial n_e/\partial t = 0$ across the minor radius.

Equation (3.65) is unsuitable for evaluating τ_{pe} because of the difficulty of obtaining values of n_e and v_r at the limiter. This difficulty can be overcome by adopting an averaging procedure (Woods 1987).

We note that the balance between S_e and $\partial(rn_e v_r)/(r\partial r)$ must occur across the entire minor radius for steady-state conditions. Thus

$$\int_0^a S_e r\, dr = [rn_e v_r]_{r=a}, \tag{3.67}$$

and

$$\int_0^a dr \int_0^r S_e r^*\, dr^* = \int_0^a n_e v_r\, r dr. \tag{3.68}$$

If we now define the ratio

$$A_p \equiv \frac{\frac{1}{a}\int_0^a dr \int_0^r S_e r^*\, dr^*}{\int_0^a S_e r\, dr}, \tag{3.69}$$

by (3.67) and (3.68) the electron particle confinement time can be expressed as

$$\tau_{pe} = aA_p \frac{\langle n_e \rangle}{\langle n_e v_r \rangle}. \tag{3.70}$$

We can calculate the ion confinement time τ_{pi} in the same way as the electron confinement time to obtain

$$\tau_{pi} = aA_{pi} \frac{\langle n_i \rangle}{\langle n_i v_r \rangle}, \tag{3.71}$$

where

$$A_{pi} \equiv \frac{\frac{1}{a}\int_0^a dr \int_0^r S_i r^* dr^*}{\int_0^a S_i r dr}, \tag{3.72}$$

and S_i is the ion source term. Suppose the charge number Z is constant across the minor radius. Then as $Zn_i = n_e$ and, as we will shortly argue, $ZS_i \simeq S_e$, it follows from (3.70) and (3.71) that $A_{pi} = A_p$. It follows from the previously noted condition of ambipolarity that $\langle n_i v_r \rangle / \langle n_i \rangle = \langle n_e v_r \rangle / \langle n_e \rangle$ whence $\tau_{pe} = \tau_{pi}$. Thus the confinement time of the plasma is equally well given by τ_{pe} or τ_{pi}.

The ratio A_p may be evaluated by supplying additional information about the distribution of the source term across the minor radius. The two main sources of electrons in plasma discharges of the type we have been considering are the ionization of impurities in highly contaminated plasmas and neutral gas recycling in clean discharges. A typical value for Z^* in HBTX is two with impurities being distributed across the minor radius (Bodin 1987). Thus HBTX discharges are relatively uncontaminated and it is reasonable to assume that the main source of electrons is the ionization of neutrals in the plasma. As this refueling mechanism yields Z electrons for every ion, it follows that the ion source term and the electron source term are related by $ZS_i = S_e$.

3.3.1 The Electron Source Distribution

There are many atomic and molecular reactions which occur in a plasma boundary and contribute to the generation of electrons. In a hydrogeneous discharge the species H_2, H_2^*, H_2^+, H, H^*, H^-, H^+, (where the * denotes an excited state, of which there may be several) are all present in the boundary region. These species interact with each other as well as with electrons and the local radiation field. The important interactions for a toroidal plasma are:

(a) $e + H_2 \rightarrow e + H^* + H^*$,

(b) $e + H_2 \rightarrow 2e + H^+ + H$,

(c) $e + H_2 \rightarrow 2e + H_2^+$,

(d) $e + H_2^+ \rightarrow 2e + H^+ + H$,

(e) $e + H \rightarrow 2e + H^+$,

(f) $H_{fast} + H_{slow}^+ \rightleftharpoons H_{slow}^+ + H_{fast}$.

Harrison (1986) has given a good introductory account of the atomic collision physics relevant in the plasma boundary. The dominant atomic and molecular processes associated with the recycling of hydrogen are shown in figure 3.8 (from Harrison 1986).

Johnson has written a program labelled HSLAB (Johnson, Culham Laboratory U.K., private communication) to calculate the total source of H^+ and e^-

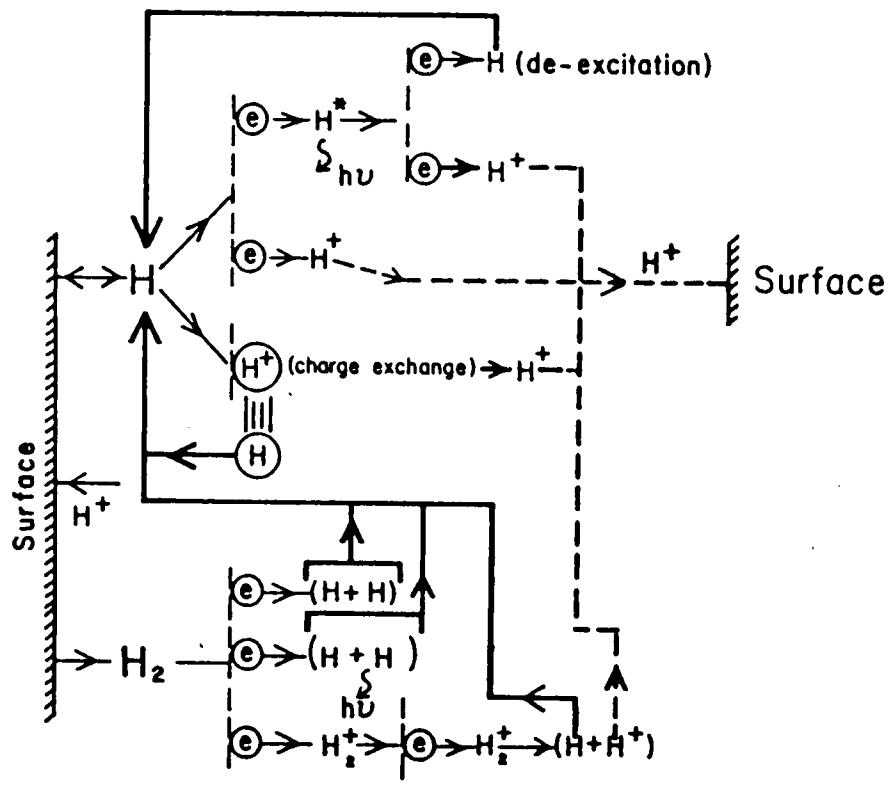

Figure 3.8: The dominant atomic and molecular processes associated with the recycling of hydrogen (from Harrison 1986).

due to the main atomic and molecular processes in the plasma boundary for a given electron density and electron and ion temperatures. The program HSLAB uses slab geometry. Because the curvature of the toroidal confinement vessel is unimportant near the discharge wall on length-scales significantly less than the minor radius, slab geometry is sufficiently accurate for the distances in from the wall that we shall be concerned with.

The programme has been run for a range of central electron temperatures and densities using (3.57) and (3.58) for n_e and T_e, and assuming that the electron temperature at the limiter $T_{el} = 0.1T_{e0}$ and $T_i = T_e$. It was also assumed that the temperature and densities decayed exponentially in distance from the limiter to the wall. A typical plot of the total H^+ and e^- sources calculated is shown in figure 3.9.

Values for A_p defined in (3.69) have been calculated from the data generated by HSLAB for various values of n_{e0} and T_{e0}, adopting the typical HBTX values $\alpha_n = 0.5$ and $\alpha_t = 0.25$. The values of A_p are listed in table 3.1.

These calculations show that A_p is not a sensitive function of temperature or

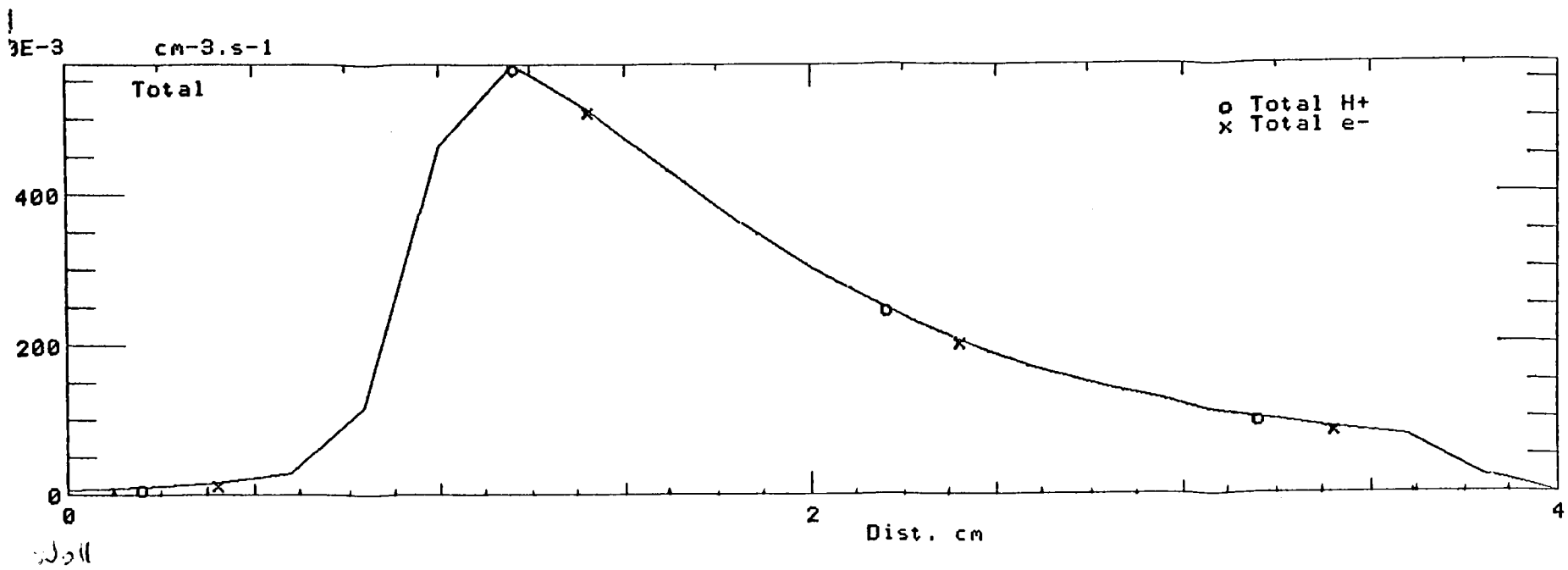

Figure 3.9: A typical plot of the ion and electron source distributions. Parameters are: $n_{e0} = 1.0 \times 10^{19}\mathrm{m}^{-3}$ and $T_{e0} = 100\mathrm{eV}$.

		$n_{e0}(\times 10^{19}\mathrm{m}^{-3})$	
		1.0	2.0
T_{e0}(eV)	100	0.071	0.057
	300	0.064	0.048

Table 3.1: Values of A_p for central values of T_e and n_e calculated from HSLAB data

		$n_{e0}(\times 10^{19}\mathrm{m}^{-3})$	
		1.0	2.0
T_{e0}(eV)	100	0.075	0.054
	300	0.066	0.048

Table 3.2: Values of A_p fitted to the HSLAB data

density. We surmise from the data that a sufficiently accurate model of A_p for our purposes is given by

$$A_p = K\left(\frac{n_{e0}}{10^{19}}\right)^{\gamma_n}\left(\frac{\tilde{T}_{e0}}{10^2}\right)^{\gamma_t}, \tag{3.73}$$

where K, γ_n and γ_t are adjustable parameters chosen to fit the calculations of A_p, and $\tilde{T}_{e0}$ has units of eV.

The values $K = 0.075$, $\gamma_n = -0.2$, and $\gamma_t = -0.12$ give a 5% fit to the values of A_p listed in table 3.1 (see table 3.2).

Changing the units of electron temperature to Kelvin, we obtain

$$A_p = 0.075\left(\frac{n_{e0}}{10^{19}}\right)^{-0.2}\left(\frac{T_{e0}}{1.16\times 10^6}\right)^{-0.12}. \tag{3.74}$$

This is the expression for A_p that we shall use in subsequent calculations.

An analysis of S_e in HBTX has been made by Carolan *et al.* (1987) from fluoroscopic measurments of neutral gas density. A typical plot of the results of their analysis is shown in figure 3.10, which is in good qualitative agreement with the results from HSLAB (note that the plasma wall is on the left in figure 3.9 and the right in figure 3.10).

3.3.2 The Plasma Radial Velocity

An expression for the plasma radial velocity can be obtained from the momentum equation. Neglecting inertia, we have that

$$\nabla \cdot \boldsymbol{p} = qn(\boldsymbol{E} + \boldsymbol{v} \times \boldsymbol{B}) + \boldsymbol{R} \tag{3.75}$$

for each fluid species, where q is the particle species charge, $\boldsymbol{p}$ is the pressure tensor, $\boldsymbol{R}$ is the drag force and $\boldsymbol{v}$ is the velocity field for the ion or electron fluid

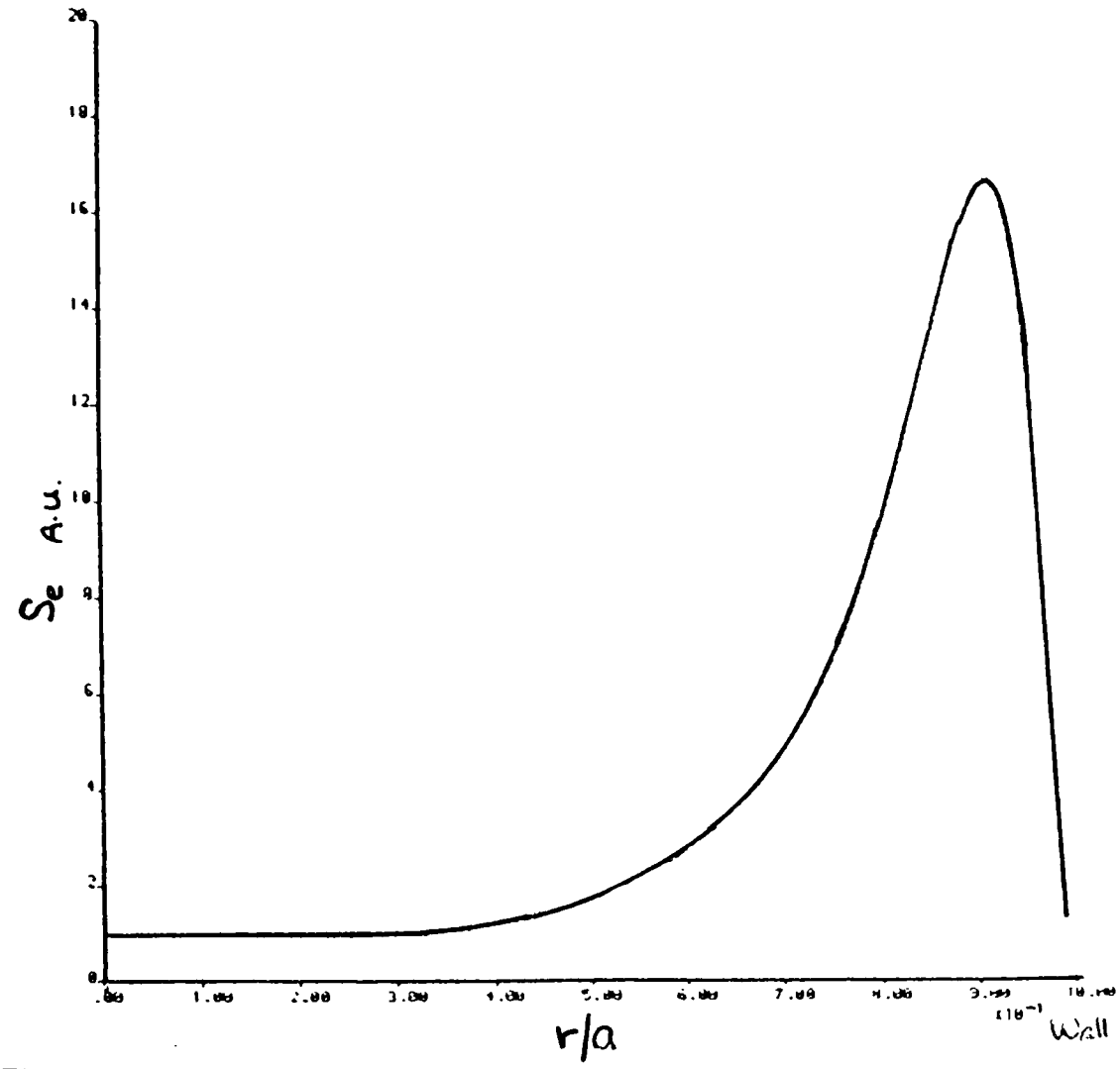

Figure 3.10: S_e versus r (from Carolan *et al.* 1987)

in question. If we solve equation (3.75) for $\boldsymbol{v}_\perp \equiv \boldsymbol{v} \cdot (\mathbf{1} - \boldsymbol{bb})$, we obtain

$$\boldsymbol{v}_\perp = \frac{\boldsymbol{E} \times \boldsymbol{b}}{B} + \frac{1}{\rho\omega_c}(\boldsymbol{R} - \nabla \cdot \boldsymbol{p}) \times \boldsymbol{b}. \tag{3.76}$$

The plasma radial velocity may be obtained from (3.76) by noting that $v_r = \boldsymbol{v}_\perp \cdot \hat{\boldsymbol{r}}$. The condition of ambipolar diffusion requires that $v_{re} = v_{ri}$, the subscript e, i denoting electron or ion velocity respectively. This places a restriction on $\nabla \cdot \boldsymbol{p}$ and an account of this condition is made later in this chapter. For our present purposes it is sufficient to note that the radial velocity may be determined by equation (3.76) written for either the electron or the ion fluids. For reasons that will become clear later we will solve for v_{re}.

Since $v_{re} = v_{ri} = v_r$ say, upon writing (3.76) for the electron fluid, and solving for v_r we have that

$$v_r = \frac{\boldsymbol{E} \cdot \boldsymbol{b} \times \hat{\boldsymbol{r}}}{B} + \frac{1}{\rho_e\omega_{ce}}(\boldsymbol{R}_e - \nabla \cdot \boldsymbol{p}_e) \cdot \boldsymbol{b} \times \hat{\boldsymbol{r}}. \tag{3.77}$$

It follows directly that

$$\langle n_e v_r \rangle = \frac{2}{a^2}\int_0^a \left\{\frac{\boldsymbol{E}}{B} + \frac{1}{\rho_e\omega_{ce}}\boldsymbol{R}_e - \frac{1}{\rho_e\omega_{ce}}\nabla \cdot \boldsymbol{p}_e\right\} \cdot \boldsymbol{b} \times \hat{\boldsymbol{r}} n_e r\, dr. \tag{3.78}$$

The integral in (3.78) may be evaluated using the model profiles adopted in the previous section and equations for $\boldsymbol{E}$, $\boldsymbol{R}_e$ and $\nabla \cdot \boldsymbol{p}_e$. We shall consider each of the three terms in the integral on the right hand side of (3.78) separately in the following sections.

The Electric Field Term

When steady state conditions prevail the physical origin of the electric field in the plasma is the changing magnetic flux through the center of the torus driven by the transformer field windings.

Rather than using the relation $E_\varphi = V_L/2\pi R_0$, we will obtain an estimate of E_φ from a simplified form of Ohm's law valid at the minor axis. By this method we can obtain an estimate of E_φ which is related directly to the current densities, which are known. From (1.22) we have that

$$\boldsymbol{\eta} \cdot \boldsymbol{j} = \boldsymbol{E} + \boldsymbol{v} \times \boldsymbol{B} - \frac{1}{en_e} \boldsymbol{j} \times \boldsymbol{B} + \frac{1}{en_e} \nabla \cdot \boldsymbol{p}_e. \tag{3.79}$$

On the minor axis $\nabla \cdot \boldsymbol{p}_e = 0$ (cf. (3.57) and (3.58)), $j_\theta = 0$, $B_\theta = 0$ and we may assume v_r to be negligible. With these assumptions the toroidal component of (3.79) evaluated on the minor axis yields

$$\eta_{||}(0) j_\varphi(0) = E_\varphi, \tag{3.80}$$

where we have used the substitution $\boldsymbol{\eta} = \eta_{||}\boldsymbol{bb} + \eta_\perp(\mathbf{1} - \boldsymbol{bb})$ and E_φ may be considered constant across the minor radius if we neglect toroidal effects. Adopting the definition

$$\langle n_e v_r^E \rangle \equiv \frac{2}{a^2} \int_0^a \frac{\boldsymbol{E} \cdot \boldsymbol{b} \times \hat{\boldsymbol{r}}}{B} n_e r \, dr, \tag{3.81}$$

and noting that $\boldsymbol{E} \cdot \boldsymbol{b} \times \hat{\boldsymbol{r}} = -E_\varphi b_\theta$, we obtain from (3.80) that

$$\langle n_e v_r^E \rangle = -\frac{2}{a^2} \int_0^a \eta_{||}(0) j_\varphi(0) \frac{b_\theta n_e}{B} r \, dr. \tag{3.82}$$

The Fluid Drag Term

The constitutive relation (1.36) for the drag force between the ion and electron fluids is, neglecting the thermoelectric effect,

$$\frac{\boldsymbol{R}_e}{en_e} = \boldsymbol{\eta} \cdot \boldsymbol{j}. \tag{3.83}$$

Noting that $\rho_e \omega_{ce} = -eBn_e$ and defining

$$\langle n_e v_r^R \rangle \equiv \frac{2}{a^2} \int_0^a \frac{1}{\rho_e \omega_{ce}} \boldsymbol{R}_e \cdot \boldsymbol{b} \times \hat{\boldsymbol{r}} n_e r \, dr, \tag{3.84}$$

we obtain, with the help of (3.83)

$$\langle n_e v_r^R \rangle = \frac{2}{a^2} \int_0^a \frac{\boldsymbol{\eta} \cdot \boldsymbol{j} \cdot \boldsymbol{b} \times \hat{\boldsymbol{r}}}{B} n_e r \, dr. \tag{3.85}$$

Using the relations $\boldsymbol{\eta} = \eta_{||} \boldsymbol{bb} + \eta_\perp (\mathbf{1} - \boldsymbol{bb})$ and $\boldsymbol{j} \times \boldsymbol{B} = \nabla p$ we find that

$$\begin{aligned} \boldsymbol{\eta} \cdot \boldsymbol{j} \cdot \boldsymbol{b} \times \hat{\boldsymbol{r}} &= \boldsymbol{j} \cdot \eta_{||} \boldsymbol{bb} \cdot (\boldsymbol{b} \times \hat{\boldsymbol{r}}) + \boldsymbol{j} \cdot \eta_\perp (\mathbf{1} - \boldsymbol{bb}) \cdot (\boldsymbol{b} \times \hat{\boldsymbol{r}}) \\ &= \eta_\perp \boldsymbol{j} \cdot \boldsymbol{b} \times \hat{\boldsymbol{r}} \\ &= \frac{\eta_\perp}{B} (\boldsymbol{j} \times \boldsymbol{B}) \cdot \hat{\boldsymbol{r}} \\ &= \frac{\eta_\perp p'}{B}. \end{aligned} \tag{3.86}$$

Substituting (3.86) into (3.85), we obtain

$$\langle n_e v_r^R \rangle = -\frac{2}{a^2} \int_0^a \eta_\perp \frac{p'}{B^2} n_e r \, dr. \tag{3.87}$$

The Pressure Tensor Term

We can define the contribution of the pressure tensor to the radial diffusion velocity to be (cf. (3.78))

$$\langle n_e v_r^\pi \rangle \equiv -\frac{2}{a^2} \int_0^a \frac{1}{\rho_e \omega_{ce}} \nabla \cdot \boldsymbol{p}_e \cdot (\boldsymbol{b} \times \hat{\boldsymbol{r}}) \, n_e r \, dr. \tag{3.88}$$

Only the poloidal and toroidal components of $\nabla \cdot \boldsymbol{p}_e = \nabla \cdot (p\mathbf{1} + \boldsymbol{\pi}_{1e} + \boldsymbol{\pi}_{2e})$ contribute to this integral. Since $\nabla \cdot (\mathbf{1} p_e + \boldsymbol{\pi}_{1e})$ has a radial component only, we can replace $\nabla \cdot \boldsymbol{p}_e$ by the divergence of the second-order viscous stress tensor $\nabla \cdot \boldsymbol{\pi}_{2e}$.

The term $\nabla \cdot \boldsymbol{\pi}_{2e}$ involves the second derivative of $\boldsymbol{v}_e$. The empirical profiles for j and n_e that will be used to estimate $\boldsymbol{v}_e$ cannot be expected to yield realistic profiles for second derivatives, but this problem can be circumvented by integrating (3.88) by parts. Making the substitution $\nabla \cdot \boldsymbol{p}_e \cdot (\boldsymbol{b} \times \hat{\boldsymbol{r}}) = \nabla \cdot \boldsymbol{\pi}_{2e} \cdot (b_\theta \hat{\boldsymbol{\theta}} - b_\varphi \hat{\boldsymbol{\varphi}})$ we have that

$$\langle n_e v_r^\pi \rangle = \frac{2}{a^2} \int_0^a \frac{1}{eB} [b_\varphi \hat{\boldsymbol{\theta}} \cdot \nabla \cdot \boldsymbol{\pi}_{2e} - b_\theta \hat{\boldsymbol{\varphi}} \cdot \nabla \cdot \boldsymbol{\pi}_{2e}] r \, dr. \tag{3.89}$$

With the help of (2.37), equation (3.89) may be rewritten as

$$\langle n_e v_r^\pi \rangle = -\frac{2}{a^2} \int_0^a \frac{1}{eB} [b_\varphi \frac{1}{r^2} \{r^2 \alpha_1\}' + b_\theta \frac{1}{r} \{r \alpha_2\}'] r \, dr, \tag{3.90}$$

where the functions α_1 and α_2 are defined by

$$\alpha_1 \equiv \frac{2 p_e \tau_{1e}}{\omega_{ce}} [b_\varphi \Theta + 2 b_\theta (2 b_\theta^2 - b_\varphi^2) \Xi], \tag{3.91}$$

$$\alpha_2 \equiv \frac{2 p_e \tau_{1e}}{\omega_{ce}} [b_\theta \Theta + 2 b_\varphi (2 b_\varphi^2 - b_\theta^2) \Xi], \tag{3.92}$$

and Θ and Ξ are defined by equations (2.34) and (2.35).

We can simplify (3.90) somewhat by neglecting variations in B across the cross-section. Assuming B to be constant and integrating (3.90) by parts we estimate that

$$\langle n_e v_r^\pi \rangle = -\frac{2}{a^2 eB} \Big\{ [r \alpha_1 b_\varphi + r \alpha_2 b_\theta]_0^a - \int_0^a [r (b_\varphi / r)' \alpha_1 + b_\theta' \alpha_2] r \, dr \Big\}. \tag{3.93}$$

Since $p_e(a) \approx 0, \alpha_1(a) \simeq \alpha_2(a) \simeq 0$ and the first term on the right hand side of (3.93) vanishes to yield

$$\langle n_e v_r^\pi \rangle = \frac{2}{a^2 eB} \int_0^a [r (b_\varphi / r)' \alpha_1 + b_\theta' \alpha_2] r \, dr. \tag{3.94}$$

In order to evaluate this integral we need expressions for the functions α_1 and α_2 defined by (3.91) and (3.92) in terms of experimental profiles. This leads us into a general consideration of a suitable expression for the viscous stress tensor.

An Estimate of the Viscous Stress Tensor

Equation (2.37) shows that $\boldsymbol{\pi}_{2e}$ depends on the electron velocity field, which is unknown. However, the condition for ambipolar diffusion allows us to determine

a suitable approximation for $v_{e\varphi}$ and $v_{e\theta}$. Such an approximation can be found because, as will be shown below, the condition $v_{re} = v_{ri}$ requires a relationship between $\nabla \cdot \pi_{2e}$ and $\nabla \cdot \pi_{2i}$. This, in turn, implies a relationship between v_e and v_i. Using this relationship and $j = en_e(v_i - v_e)$, we can determine v_e in terms of the known quantity j.

If we write (3.77) for the electron and ion fluids separately, then $v_{re} = v_{ri}$ implies that

$$\frac{1}{\rho_e \omega_{ce}}(\boldsymbol{R}_e - \nabla \cdot \boldsymbol{p}_e) \cdot \boldsymbol{b} \times \hat{\boldsymbol{r}} = \frac{1}{\rho_i \omega_{ci}}(\boldsymbol{R}_i - \nabla \cdot \boldsymbol{p}_i) \cdot \boldsymbol{b} \times \hat{\boldsymbol{r}}, \tag{3.95}$$

or

$$\frac{\nabla \cdot \boldsymbol{\pi}_{2e} \cdot (\boldsymbol{b} \times \hat{\boldsymbol{r}})}{\rho_e \omega_{ce}} + \frac{\nabla \cdot \boldsymbol{\pi}_{2i} \cdot (\boldsymbol{b} \times \hat{\boldsymbol{r}})}{\rho_i \omega_{ci}} = 0, \tag{3.96}$$

where we have used $\boldsymbol{R}_e = -\boldsymbol{R}_i$.

Using equation (2.37) for $\nabla \cdot \boldsymbol{\pi}$ evaluated for the electron and ion fluids, we find after some algebra that equation (3.96) is satisfied if

$$\frac{1}{r^2}\Big\{\frac{r^2 p_e \tau_{1e}}{\omega_{ce}}[-b_\varphi \Theta_e - 2b_\theta(2b_\theta^2 - b_\varphi^2)\Xi_e]\Big\}' = \frac{Z}{r^2}\Big\{\frac{r^2 p_i \tau_{1i}}{\omega_{ci}}[-b_\varphi \Theta_i - 2b_\theta(2b_\theta^2 - b_\varphi^2)\Xi_i]\Big\}' \tag{3.97}$$

and

$$\frac{1}{r}\Big\{\frac{r p_e \tau_{1e}}{\omega_{ce}}[-b_\theta \Theta_e - 2b_\varphi(2b_\varphi^2 - b_\theta^2)\Xi_e]\Big\}' = \frac{Z}{r}\Big\{\frac{r p_i \tau_{1i}}{\omega_{ci}}[-b_\theta \Theta_i - 2b_\varphi(2b_\varphi^2 - b_\theta^2)\Xi_i]\Big\}', \tag{3.98}$$

where

$$\Theta_e \equiv \frac{1}{2}\Big\{r^2\Big[\Big(\frac{v_{e\theta}}{r}\Big)'\Big]^2 + \Big[v'_{e\varphi}\Big]^2\Big\}, \tag{3.99}$$

$$\Theta_i \equiv \frac{1}{2}\Big\{r^2\Big[\Big(\frac{v_{i\theta}}{r}\Big)'\Big]^2 + \Big[v'_{i\varphi}\Big]^2\Big\}, \tag{3.100}$$

$$\Xi_e \equiv \frac{1}{4} r \Big(\frac{v_{e\theta}}{r}\Big)' v'_{e\varphi}, \tag{3.101}$$

$$\Xi_i \equiv \frac{1}{4} r \Big(\frac{v_{i\theta}}{r}\Big)' v'_{i\varphi}. \tag{3.102}$$

These functions follow from Θ and Ξ, defined by (2.34) and (2.35) evaluated for the electron and ion fluids. Equations (3.97) and (3.98) will be satisfied if

$$\Theta_i = G\Theta_e, \qquad \Xi_i = G\Xi_e, \tag{3.103}$$

where

$$G \equiv -Z\frac{\omega_{ce}p_e\tau_{1e}}{\omega_{ci}p_i\tau_{1i}}, \tag{3.104}$$

assuming that the charge number is constant across the minor radius. The definitions (3.99) to (3.102), and the conditions (3.103) yield

$$r^2[(\frac{v_{i\theta}}{r})']^2 + [v'_{i\varphi}]^2 = G\Big\{r^2[(\frac{v_{e\theta}}{r})']^2 + [v'_{e\varphi}]^2\Big\}, \tag{3.105}$$

and

$$r(\frac{v_{i\theta}}{r})'v'_{i\varphi} = Gr(\frac{v_{e\theta}}{r})'v'_{e\varphi}. \tag{3.106}$$

Equations (3.105) and (3.106) will be satisfied if

$$r(\frac{v_{i\theta}}{r})' = G^{1/2}r(\frac{v_{e\theta}}{r})', \tag{3.107}$$

and

$$v'_{i\varphi} = G^{1/2}v'_{e\varphi}. \tag{3.108}$$

Using equations (3.107) and (3.108) and the relation $\boldsymbol{j} = en_e(\boldsymbol{v}_i - \boldsymbol{v}_e)$ we can derive the expressions

$$v'_{e\varphi} = -\frac{1}{1-G^{1/2}}(\frac{j_\varphi}{en_e})', \tag{3.109}$$

and

$$r(\frac{v_{e\theta}}{r})' = -\frac{1}{1-G^{1/2}}r(\frac{j_\theta}{ren_e})'. \tag{3.110}$$

From the definition of G and equations (1.14) for τ_{1e} and τ_{1i} we can show

$$\begin{aligned} G &= \frac{m_e}{m_i}\frac{n_ekT_e}{n_ikT_i}\frac{0.73\tau_e}{0.96\tau_i}Z \\ &\simeq 6.83\times10^{-6}Z^4\Big(\frac{T_e}{T_i}\Big)^{5/2}A^{-3/2}, \end{aligned} \tag{3.111}$$

where $A \equiv m_i/m_p$ (m_p is the mass of a proton). For $A = 1$, $Z = 1$ and $T_i = T_e$ we have that $G^{1/2} \simeq 3\times10^{-3}$ and so to a good approximation

$$v'_{e\varphi} = -(\frac{j_\varphi}{en_e})', \tag{3.112}$$

and

$$r(\frac{v_{e\theta}}{r})' = -r(\frac{j_\theta}{ren_e})'. \tag{3.113}$$

Since we have empirical profiles for j_θ, j_φ and n_e, equations (3.112) and (3.113) allow us to make an estimate of $\nabla\cdot\boldsymbol{\pi}_{2e}$.

3.3.3 An Estimate of the Particle Confinement Time

We are now able to estimate the particle confinement time by substituting the empirical profiles developed in section 3.2 into equation (3.78) and using the approximations for the three terms on the right hand side of this equation found in the preceding sections. By definitions (3.81), (3.84) and (3.88), and equation (3.78) we have that

$$\langle n_e v_r \rangle = \langle n_e v_r^E \rangle + \langle n_e v_r^R \rangle + \langle n_e v_r^\pi \rangle. \tag{3.114}$$

Collecting the approximations for the three terms on the right hand side of (3.114) (given by (3.82), (3.85) and (3.94)) we obtain

$$\langle n_e v_r \rangle = \frac{2}{a^2} \int_0^a [-\eta_{||}(0) j_\varphi(0) \frac{b_\theta n_e}{B} - \eta_\perp \frac{n_e p'}{B^2} + \frac{1}{eB} \{ r(b_\varphi / r)' \alpha_1 + b_\theta' \alpha_2 \}] r \, dr, \tag{3.115}$$

where α_1 and α_2 are defined by equations (3.91) and (3.92).

Equation (3.115) may be evaluated for the RFP by substituting the actual profiles for j_θ, j_φ, B_θ, B_φ, n_e and T_e found in these machines. In order to make a comparison between the various terms in (3.115) and also to calculate $\langle n_e v_r \rangle$, we proceed as follows.

Each of the empirical profiles set out in section 3.2 can be expressed in the form $\phi(r) = K_\phi \Psi(x)$ where $\phi(r)$ is the variable of interest, K_ϕ is a constant scaling factor and $\Psi(x)$ is a dimensionless profile shape function of order unity and a function of the non-dimensional radial variable $x \equiv r/a$. Rewriting the profile equations in this form will enable us to formulate equation (3.115) in terms of variables which are independent of the details of profile shape, multiplied by profile shape factors which depend only on changes in the plasma variables across the minor radius.

For the remainder of the chapter we will use the convention that an upper-case script symbol corresponds to the scaled variable denoted by a plain symbol. So $\mathcal{J}_\theta$ is the scaled poloidal current density corresponding to j_θ, for example.

Defining

$$\mathcal{J}_\theta(x) \equiv \frac{j_\theta(r)}{J_\theta}, \qquad \mathcal{J}_\varphi(x) \equiv \frac{j_\varphi(r)}{J_\varphi}, \qquad x \equiv r/a, \tag{3.116}$$

we obtain from (3.48) and (3.49)

$$\mathcal{J}_\theta = \sin(\pi x), \qquad \mathcal{J}_\varphi = \alpha_j + \cos(\pi x). \tag{3.117}$$

The magnetic field profiles may be scaled in a similar way. We define the scaled profiles to be

$$\mathcal{B}_\theta(x) \equiv \frac{B_\theta(r)}{B_e}, \qquad \mathcal{B}_\varphi(x) \equiv \frac{B_\varphi(r)}{B_e}, \tag{3.118}$$

where B_e is the externally imposed toroidal field. Substituting equations (3.50) and (3.51) for B_θ and B_φ into the definitions (3.118), and using (3.54), (3.55) and (3.56) to eliminate J_θ and J_φ, we obtain

$$\mathcal{B}_\theta = \frac{2\pi\theta}{\alpha_j\pi^2 - 4}\left[\frac{\pi}{2}\alpha_j x + \sin(\pi x) + \frac{1}{\pi x}\{\cos(\pi x) - 1\}\right], \tag{3.119}$$

and

$$\mathcal{B}_\varphi = 1 + \frac{\theta^2}{2}\frac{4 + \pi^2\cos(\pi x)}{\pi^2 - 4}, \tag{3.120}$$

From (3.57) and (3.58) we find that the scaled number density and temperature profiles, defined by

$$\mathcal{N}_e(x) \equiv \frac{n_e(r)}{n_{e0}}, \qquad \mathcal{T}_e(x) \equiv \frac{T_e(r)}{T_{e0}}, \tag{3.121}$$

are given by

$$\mathcal{N}_e = (1 - x^2)^{\alpha_n}, \qquad \mathcal{T}_e = (1 - x^2)^{\alpha_t}, \tag{3.122}$$

where to obtain (3.122) we have taken $n_{ea} = T_{ea} = 0$ in (3.57) and (3.58). The above equations for the scaled profiles can be used to evaluate each of the three terms in (3.115).

By substituting equations (3.116), (3.118), (3.121), (3.91) and (3.92) into (3.115), we find after some algebra that

$$\langle n_e v_r \rangle = A_E F_E + A_R F_R + A_\pi F_\pi, \tag{3.123}$$

where A_E, A_R and A_π, defined below, are functions of J_θ, J_φ, B_e, n_{e0} and T_{e0}, and F_E, F_R, and F_π, also defined below, are integrals involving the scaled profiles.

The terms

$$A_E \equiv -3.64 \times 10^{-6} \frac{m_e}{e^2}(\alpha_j + 1) J_\varphi Z^* \ln \Lambda \frac{n_{e0}}{B_e T_{e0}^{\frac{3}{2}}}, \tag{3.124}$$

$$F_E \equiv \int_0^1 b_\theta \frac{\mathcal{N}_e}{\mathcal{B}} x \, dx, \tag{3.125}$$

where $\mathcal{B} = (\mathcal{B}_\theta^2 + \mathcal{B}_\varphi^2)^{1/2}$, are the scaling constant and profile shape factor corresponding to the electric field term. For the flux arising from the drag force we have

$$A_R \equiv 3.64 \times 10^{-6} \frac{2km_e}{e^2} Z^* \ln \Lambda \frac{n_{e0}^2}{B_e^2 T_{e0}^{\frac{1}{2}}} \frac{1}{a}, \tag{3.126}$$

$$F_R \equiv -\int_0^1 \frac{\mathcal{N}_e}{\mathcal{B}\mathcal{T}_e^{5/2}} (\mathcal{N}_e \mathcal{T}_e)' x \, dx \tag{3.127}$$

which are are the drag force scaling constant and profile shape factor, and

$$A_\pi \equiv 8.04 \times 10^5 \frac{km_e}{e^4} \frac{T_{e0}^{\frac{5}{2}}}{Z^* \ln \Lambda} \frac{J_\varphi^2}{B_e^2} \frac{1}{n_{e0}^2 a^3}, \tag{3.128}$$

$$\begin{aligned} F_\pi \equiv -\int_0^1 \frac{\mathcal{T}_e^{\frac{5}{2}}}{\mathcal{B}^2} [x(b_\varphi/x)' \{ b_\varphi \Theta_{es} + b_\theta (b_\theta^2 - b_\varphi^2/2) 4\Xi_{es} \} \\ + b_\theta' \{ b_\theta \Theta_{es} + b_\varphi (b_\varphi^2 - b_\theta^2/2) 4\Xi_{es} \}] x dx \end{aligned} \tag{3.129}$$

are the scaling constant and profile shape factor for the pressure term, where

$$\Theta_{es} \equiv \frac{1}{2} \left\{ \frac{J_\theta^2}{J_\varphi^2} x^2 [(\frac{\mathcal{J}_\theta}{x\mathcal{N}_e})']^2 + [(\frac{\mathcal{J}_\varphi}{\mathcal{N}_e})']^2 \right\}, \tag{3.130}$$

$$\Xi_{es} \equiv \frac{1}{4} \frac{J_\theta}{J_\varphi} x (\frac{\mathcal{J}_\theta}{x\mathcal{N}_e})' (\frac{\mathcal{J}_\varphi}{\mathcal{N}_e})' \tag{3.131}$$

are the scaled forms of Θ_e and Ξ_e defined by (3.99) and (3.101) respectively.

The profile shape factors F_E, F_R, and F_π can be estimated with the empirical profiles given in section 3.2, and have been calculated numerically for various values of θ, α_t and α_n. We shall restrict attention to discharges where reversal occurs. From Figure 3.2 and (3.7) we require $\theta \geq 1.4$ for reversal of the toroidal field to occur. We have chosen a range of values for α_n and α_t around their typical values $\alpha_n = 0.5$ and $\alpha_t = 0.25$. The profile shape factors are listed in Tables 3.3, 3.4 and 3.5.

$\theta = 1.4$

α_n	0.3	0.5	0.7	0.9
F_E	0.15	0.14	0.10	0.09

$\theta = 1.6$

α_n	0.3	0.5	0.7	0.9
F_E	0.13	0.11	0.09	0.08

$\theta = 1.8$

α_n	0.3	0.5	0.7	0.9
F_E	0.11	0.09	0.08	0.07

$\theta = 2.0$

α_n	0.3	0.5	0.7	0.9
F_E	0.10	0.08	0.07	0.06

Table 3.3: Values of F_E

$\theta = 1.4$

	α_n			
α_t	0.3	0.5	0.7	0.9
0.05	0.19	0.18	0.16	0.14
0.15	0.27	0.23	0.19	0.16
0.25	0.36	0.28	0.22	0.18
0.35	0.45	0.34	0.26	0.21
0.45	0.57	0.40	0.30	0.23

$\theta = 1.6$

	α_n			
α_t	0.3	0.5	0.7	0.9
0.05	0.17	0.16	0.14	0.12
0.15	0.24	0.20	0.16	0.14
0.25	0.31	0.24	0.19	0.16
0.35	0.40	0.29	0.23	0.18
0.45	0.50	0.35	0.26	0.20

$\theta = 1.8$

	α_n			
α_t	0.3	0.5	0.7	0.9
0.05	0.15	0.14	0.12	0.11
0.15	0.21	0.17	0.15	0.12
0.25	0.27	0.21	0.17	0.14
0.35	0.35	0.26	0.20	0.16
0.45	0.43	0.31	0.23	0.18

$\theta = 2.0$

	α_n			
α_t	0.3	0.5	0.7	0.9
0.05	0.13	0.12	0.11	0.10
0.15	0.18	0.15	0.13	0.11
0.25	0.24	0.19	0.15	0.13
0.35	0.31	0.23	0.18	0.14
0.45	0.38	0.27	0.20	0.16

Table 3.4: Values of F_R

$\theta = 1.4$

	α_n			
α_t	0.3	0.5	0.7	0.9
0.05	1.7	1.9	2.3	2.5
0.15	1.4	1.5	1.7	1.7
0.25	1.2	1.2	1.3	1.3
0.35	1.0	1.0	1.1	1.0
0.45	0.90	0.89	0.87	0.81

$\theta = 1.6$

	α_n			
α_t	0.3	0.5	0.7	0.9
0.05	1.4	1.4	1.6	1.9
0.15	1.1	1.2	1.2	1.4
0.25	0.99	0.99	1.0	1.0
0.35	0.86	0.85	0.83	0.80
0.45	0.75	0.73	0.70	0.65

$\theta = 1.8$

	α_n			
α_t	0.3	0.5	0.7	0.9
0.05	1.2	1.2	1.3	2.3
0.15	0.99	1.0	1.0	1.5
0.25	0.85	0.84	0.85	1.0
0.35	0.74	0.72	0.70	0.76
0.45	0.65	0.62	0.59	0.59

$\theta = 2.0$

	α_n			
α_t	0.3	0.5	0.7	0.9
0.05	1.1	1.1	1.3	2.7
0.15	0.89	0.90	0.97	1.6
0.25	0.76	0.75	0.77	1.1
0.35	0.66	0.64	0.63	0.75
0.45	0.57	0.55	0.52	0.56

Table 3.5: Values of F_π

It can be seen from the equations for A_E, A_R and A_π that (3.123) has a complicated dependence on number density, temperature and θ. To obtain a final expression for the particle confinement time that is not unduly complicated in form, we will retain only the largest term in (3.123).

Taking the ratios of A_E and A_R to A_π we find that

$$\frac{A_E}{A_\pi} = -4.53 \times 10^{-12} \frac{e^2}{k}(\alpha_j + 1)(Z^* \ln \Lambda)^2 \frac{n_{e0}^3}{T_{e0}^4} \frac{B_e}{J_\varphi} a^3, \tag{3.132}$$

and

$$\frac{A_R}{A_\pi} = 9.06 \times 10^{-12} e^2 (Z^* \ln \Lambda)^2 \frac{n_{e0}^4}{T_{e0}^3 J_\varphi^2} a^2. \tag{3.133}$$

Values for $(A_e F_E)/(A_\pi F_\pi)$ which result on adopting the empirical relation between T_{e0} and n_{e0} given by equation (3.61) are listed in Table 3.6 for the typical HBTX values $\alpha_n = 0.5$, $\alpha_t = 0.25$, $Z^* = 2$, $\ln \Lambda = 15$ and $I_\varphi = 220$kA.

An estimate of A_R/A_π shows that this ratio is small for all values of density in the range $1 \leq 10^{-19} n_{e0} \leq 4$.

From these calculations it is clear that

$$|\langle n_e v_r^\pi \rangle| > |\langle n_e v_r^E \rangle| \gg |\langle n_e v_r^R \rangle| \tag{3.134}$$

$10^{-19}n_{e0}$	1	1.5	2	2.5	3	3.5	4
$(A_E F_E)/(A_\pi F_\pi)$	-0.001	-0.009	-0.033	-0.089	-0.18	-0.35	-0.59

Table 3.6: Values of the ratio $(A_E F_E)/(A_\pi F_\pi)$

for $1 \leq 10^{-19}n_{e0} \leq 4$ and $I_\varphi = 220$kA. We can expect inequality (3.134) to be valid for currents greater than 220kA as β_p decreases and T_{e0} increases with increasing current. This implies that the ratio A_E/A_π is a decreasing function of I_φ (cf. equation (3.132)).

Accordingly, we may take as a first approximation that

$$\langle n_e v_r \rangle = A_\pi F_\pi. \tag{3.135}$$

From (3.55) and (3.56) for J_φ and B_e we have

$$\frac{J_\varphi^2}{B_e^2} = \frac{4\theta^2}{\mu_0^2 a^2}\{\alpha_j - 4/\pi^2\}^{-2}. \tag{3.136}$$

Substituting (3.136) into (3.135), we obtain

$$\langle n_e v_r \rangle = 1.80 \times 10^{41} \frac{1}{Z^* \ln \Lambda} \frac{T_{e0}^{5/2}}{n_{e0}^2} \frac{\theta^2}{a^5} F_\pi, \tag{3.137}$$

where F_π is specified in Table 3.5. Substituting equation (3.137) into equation (3.70) for the electron confinement time, we find that

$$\tau_{pe} = 5.6 \times 10^{-42} Z^* \ln \Lambda \frac{n_{e0}^3}{T_{e0}^{5/2}} \frac{a^6}{\theta^2} \frac{A_p}{(1+\alpha_n)F_\pi}. \tag{3.138}$$

It must be noted that the coefficient 5.6×10^{-42} cannot be accurate as we have made some approximations en route, but this equation should at least give the correct scaling law.

3.4 The Energy Confinement Time

For the reasons discussed in Chapter 1, the unexpectedly small values for the energy confinement time τ_E observed in toroidal confinement machines is one of the key problems in fusion research. In this section, we shall apply the cross-field transport coefficients developed by Woods to the RFP and evaluate their usefulness in explaining the energy confinement properties of these machines.

3.4.1 An Expression for the Energy Confinement Time

The energy confinement time τ_E can be calculated in the same way that the electron energy confinement time τ_{Ee} was calculated in 1.3.3. We begin with the total energy equation expressed in the form

$$\frac{\partial}{\partial t}(\tfrac{3}{2}p) + \nabla \cdot (\tfrac{5}{2}p\boldsymbol{v} + \boldsymbol{Q}) = \boldsymbol{v} \cdot \nabla p + R_{ei} \cdot (\boldsymbol{v}_i - \boldsymbol{v}_e) - \boldsymbol{\pi}_i : \nabla \boldsymbol{v}_i - \boldsymbol{\pi}_e : \nabla \boldsymbol{v}_e - \Phi_e - \Phi_i, \tag{3.139}$$

where $\boldsymbol{Q} = \boldsymbol{Q}_e + \boldsymbol{Q}_i$ is the total heat flux vector. After some analysis it can be shown that

$$\frac{\partial \ln W}{\partial t} + \frac{1}{\tau_E} = \frac{1}{\tau_E^*} - \frac{1}{\tau_E^R}, \tag{3.140}$$

where

$$\tau_E \equiv W/[r(\tfrac{5}{2}pv_r + Q_r)]_{r=a}, \tag{3.141}$$

$$\tau_E^* \equiv W/\int_0^a (\boldsymbol{v} \cdot \nabla p + R_{ei} \cdot (\boldsymbol{v}_i - \boldsymbol{v}_e) - \boldsymbol{\pi}_i : \nabla \boldsymbol{v}_i - \boldsymbol{\pi}_e : \nabla \boldsymbol{v}_e) r\, dr, \tag{3.142}$$

$$\tau_E^R \equiv W/\int_0^a (\Phi_i + \Phi_e) r\, dr. \tag{3.143}$$

The term

$$W \equiv \int_0^a \tfrac{3}{2}k(n_e T_e + n_i T_i) r\, dr \tag{3.144}$$

is proportional to the total thermal energy in the torus, and $Q_r = \boldsymbol{Q} \cdot \hat{\boldsymbol{r}}$ is the total radial heat flux.

As with equation (3.65) for τ_{pe}, (3.141) is unsuitable for evaluating τ_E because of the uncertainties in estimates of p, v_r, and Q_r at the limiter. We can, however, avoid this difficulty by employing the averaging method developed by Woods, which we used to estimate τ_{pe} in section 3.3.

To eliminate the mass flux term $[rn_e v_r]_{r=a}$ in (3.65) for τ_{pe}, we assumed steady-state conditions which gave a balance between the mass source term S_e and $\nabla \cdot (n_e \boldsymbol{v}_r)$. This balance enabled $[rn_e v_r]_{r=a}$ to be equated to averaged quantities, eliminating the need for estimating quantities at the limiter. The analogous procedure for determining $[r(\frac{5}{2}pv_r + Q_r)]_{r=a}$ involves volume-weighted averages of the energy source term which appears on the right-hand side of equation (3.139).

If we assume steady-state conditions, the required result is

$$\tau_E = aA_eW/\int_0^a (\tfrac{5}{2}pv_r + Q_r)r\,dr, \tag{3.145}$$

where A_e is defined by

$$A_e \equiv \frac{1}{a}\int_0^a dr \int_o^r \mathcal{P}r^*\,dr^* / \int_0^a \mathcal{P}r\,dr, \tag{3.146}$$

in which

$$\mathcal{P} \equiv \boldsymbol{v}\cdot\nabla p + \boldsymbol{R}_{ei}\cdot(\boldsymbol{v}_i - \boldsymbol{v}_e) - \boldsymbol{\pi}_i : \nabla\boldsymbol{v}_i - \boldsymbol{\pi}_e : \nabla\boldsymbol{v}_e \tag{3.147}$$

is the energy source term. Radiation losses do not appear in (3.147) as they have been separated into the radiation energy confinement time τ_E^R.

There are difficulties associated with evaluating (3.145). As we will demonstrate in the next section, the convective term in (3.145) dominates the losses due to conduction in the outer region of the torus. This suggests that the $\boldsymbol{v}\cdot\nabla p$ term appearing in the equation for $\mathcal{P}$ cannot be neglected, and thus to evaluate A_E we require a knowledge of $v_r(r)$. Without an accurate model for $S_e(r)$ or reasonable estimates of the second derivatives of j, n_e and T_e, it is impossible to calculate $v_r(r)$. Furthermore, since v_r is driven by viscosity, the viscous dissipation functions $\boldsymbol{\pi}_i : \nabla\boldsymbol{v}_i$ and $\boldsymbol{\pi}_e : \nabla\boldsymbol{v}_e$ cannot be consistently neglected. To avoid these difficulties we will proceed as follows.

If we assume that Q_r may be neglected in favor of $5pv_r/2$ in equation (3.141) for τ_E, an assumption we shall justify in the following section, we obtain

$$\tau_E = \frac{\int_0^a \frac{3}{2}pr\,dr}{[r\frac{5}{2}pv_r]_{r=a}}. \tag{3.148}$$

On assuming that $T_e = T_i$ and $Zn_i = n_e$ where Z is constant over the minor radius, (3.148) becomes

$$\tau_E = \frac{\int_0^a \frac{3}{2}n_eT_er\,dr}{\frac{5}{2}[rn_eT_ev_r]_{r=a}}. \tag{3.149}$$

It follows from the empirical profiles for n_e and T_e that their product may be expressed in the form

$$n_eT_e = n_{e0}T_{e0}(1 - r^2/a^2)^{\alpha_n+\alpha_t}. \tag{3.150}$$

If we now substitute (3.150) into (3.149) and compare the resulting expression with equation (3.65) for the particle confinement time, it is apparent that

$$\tau_E = \frac{\frac{3}{2}\int_0^a n_e^\dagger r\, dr}{\frac{5}{2}\left[r n_e^\dagger v_r\right]_{r=a}} = \frac{3}{2}\tau_{pe}(n_e^\dagger), \tag{3.151}$$

where $n_e^\dagger = n_{e0}(1 - r^2/a^2)^{\alpha_n+\alpha_t}$. It follows from the analysis immediately preceeding equation (3.70) (see section 3.3) that

$$\tau_E = \frac{3}{5} a A_p^\dagger \frac{\langle n_e^\dagger \rangle}{\langle n_e^\dagger v_r \rangle}, \tag{3.152}$$

where

$$A_p^\dagger \equiv \frac{\frac{1}{a}\int_0^a dr \int_0^r S_e(1 - r^2/a^2)^{\alpha_t} r^*\, dr^*}{\int_0^a S_e(1 - r^2/a^2)^{\alpha_t} r\, dr}. \tag{3.153}$$

Substituting the mass source function $S_e = S_0\delta(r - r_0)$ into (3.153), we obtain that

$$A_p^\dagger = A_p = 1 - r_0/a. \tag{3.154}$$

The factor $\langle n_e^\dagger v_r \rangle$ in (3.152) can be calculated by replacing n_e with $n_e^\dagger$ in (3.90). The analysis following (3.90) is essentially unchanged, and we obtain the result that

$$\langle n_e^\dagger v_r \rangle = 1.80 \times 10^{41} \frac{1}{Z^* \ln\Lambda} \frac{T_{e0}^{5/2}\theta^2}{n_{e0}^2 a^5} F_\pi^\dagger, \tag{3.155}$$

where

$$F_\pi^\dagger \equiv -\int_0^1 \frac{\mathcal{T}_e^{\frac{7}{2}}}{\mathcal{B}^2}\left[x\left(\frac{b_\varphi}{x}\right)'\left\{b_\varphi\Theta_{es} + b_\theta 2(2b_\theta^2 - b_\varphi^2)\Xi_{es}\right\} + b_\theta'\left\{b_\theta\Theta_{es} + b_\varphi 2(2b_\varphi^2 - b_\theta^2)\Xi_{es}\right\}\right] x\, dx. \tag{3.156}$$

Values for $F_\pi^\dagger$ are listed in Table 3.7.

By substituting (3.155) into (3.152) and noting that $\langle n_e^\dagger \rangle = \frac{1}{1+\alpha_n+\alpha_t} n_{e0}$, we obtain the energy confinement time

$$\tau_E = 3.3 \times 10^{-42} Z^* \ln\Lambda \frac{n_{e0}^3 a^6}{T_{e0}^{\frac{5}{2}}\theta^2} \frac{A_p}{(1 + \alpha_n + \alpha_t) F_\pi^\dagger}. \tag{3.157}$$

To derive (3.157) for τ_E we made the assumption that the energy losses from the torus are dominated by convection. To justify this assumption we need to make an estimate of the radial heat flux which, in turn, requires a value for the plasma thermal diffusivity.

$\theta = 1.4$

α_t \ α_n	0.3	0.5	0.7	0.9
0.05	1.6	1.8	2.1	2.3
0.15	1.3	1.3	1.4	1.5
0.25	1.0	1.0	1.1	1.0
0.35	0.85	0.84	0.82	0.75
0.45	0.72	0.70	0.66	0.59

$\theta = 1.6$

α_t \ α_n	0.3	0.5	0.7	0.9
0.05	1.3	1.4	1.5	1.8
0.15	1.0	1.1	1.1	1.1
0.25	0.86	0.85	0.83	0.80
0.35	0.71	0.69	0.66	0.60
0.45	0.61	0.58	0.53	0.47

$\theta = 1.8$

α_t \ α_n	0.3	0.5	0.7	0.9
0.05	1.1	1.2	1.3	2.1
0.15	0.90	0.90	0.92	1.2
0.25	0.74	0.72	0.70	0.76
0.35	0.61	0.59	0.56	0.54
0.45	0.52	0.49	0.45	0.41

$\theta = 2.0$

α_t \ α_n	0.3	0.5	0.7	0.9
0.05	1.0	1.0	1.2	2.4
0.15	0.81	0.80	0.84	1.3
0.25	0.66	0.64	0.63	0.75
0.35	0.54	0.52	0.49	0.50
0.45	0.46	0.43	0.40	0.37

Table 3.7: Values of $F_\pi^\dagger$

3.4.2 The Plasma Thermal Diffusivity

An expression for the second-order heat flux in a RFP was developed in Chapter 2, the relevant result being (cf. (2.30))

$$\boldsymbol{Q} = -\frac{5}{2}\frac{kp}{\mathcal{Q}B}\frac{2r\Gamma(q^2+\epsilon^2)^{1/2}}{C}\boldsymbol{b}\times\nabla\boldsymbol{v}\cdot\nabla T. \tag{3.158}$$

where $\mathcal{Q}$ is the fluid species charge. Substituting $\boldsymbol{b} = b_\theta\hat{\boldsymbol{\theta}} + b_\varphi\hat{\boldsymbol{\varphi}}$ into (3.158), we obtain for the radial heat flux

$$Q_r = \hat{\boldsymbol{r}}\cdot\boldsymbol{Q} = -\frac{5}{2}\frac{kp}{\mathcal{Q}B}\frac{2r\Gamma(q^2+\epsilon^2)^{1/2}}{C}HT', \tag{3.159}$$

where H is defined by

$$H \equiv \boldsymbol{b}\times\hat{\boldsymbol{r}}\cdot\nabla\boldsymbol{v}\cdot\hat{\boldsymbol{r}} = \tfrac{1}{2}r(\frac{v_\theta}{r})'b_\varphi - \tfrac{1}{2}v_\varphi' b_\theta. \tag{3.160}$$

Let H_i and H_e be H evaluated for the ion and electron fluids respectively. Then it follows from (3.106) and (3.107) that

$$H_i = -G^{1/2}H_e, \tag{3.161}$$

where G is defined by (3.104). It follows from (3.161) and (3.159) that

$$\frac{Q_{er}}{Q_{ir}} = \frac{8.91}{Z^2}\left(\frac{T_i}{T_e}\right)^{\frac{3}{4}} A^{\frac{3}{4}} \frac{T_e'}{T_i'}, \tag{3.162}$$

where $A \equiv M_i/M_p$ is the ion to proton mass ratio. For typical RFP values of $T_i \approx T_e$, $T_i' \approx T_e'$ and a hydrogenous plasma, equation (3.162) yields $Q_{er} \sim 9Q_{ir}$. As we are making an estimate of Q_r, we shall neglect Q_{ir} in subsequent calculations.

We can find an estimate of Q_{er} as follows. From (3.112), (3.113) and (3.160) evaluated for the electron fluid, we obtain

$$\begin{aligned} H_e &= -\frac{1}{1-G^{1/2}}\{\tfrac{1}{2}r\left(\frac{j_\theta}{en_e r}\right)' b_\varphi - \tfrac{1}{2}\left(\frac{j_\varphi}{en_e}\right)' b_\theta\} \\ &\simeq -\frac{1}{2e}\{r\left(\frac{j_\theta}{n_e r}\right)' b_\varphi - \left(\frac{j_\varphi}{n_e}\right)' b_\theta\}. \end{aligned} \tag{3.163}$$

Substituting (3.163) into (3.159) evaluated for the electron fluid and adopting the normalised profiles for j_θ, j_φ, n_e, T_e and B defined in section 3.2.2, yields

$$Q_{er} = \frac{5k^{3/2}m_e^{1/2}}{\sqrt{8}e^2}\frac{T_{e0}^{3/2}J_\varphi}{B_e}\Gamma\mathcal{F}_e, \tag{3.164}$$

where

$$\mathcal{F}_e \equiv \frac{x^2\mathcal{N}_e\mathcal{T}_e^{1/2}\mathcal{T}_e'}{\mathcal{B}b_\theta}\left\{\frac{J_\theta}{J_\varphi}x(\frac{\mathcal{J}_\theta}{x\mathcal{N}_e})'b_\varphi - (\frac{\mathcal{J}_\varphi}{\mathcal{N}_e})'b_\theta\right\}, \qquad \left(' \equiv \frac{\partial}{\partial x}\right), \tag{3.165}$$

and we have used the result $(q^2+\epsilon^2)^{1/2} = (\epsilon^2 B_\varphi^2/B_\theta^2 + \epsilon^2)^{1/2} = \epsilon/B_\theta$. Noting that $j \times \boldsymbol{B} = \nabla p$, we can rewrite $\mathcal{F}_e$ as

$$\mathcal{F}_e = \frac{x^2\mathcal{T}_e^{1/2}\mathcal{T}_e'}{\mathcal{B}b_\theta}\left\{\frac{J_\theta}{J_\varphi}x(\frac{\mathcal{J}_\theta}{x})'b_\varphi - \mathcal{J}_\varphi' b_\theta + \frac{1}{J_\varphi}\frac{\mathcal{N}_e'}{\mathcal{N}_e}\frac{p'}{B}\right\}. \tag{3.166}$$

From the estimate $p'/J_\varphi B \sim \langle p\rangle/aJ_\varphi B_{\theta a} = \beta_p(\alpha_j - 4/\pi^2)/4B_{\theta a}$, it is clear that the number density gradient term in (3.166), which is of the order β_p, can be neglected.

As we shall explain, it follows from (3.164) that convection must be the dominant transport process in the RFP, at least in the region $a/2 \leq r \leq a$. The strongest reason for this conclusion is that an evaluation of $\mathcal{F}_E$ using the experimentally determined profiles for j_θ, j_φ, n_e and T_e leads to the result that

x	$\Gamma^{1/2}\mathcal{F}_E$
0.1	-4.5×10^{-5}
0.2	-7.4×10^{-4}
0.3	-4.0×10^{-3}
0.4	-1.3×10^{-2}
0.5	-3.4×10^{-2}
0.6	-7.4×10^{-2}
0.7	-0.13
0.8	-0.22
0.9	-0.30
0.975	-0.33

Table 3.8: Values of the factor $\Gamma\mathcal{F}_E$ as a function of $x \equiv r/a$

$Q_{er} < 0$, i.e. the heat flux due to conduction is inward. This is a consequence of H_e being negative for the empirical profiles adopted for j_θ and j_φ. The sign of H_e could be changed by a judicious choice of the current density profiles near the axis where the two terms determining H_e are in near balance (cf. (3.163)). However, any reasonable choice for j_θ and j_φ in the RFP will be such that j'_θ has a zero in the neighbourhood of $r \sim a/2$ where $j'_\varphi < 0$. Furthermore, in the outer region of the discharge, the j'_φ term dominates H_e ($b_\theta \gg b_\varphi$). Thus we conclude that H_e will be negative, at least in the outer region of the discharge, for any current profiles representative of those found in the RFP.

The variation of Q_{er} across the minor radius is determined by the factor $\Gamma^{1/2}\mathcal{F}_E$, and a list of values for this factor can be found in table 3.8 The factor Γ has been calculated by substituting equation (3.50) for B_θ into (1.89) and neglecting the small β_p contribution to Λ (see the discussion below).

It follows from these considerations that Woods' theory predicts the radial heat flux in the RFP to be inward, in the outer region of the discharge at least. Hence for Woods' theory of second-order heat transport applied to the RFP to be correct, it appears that convection must dominate conduction in the outer region of the discharge.

We shall investigate this hypothesis by considering the ratio of conduction to

convection. Defining $R \equiv -\langle Q_{er} \rangle / \langle \frac{5}{2} p v_r \rangle$, we obtain from (3.164) and (3.155)

$$R = 2.7 \times 10^{-31} \frac{J_\varphi Z^* \ln \Lambda}{B_e \theta^2} \frac{n_{e0}^2}{T_{e0}^2} a^5 \frac{\langle \Gamma \mathcal{F}_E \rangle}{F_\pi^\dagger}, \tag{3.167}$$

where $\langle \Gamma \mathcal{F}_E \rangle \equiv (2/a^2) \int_0^a \Gamma \mathcal{F}_E \, r dr$.

In order to estimate R we must now calculate the factor Γ, defined in (1.89). We have that

$$\begin{aligned} \Gamma &= \frac{B_\varphi^2 - \Lambda B_\theta^2}{B^2} \\ &= \frac{B_\varphi^2 - (\beta_p - \beta_{p0} + l_i/2 - 1) B_\theta^2}{B^2} \\ &= 1 - b_\theta^2 (\beta_p - \beta_{p0} + l_i/2), \end{aligned} \tag{3.168}$$

where, from (1.84),

$$l_i(x) = \frac{2}{\mathcal{B}_\theta^2(x)} \int_0^x \mathcal{B}_\theta^2(x^*) \, dx^*. \tag{3.169}$$

Substituting for $\mathcal{B}_\theta$ in (3.169) and integrating numerically results in the values for l_i listed in table 3.10. As $\beta_p - \beta_{p0}$ adds only a small correction to Γ, as a first approximation we may neglect these terms in (3.168).

Values of Γ obtained from (3.168) (neglecting the β_p term) are listed in table 3.10. We can see from these calculations that Γ is going to decrease the thermal conductivity, and by assuming that $\Gamma = 1$, we will obtain an upper estimate for the ratio R viz:

$$R = 2.7 \times 10^{-31} \frac{J_\varphi Z^* \ln \Lambda}{B_e \theta^2} \frac{n_{e0}^2}{T_{e0}^2} a^5 \frac{\langle \mathcal{F}_E \rangle}{F_\pi^\dagger}, \tag{3.170}$$

Values for $\langle \mathcal{F}_E \rangle$ are listed in Table 3.9.

We find from (3.170) that, assuming $\Gamma = 0.3$ and for the typical HBTX values $n_{e0} = 3 \times 10^{19} \mathrm{m}^{-3}$, $Z^* = 2$, $\theta = 1.6$, $B_e = 0.1\mathrm{T}$, $I_\varphi = 220\mathrm{kA}$ and (from (3.61)) $T_{e0} = 3.6 \times 10^6 \mathrm{K}$, that $R \sim 0.1$. We conclude that conduction is not the dominant process determining the energy confinement time. In view of the empirical evidence, i.e. that the radial heat flux is outward, we will assume that Q_{er} may be neglected in favor of $5pv_r/2$ for the purposes of energy confinement time calculations.

$\theta = 1.4$

α_t \ α_n	0.3	0.5	0.7	0.9
0.05	0.05	0.08	0.10	0.12
0.15	0.12	0.17	0.22	0.27
0.25	0.15	0.21	0.27	0.33
0.35	0.17	0.23	0.28	0.34
0.45	0.17	0.22	0.28	0.33

$\theta = 1.6$

α_t \ α_n	0.3	0.5	0.7	0.9
0.05	0.06	0.08	0.10	0.11
0.15	0.14	0.17	0.21	0.25
0.25	0.17	0.21	0.26	0.30
0.35	0.19	0.23	0.27	0.31
0.45	0.19	0.22	0.26	0.30

$\theta = 1.8$

α_t \ α_n	0.3	0.5	0.7	0.9
0.05	0.07	0.08	0.09	0.10
0.15	0.15	0.17	0.20	0.22
0.25	0.19	0.22	0.24	0.27
0.35	0.20	0.23	0.26	0.28
0.45	0.20	0.23	0.25	0.27

$\theta = 2.0$

α_t \ α_n	0.3	0.5	0.7	0.9
0.05	0.07	0.08	0.09	0.09
0.15	0.16	0.17	0.19	0.20
0.25	0.20	0.22	0.23	0.24
0.35	0.21	0.23	0.24	0.25
0.45	0.21	0.22	0.24	0.25

Table 3.9: Values of $(a^2/2)\langle \mathcal{F}_E \rangle$

x	0.1	0.2	0.3	0.4	0.5	0.6	0.7	0.8	0.9	1.0
l_i	0.005	0.081	0.049	0.093	0.159	0.259	0.411	0.648	1.024	1.607
Γ	1.000	0.999	0.994	0.981	0.952	0.898	0.809	0.677	0.492	0.220

Table 3.10: Values of l_i and Γ

3.4.3 The Energy Confinement Time for Non Steady-State Conditions

All the confinement calculations to this point have been made assuming steady-state number density and temperature profiles. However, in the RFP these assumptions are not always valid. In HBTX, wall loading (the diffusion of gas from the confinement vessel walls into the plasma) maintains a steady-state number density profile, but this is not the case for all machines. In ETA-BETA-II, for example, both the number density and temperature profiles vary throughout a typical discharge.

A Non Steady-State Number Density Profile

Time variations in the number density profile can be accommodated in a calculation of τ_E by treating $\partial n_e/\partial t$ as an equivalent mass source term. Since—granted the assumptions in the preceeding section—τ_E can be calculated from τ_{pe} (cf. (3.151)), it is sufficient at this point to calculate the effect of a non-zero $\partial n_e/\partial t$ on τ_{pe}.

We begin by defining an 'effective' source term

$$S_e^* = S_e - \frac{\partial n_e}{\partial t}. \tag{3.171}$$

Following the same analysis as in section 3.3, we obtain the result that

$$\tau_{pe} = aA_p^* \frac{\langle n_e \rangle}{\langle n_e v_r \rangle}, \tag{3.172}$$

where

$$A_p^* \equiv \frac{\frac{1}{a}\int_0^a dr \int_0^r S_e^* r^* dr^*}{\int_0^a S_e^* r dr}. \tag{3.173}$$

We can simplify the analysis somewhat by assuming that the mass source term is reasonably well approximated by $S_e = S_0\delta(r - r_0)$. By substituting for S_e in (3.173), we find that

$$A_p^* = \frac{aS_0r_0(1 - r_0/a) - \frac{1}{a}\int_0^a dr \int_0^r \frac{\partial n_e}{\partial t} r^* dr^*}{aS_0r - \int_0^a \frac{\partial n_e}{\partial t} r\, dr}. \tag{3.174}$$

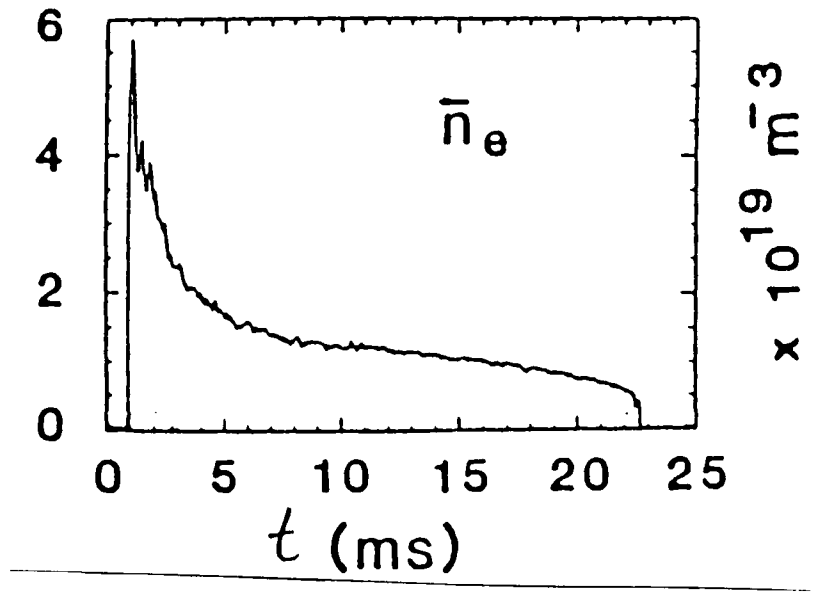

Figure 3.11: Plot of n_e versus t for ZT-40M (from Wurden *et al.* 1987)

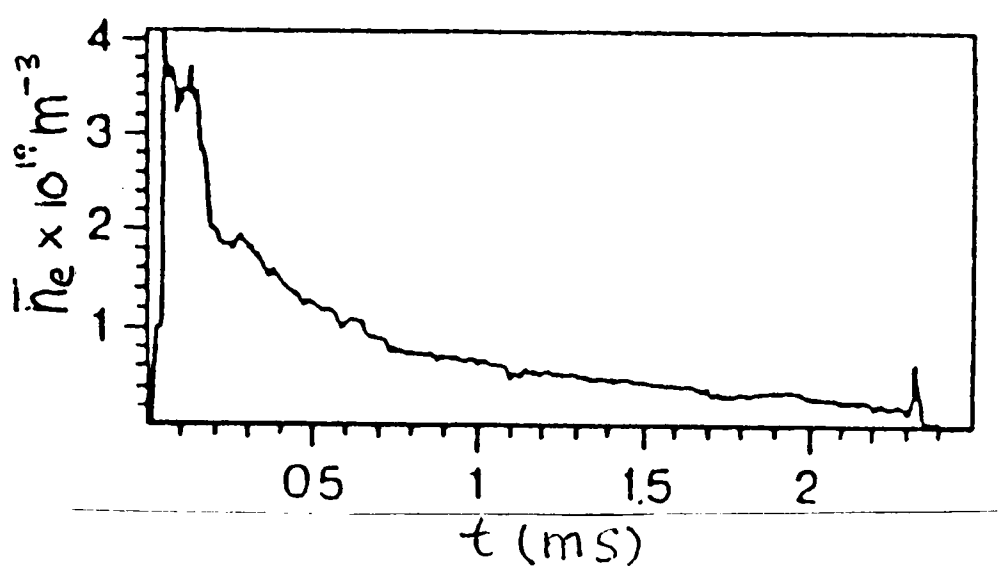

Figure 3.12: Plot of n_e versus t for ETA-BETA-II (from Innocente *et al.* 1987)

If we assume that the density profiles assumed for HBTX are representative of those found in RPF machines in general, and that the time variation in n_e is of the form $n_e(r,t) = n_e(r,0)e^{-t/\tau_n}$, then

$$n_e(r,t) = n_{e0}(1 - r^2/a^2)^{\alpha_n} e^{-t/\tau_n}. \tag{3.175}$$

In (3.175), τ_n is a time constant that characterizes the decay time of the number density profile, and which is assumed to be of the same order as the discharge duration. There is some experimental evidence for an exponential decay law for number density profiles in discharges without fuel pellet injection, gas puffing or wall loading. Representative plots of n_e versus t in the absence of gas puffing and pellet injection are shown in Figures 3.11 and 3.12.

Substitution of (3.175) into (3.174) yields

$$A_p^* = \frac{S_0 r_0(1 - r_0/a) - f_t \dfrac{a n_{e0}}{2(1+\alpha_n)}\left\{1 - 2^{2\alpha_n+2}\dfrac{\Gamma^2(2\alpha_n+2)}{\Gamma(4\alpha_n+4)}\right\}}{S_0 r_0 - f_t \dfrac{a n_{e0}}{2(1+\alpha_n)}}, \tag{3.176}$$

where

$$f_t \equiv \frac{1}{n_e(r,0)}\frac{\partial n_e}{\partial t} = -\frac{1}{\tau_n}e^{-t/\tau_n}, \tag{3.177}$$

and Γ denotes the gamma function. In (3.176) we have used the standard result: $\int_0^1 (1-x^2)^{\alpha+1}\,dx = 2^{(2\alpha+1)}\Gamma^2(2\alpha+2)/\Gamma(4\alpha+4)$.

We can rewrite (3.176) by dividing both numerator and denominator of (3.176) by $S_0 r_0$ to obtain

$$A_p^* = \frac{1 - \dfrac{r_0}{a} + \gamma\left\{1 - 2^{2\alpha_n+2}\dfrac{\Gamma^2(2\alpha_n+2)}{\Gamma(4\alpha_n+4)}\right\}}{1+\gamma}, \tag{3.178}$$

where

$$\gamma \equiv -f_t \frac{a n_{e0}}{2 r_0 S_0 (1+\alpha_n)}. \tag{3.179}$$

The function γ has a particular physical significance. Noting that

$$\left\langle \frac{\partial n_e}{\partial t} \right\rangle = f_t \frac{n_{e0}}{1+\alpha_n} \tag{3.180}$$

and

$$\begin{aligned} \langle S_e \rangle &\equiv \frac{2}{a^2}\int_0^a S_0 \delta(r - r_0)\, r\, dr \\ &= \frac{2 r_0}{a} S_0, \end{aligned} \tag{3.181}$$

it follows from (3.179) that

$$\gamma = -\frac{\left\langle \dfrac{\partial n_e}{\partial t} \right\rangle}{\langle S_e \rangle}. \tag{3.182}$$

That is, γ is the ratio of the volume-weighted average of $\partial n_e/\partial t$ with the similarly averaged electron source term.

We can obtain an estimate for γ as follows. In the absence of pellet injection, the main source of electrons in the plasma comes from the ionization of recycled,

		r_0/a				
		0.6	0.7	0.8	0.9	0.95
f_α	0.1	0.58	0.57	0.56	0.55	0.55
	0.2	0.56	0.54	0.52	0.50	0.49
	0.5	0.50	0.45	0.40	0.35	0.33
	1.0	0.40	0.30	0.20	0.10	0.05

Table 3.11: Values of A_p^*

neutral gas. This point was argued in regard to HBTX in section 3.3.2 and may be assumed to hold for ETA-BETA-II where impurity levels are commensurate with those found in HBTX. We shall assume that a fraction f_α of the plasma flux to the discharge limiter is recycled, i.e.

$$\int_0^a S_e r\, dr = f_\alpha [r n_e v_r]_{r=a}. \tag{3.183}$$

Substituting (3.183) into mass conservation written for the electron fluid yields

$$\frac{\langle \frac{\partial n_e}{\partial t} \rangle}{\langle S_e \rangle} = 1 - \frac{1}{f_\alpha}, \tag{3.184}$$

whence (3.178) may be written

$$A_p^* = f_\alpha (1 - r_0/a) + (1 - f_\alpha)\Big\{1 - 2^{2\alpha_n+2} \frac{\Gamma^2(2\alpha_n + 2)}{\Gamma(4\alpha_n + 4)}\Big\}. \tag{3.185}$$

Values of A_p^* for $\alpha_n = 0.5$ and various values of f_α and r_0/a are listed in Table 3.11.

Integration the mass conservation equation for the electrons, (3.62), yields

$$\int_0^a \frac{\partial n_e}{\partial t} r dr + [r n_e v_r]_{r=a} = \int_0^a S_e\, r dr. \tag{3.186}$$

With the help of (3.183), (3.186) may be rewritten as

$$f_\alpha = 1 + \frac{\int_0^a \frac{\partial n_e}{\partial t} r dr}{[r n_e v_r]_{r=a}}. \tag{3.187}$$

From the definition of the electron confinement time τ_{pe} and (3.187), we obtain

$$f_\alpha = 1 + \tau_{pe} \frac{\partial}{\partial t} \ln\Big(\int_0^a n_e r\, dr\Big). \tag{3.188}$$

Substituting (3.175) into (3.188), we obtain

$$f_\alpha = 1 - \frac{\tau_{pe}}{\tau_n} e^{-t/\tau_n}. \tag{3.189}$$

We can obtain an estimate for f_α from (3.189), by using experimental values for τ_{pe} and τ_n. Although employing an experimental value for τ_{pe} to obtain an estimate for τ_E introduces a circularity into the analysis, without an independent measurement of S_e this difficulty is unavoidable.

For the reasons outlined earlier in this chapter, experimental estimations of the particle confinement time are difficult to make. However, from equation (3.151) we have that $\tau_{pe} \sim 5\tau_E/2$ for a discharge where losses are dominated by convection. For ETA-BETA-II, $\tau_E \sim 100\mu$s (Ortolani and Valisa 1987). A value for τ_n can be estimated from the decay rate of the number density in the absence of pellet injection and wall loading. From results due to Innocente and Martini (1987) (see Figure 3.6), $\tau_n \sim 500\mu$s. Taking an average value of $t = 1$ms for the exponential factor in (3.189), we obtain the estimate $f_\alpha \sim 0.93$. From (3.184) (3.181) and our estimate for f_α, we find that $\gamma \sim 0.07$

A Non Steady-State Temperature Profile

If we were to perform an analysis of τ_E which included energy losses due to conduction, time variations in T_e and T_i could be accommodated in the same way that number density variations were accounted for. That is, an 'effective steady-state' energy source term $u_E^* \equiv u_E - (3/2)(\partial p v_r)/\partial t$ would be used when estimating the energy flux term $[r(5pv_r/2 + Q_r)]_{r=a}$ at the limiter.

However, as we are assuming that convection driven by viscosity dominates energy losses, such an analysis is not appropriate. Our result, $\tau_E = (3/5)\tau_{pe}(n_e^\dagger)$, which we derived for steady-state conditions, is also valid for non-steady state temperature profiles, provided that convection dominates energy losses. Thus equation (3.157) correctly describes the energy confinement time in non-steady state conditions, provided A_p is replaced by A_p^* if time variations in the number density profile are present.

3.5 Comparision with Experiment

In section 3.3 and 3.4 we derived expressions for the energy confinement time τ_E and the electron confinement time τ_{pe} in RFPs. It is difficult to compare these times with experiment for two reasons.

First, because of the problems associated with making measurements of variables in plasma discharges, there are too few measurements of the necessary parameters. This is particularly true for the RFP, as experiments with these machines are not funded at the same level as those with the tokamak. For example, to the author's knowledge, accurate measurements of the radial variation in number density and temperature profiles for HBTX have not been published.

Secondly, *raw* data are not often published, so that it is not always clear what models have been employed to arrive at the results presented.

Notwithstanding these difficulties, we shall attempt to compare equations (3.138) and (3.157) for τ_{pe} and τ_E with experiment.

3.5.1 The Particle Confinement Time

Equation (3.138) for the electron confinement time is

$$\tau_{pe} = 5.6 \times 10^{-42} Z^* \ln\Lambda \frac{n_{e0}^3}{T_{e0}^{\frac{5}{2}}} \frac{a^6}{\theta^2} \frac{A_p}{(1+\alpha_n)F_\pi}, \tag{3.190}$$

where F_π is given in Table 3.5 and A_p, defined by (3.69), depends on the distribution of the electron source term S_e across the minor radius.

We made an estimate of A_p in section 3.3.1 and found

$$A_p = 0.075\left(\frac{n_{e0}}{10^{19}}\right)^{-0.2}\left(\frac{T_{e0}}{1.16\times 10^6}\right)^{-0.12}. \tag{3.191}$$

It is not possible to test the scaling laws implied by (3.190), as empirical scaling laws for τ_p are not available in the literature. We do, however, have an estimate of $\tau_p^* \equiv \langle n_e\rangle/\langle S_e\rangle$. Spectroscopic measurements of a Carbon V transition line in HBTX (Carolan *et al.* 1987) have indicated that $\tau_p^* \simeq 100\mu$s. Taking the typical HBTX values $n_{e0} = 3.0\times 10^{19}\mathrm{m}^{-3}$, $\theta = 1.6$, $\alpha_n = 0.5$, $\alpha_t = 0.25$, we find

from (3.61) that $T_{e0} = 3.6\times10^6$K and $F_\pi = 0.99$. Substituting (3.191) into (3.190) and taking $Z^* = 2$, $\ln\Lambda = 15.5$, we obtain $\tau_{pe} \sim 650\mu$s. The agreement between τ_p^* and τ_{pe} is reasonable considering the approximations made in computing both quantities, and the sensitivity of τ_{pe} to limiter position.

3.5.2 The Energy Confinement Time

The energy confinement time, τ_E has been studied experimentally for HBTX. Bodin (1987) has given a number of results which will enable us to test the scaling of (3.157) for τ_E. This equation reads

$$\tau_E = 3.3\times10^{-42} Z^* \ln\Lambda \frac{n_{e0}^3}{T_{e0}^{\frac{5}{2}}} \frac{a^6}{\theta^2} \frac{A_p}{(1+\alpha_n+\alpha_t)F_\pi^\dagger}, \tag{3.192}$$

where $F_\pi^\dagger$ is given in Table 3.7.

To test (3.192) against Bodin's observations, we need to deduce the steady-state energy balance condition by equating τ_E with the energy replacement time τ_E^*. As was noted in section 3.4, a complete calculation of τ_E^* requires a detailed knowledge of v_r and the viscous dissipation function. However, an estimate of τ_E^* made by assuming that ohmic dissipation is the dominant heating mechanism is sufficient for our present purposes.

Thus an approximate expression for τ_E^* may be obtained from (3.142) by neglecting viscosity and the $\boldsymbol{v}\cdot\nabla p$ term. We have

$$\tau_E^* = \frac{W}{\int_0^a \boldsymbol{R}_{ei}\cdot(\boldsymbol{v}_i-\boldsymbol{v}_e)\,r\,dr}, \tag{3.193}$$

where $W \equiv \int_0^a \frac{3}{2}p\,r\,dr$. From (3.83) and $\boldsymbol{j} = en_e(\boldsymbol{v}_i-\boldsymbol{v}_e)$ we obtain

$$\begin{aligned}\boldsymbol{R}_{ei}\cdot(\boldsymbol{v}_i-\boldsymbol{v}_e) &= \boldsymbol{j}\cdot\boldsymbol{\eta}\cdot\boldsymbol{j}\\ &= \eta_{||}\boldsymbol{j}\cdot\boldsymbol{bb}\cdot\boldsymbol{j}+\eta_\perp(\boldsymbol{j}\cdot\boldsymbol{j}-\boldsymbol{j}\cdot\boldsymbol{bb}\cdot\boldsymbol{j})\\ &= \eta_{||}(j_\theta b_\theta + j_\varphi b_\varphi)^2+\eta_\perp(j_\theta b_\varphi - j_\varphi b_\theta)^2. \end{aligned}\tag{3.194}$$

where we have used the substitution $\boldsymbol{\eta} = \eta_{||}\mathbf{1}+\eta_\perp(\mathbf{1}-\boldsymbol{bb})$ and $j_\theta^2+j_\varphi^2-(j_\theta b_\theta + j_\varphi b_\varphi)^2 = (j_\theta b_\varphi - j_\varphi b_\theta)^2$. The dominant term in (3.194) is the first. This follows from the estimates $j_\theta b_\theta + j_\varphi b_\varphi \sim I_\varphi/(\pi a^2)$ and $j_\theta b_\varphi - j_\varphi b_\theta = p'/B \sim p/(aB_\theta) =$

α_t	0.05	0.15	0.25	0.35	0.45
$\mathcal{F}_p$	0.52	0.55	0.58	0.61	0.65

Table 3.12: The function $\mathcal{F}_p$ for $\theta = 1.6$

$\beta_p I_\varphi/(4\pi a^2)$. So $(j_\theta b_\varphi - j_\varphi b_\theta)/(j_\theta b_\theta + j_\varphi b_\varphi) \sim \beta_p/4$ and typically $\beta_p \sim 0.1$. So we shall adopt the estimate

$$\boldsymbol{R}_{ei} \cdot (\boldsymbol{v}_i - \boldsymbol{v}_e) = \eta_{||}(j_\theta b_\theta + j_\varphi b_\varphi)^2, \tag{3.195}$$

where, from $\eta_{||} = \sigma_{||}^{-1} \simeq m_e/2e^2 n_e \tau_e$ (cf. (1.26)),

$$\eta_{||} = \frac{64.5 Z^* \ln \Lambda}{T_{e0}^{3/2}}. \tag{3.196}$$

Integrating (3.195) we obtain

$$\int_0^a \boldsymbol{R}_{ei} \cdot (\boldsymbol{v}_i - \boldsymbol{v}_e)\, r dr = \frac{64.5 Z^* \ln \Lambda}{T_{e0}^{3/2}} J_\varphi^2 a^2 \mathcal{F}_p, \tag{3.197}$$

where

$$\mathcal{F}_p \equiv \int_0^1 \left(\frac{J_\theta}{J_\varphi}\mathcal{J}_\theta b_\theta + \mathcal{J}_\varphi b_\varphi\right)^2 \mathcal{T}_e^{-3/2}\, x dx, \qquad (x \equiv r/a). \tag{3.198}$$

Values for the profile shape factor are given in Table 3.12. For W we have from (3.144)

$$\begin{aligned} W &= \int_0^a \tfrac{3}{2} k 2 n_e T_e\, r dr \\ &= \frac{3}{2}\frac{k n_{e0} T_{e0}}{1 + \alpha_n + \alpha_t} a^2, \end{aligned} \tag{3.199}$$

where we have assumed $T_i = T_e$.

Substituting (3.199) and (3.197) into (3.193) we find that

$$\tau_E^* = \frac{3k\pi^2}{2(1 + \alpha_n + \alpha_t)} \frac{(\alpha_j - 4/\pi^2)^2}{64.5 \mathcal{F}_p} \frac{n_{e0} T_{e0}^{5/2}}{I_\varphi^2 Z^* \ln \Lambda} a^4, \tag{3.200}$$

where J_φ has been eliminated by equation (3.54), viz:

$$J_\varphi = \frac{I_\varphi}{\pi a^2}(\alpha_j - 4/\pi^2)^{-1}. \tag{3.201}$$

On adopting the values $\alpha_j = 0.87$, $\alpha_n = 0.5$ and $\alpha_t = 0.25$, we obtain from (3.200)

$$\tau_E^* = 3.91 \times 10^{-25} \frac{n_{e0} T_{e0}^{5/2}}{I_\varphi^2 Z^* \ln \Lambda} a^4 \mathcal{F}_p^{-1}. \tag{3.202}$$

By equating (3.202) and (3.192) we can determine a relation between T_{e0}, n_{e0} and I_φ. To enable a comparison with experiment, we shall deduce a value for T_{e0} in terms of n_{e0} and I_φ. Equating (3.202) and (3.192), and solving for T_{e0} we obtain

$$T_{e0}^5 = 8.5 \times 10^{-18} \frac{(Z^* \ln \Lambda)^2}{\theta^2} n_{e0}^2 I_\varphi^2 a^2 \frac{A_p \mathcal{F}_p}{(1 + \alpha_n + \alpha_t) F_\pi^\dagger}, \tag{3.203}$$

where A_p is given by (3.191). On adopting the typical HBTX values $\theta = 1.6$, $\alpha_n = 0.5$, $\alpha_t = 0.25$, $Z^* = 2$ and $\ln \Lambda = 15.5$ we find that

$$T_{e0} = 5.7 \times 10^{-3} n_{e0}^{0.35} I_\varphi^{0.39} a^{0.39}, \tag{3.204}$$

where in (3.203), we have set $F_\pi^\dagger = 0.85$ and $\mathcal{F}_p = 0.58$.

It is interesting to compare (3.204) with the relations for T_e obtained by An *et al.* (1984) and Henderson and Robinson (1982). An *et al.* considered enhanced thermal conductivity due to tearing modes, and obtained the scaling law

$$T_e \propto I_\varphi^{0.7}, \tag{3.205}$$

on balancing heat losses with ohmic heating, and assuming that $n \propto I_\varphi$.

Hender and Robinson considered enhanced losses due to resistive g modes, and deduced that

$$T_e \propto I_\varphi^{0.5} a^{0.4} \tag{3.206}$$

for a collisional plasma, on adopting the empirical density dependence $n \propto I^\alpha$; $0.5 < \alpha < 1$.

Bodin (1987) has published graphs of β_p versus n_e (I_φ constant), β_p versus I_φ and T_e versus I_φ for HBTX. We test the scaling predicted by (3.204) with each of these curves below.

The Poloidal Beta as a Function of Electron Density

Equation (3.204) can be rewritten as a scaling law for β_p as follows. Noting that $B_{\theta a} = \mu_0 I_\varphi / 2\pi a$ and, if $T_i = T_e$, $\langle p \rangle = 2k n_{e0} T_{e0} / (1 + \alpha_n + \alpha_t)$, we find from (1.51)

$$\beta_p = \frac{(4\pi a)^2}{\mu_0} \frac{k n_{e0} T_{e0}}{1 + \alpha_n + \alpha_t} \frac{1}{I_\varphi^2}. \tag{3.207}$$

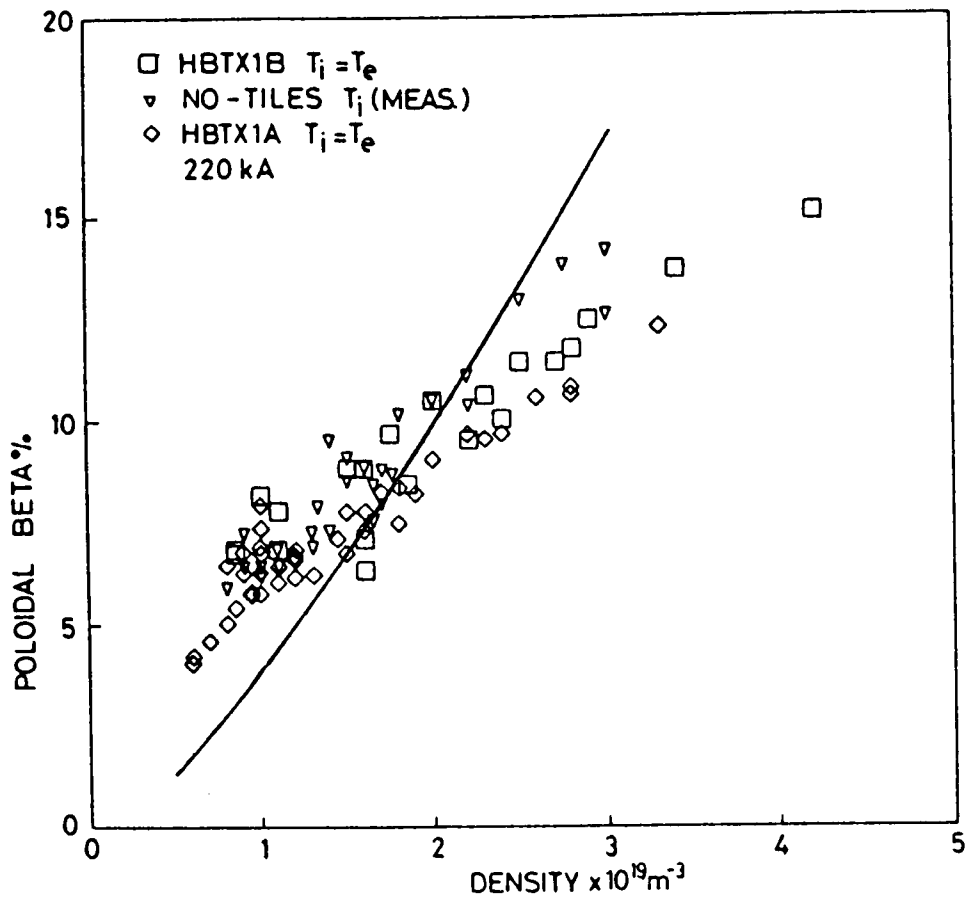

Figure 3.13: Plot of β_p versus n_e: Theory and Experiment

Substituting (3.204) into (3.207), we obtain

$$\beta_p = 2.1 \times 10^{-19} n_{e0}^{1.35} I_\varphi^{-1.61}. \tag{3.208}$$

Values of β_p are plotted against density with experimental results in Figure 3.13 for the constant current $I_\varphi = 220$kA. The agreement between theory and experiment is quite good, although the theoretical curve in Figure 3.13 is a little steeper than a line drawn through the experimental results.

The Poloidal Beta as a Function of Toroidal Current

The experimental results for β_p versus I_φ plotted in Figure 3.14 are not a constant number density, so there is a scatter of points for a given current. The values of β_p predicted by (3.208) for the typical HBTX value $n_{e0} = 3 \times 10^{19}\text{m}^{-3}$ are plotted in Figure 3.14. The fit between theory and experiment is better for high currents, but the overall agreement is satisfactory.

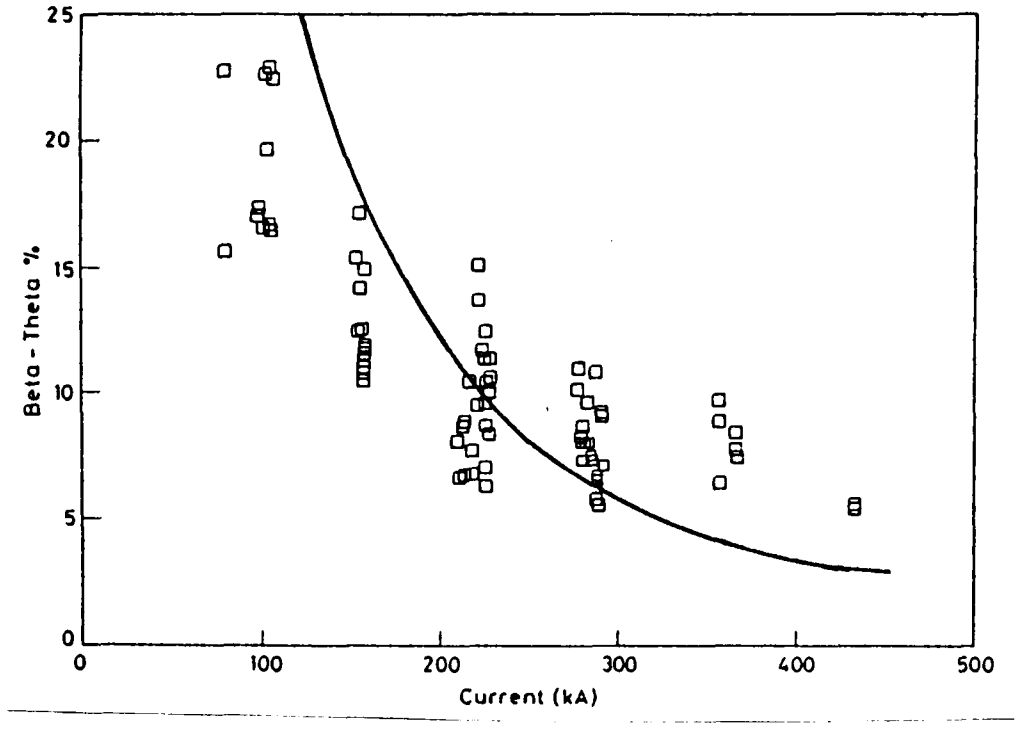

Figure 3.14: Plot of β_p versus I_φ: Theory and Experiment

The Electron Temperature as a Function of Toroidal Current

Values of $T_e = T_{e0}/(1 + \alpha_t)$ as a function of I_φ given by (3.204) for $n_{e0} = 3 \times 10^{19}\mathrm{m}^{-3}$ are compared with experimental results in Figure 3.15. The scaling law predicted by (3.204) fits the experimental data quite well, with a flattening off at higher values of current.

The Energy Confinement Time as a Function of Electron Density

We can eliminate the temperature dependence in (3.192) with the help of (3.204) to obtain

$$\tau_E = 5.3 \times 10^{-35} Z^* \ln \Lambda \frac{n_{e0}^{1.88}}{I_\varphi^{1.02}}. \tag{3.209}$$

Equation (3.209) is plotted with experimental results from HBTX in Figure 3.16.

As can be seen from the figure, the values of τ_E predicted by the theory are somewhat higher than those observed.

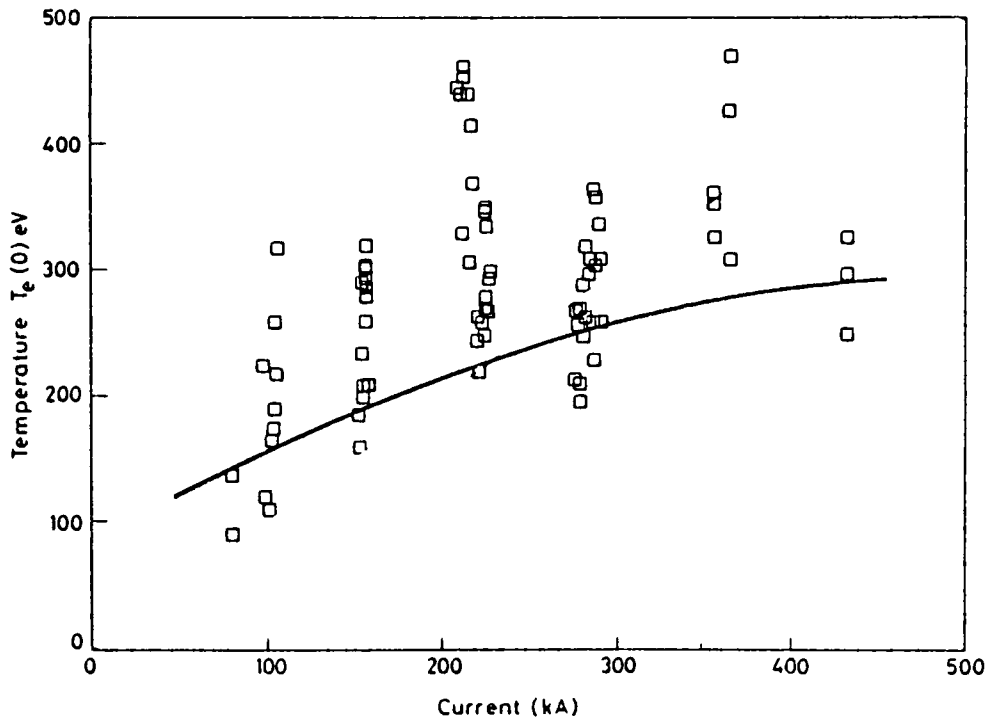

Figure 3.15: Plot of T_e versus I_φ: Theory and Experiment

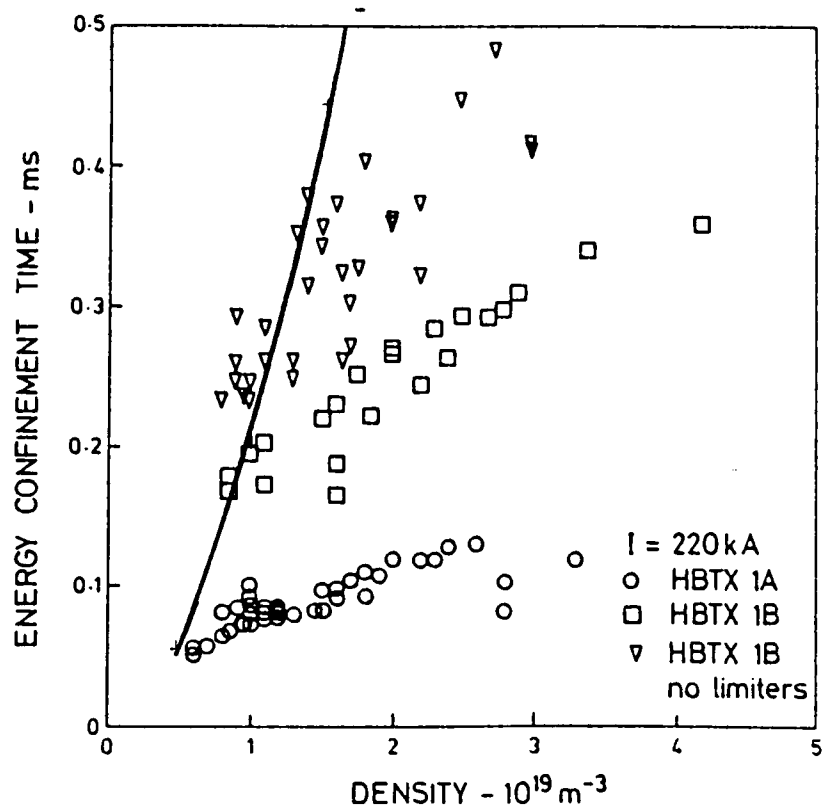

Figure 3.16: Plot of τ_E versus n_e: Theory and Experiment

Chapter 4

Snakes in Tokamaks

The injection of fuel pellets into the JET tokamak can cause high density filaments of plasma on either the $q = 1$ or $q = 3/2$ magnetic surfaces. The effects of density perturbations, known as 'snakes', were first observed in the soft-X-ray diagnostics following pellet injection into JET (Weller *et al.* 1987). There are a number of observations relating to snakes that cannot be explained adequately by accepted plasma theory. In this chapter we will attempt to answer some of the outstanding questions concerning snakes by an application of Woods' transport theory.

4.1 Observations of Snakes

Figure 4.1 shows an example of the X-ray emission during a pellet injection in JET ($a = 1.2$m, $R_0 = 3$m) which subsequently causes the formation of a snake.

Snakes are rope-like in structure and follow magnetic surfaces around the torus at rational values of the safety factor q. The favoured value is $q = 1$, but snakes have been observed at $q = 3/2$. The density perturbations extend further in the poloidal direction than they do radially, typical full-width at half-maximum-height dimensions being $l_\theta = 26$cm and $l_r = 17$cm.

Once formed, a snake is a well defined structure with a surprisingly long life-time, τ_{sl}. The temperature and density in snakes have been measured, and parameters for four typical snakes are given in Table 4.1.

The density perturbation Δn represents an increase in electron density above

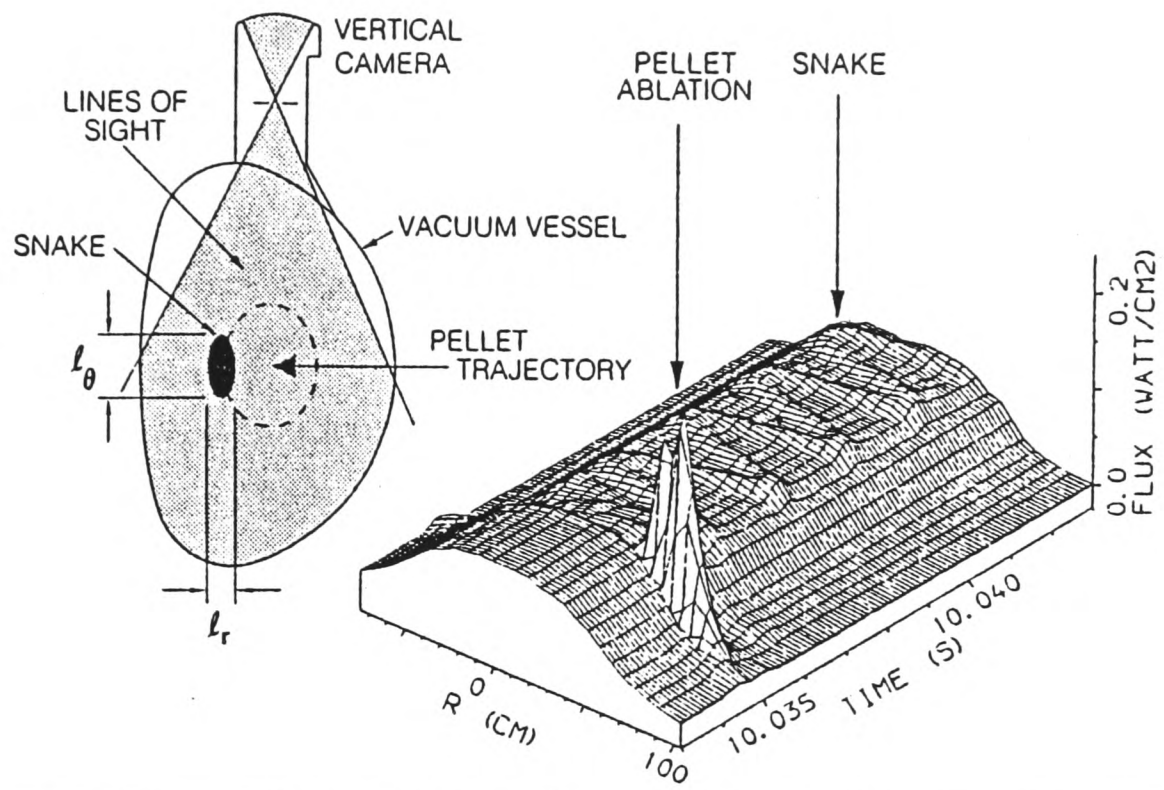

Figure 4.1: Pellet ablation (10.035s) and snake oscillation seen by the vertical soft-X-ray camera (from Edwards *et al.* 1987)

Δn ($10^{19}\mathrm{m}^{-3}$)	n_b ($10^{19}\mathrm{m}^{-3}$)	ΔT (eV)	T_b (eV)	l_θ (cm)	l_r (cm)
3.4	4.9	-135	1200	24	14
2.6	6.6	>-100	1180	24	17
1.5	6.2	>-100	1150	31	16.5
3.6	4.9	-210	650	25	19.5

Table 4.1: Parameters of typical snakes in JET. Variables refer to the electron fluid: Δn = density perturbation in snake, n_b = background density, ΔT = temperature perturbation in snake, T_b = background temperature.

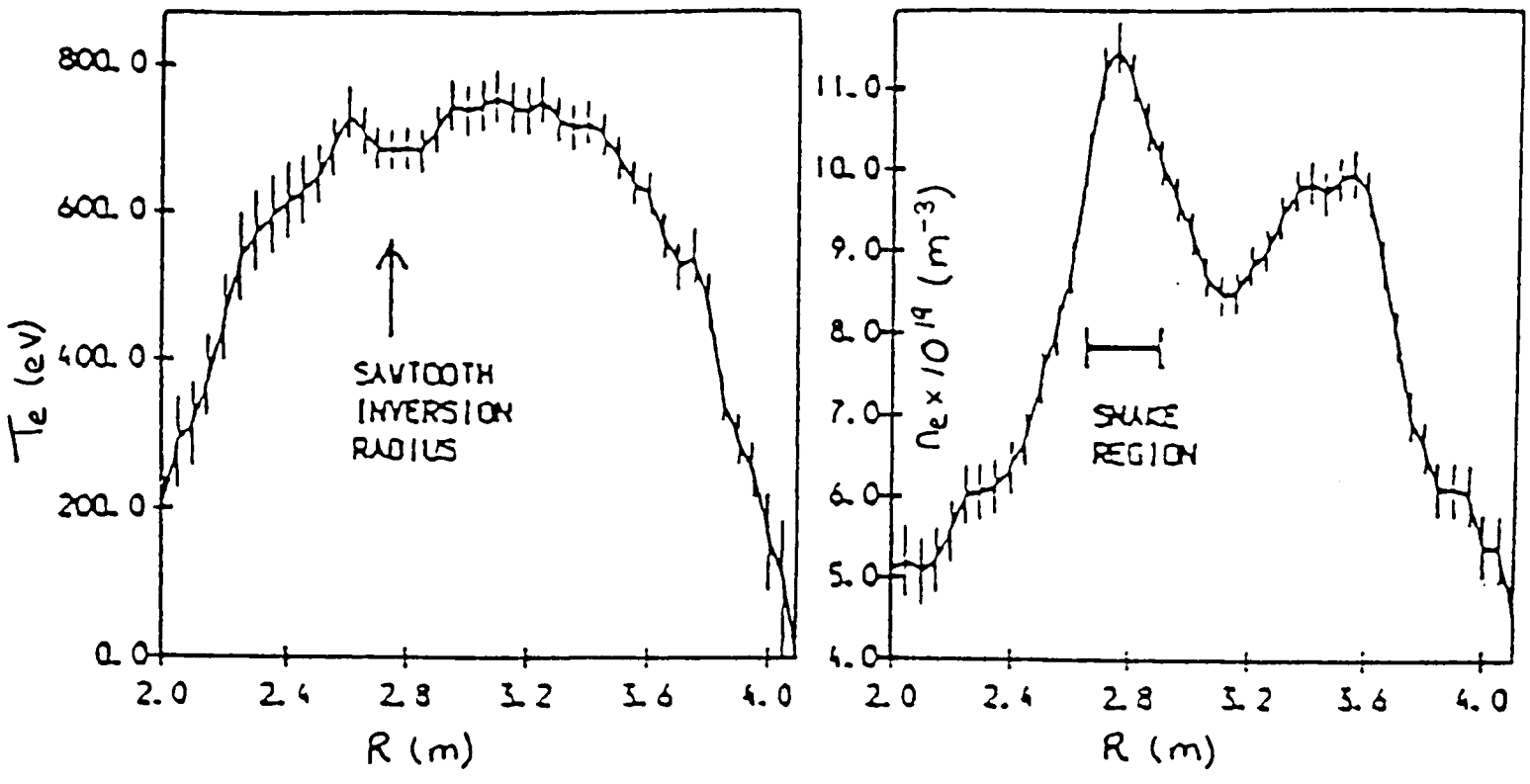

Figure 4.2: Electron density and temperature profiles in JET with a snake present (from Weller *et al.* 1987)

ambient conditions, whereas the electron temperature perturbation ΔT corresponds to a temperature drop. The density within the snake has been observed to be as much as twice that of the surrounding plasma (Weller *et al.* 1987). Following an initial large drop, the plasma temperature within the snake quickly ($\sim$ 100ms) rises to within 10% or so of the surrounding plasma temperature. Figure 4.2 shows electron temperature and density profiles 19ms after the injection of the pellet causing a snake. The temperature depression and density enhancement in the snake region can be seen quite clearly.

There is one further characteristic of snakes that is of interest to us, namely the stability of snakes. At this point we should distinguish between the snake life-time τ_{sl}, which is the time that the snake is in existence, and the snake decay time τ_{sp}, which is the time-scale for the decay of density in the snake. These two times can be different if the snake is terminated for reasons other than the loss of plasma; e.g. by a soft disruption. In the calculations that follow, we will attempt to determine the snake decay time.

Snakes are remarkably stable and can even survive sawtooth disruptions. Observations in JET indicate that snakes are sometimes terminated by a soft disruption or a very large sawtooth collapse, and generally have long decay times. The snake density can have a decay time greater than 10s, and even after their initial formation snakes have been observed to grow (Weller *et al.* 1987). This

last observation is particularly interesting as it implies the existence of an inward diffusion mechanism operating on the plasma in the snake region.

Exceptions to these observations occur if on-axis ion cyclotron resonance heating (ICRH) is applied, or the snake is coupled to 'locked' modes in the plasma (Edwards *et al.* 1987). In these cases the snake decays on time-scales of order 1s, when the snake has been observed to couple to a 'locked' mode, and of order 100ms when ICRH is applied to the plasma. We will restrict attention to cases where snakes have been observed to be stable.

4.1.1 Present Snake Theory

The main questions about snakes that concern us here are (1) What mechanism is responsible for snake formation and why are snakes observed on rational q surfaces only? (2) Why are snakes so long lived? (Neoclassical calculations indicate that snakes should decay on a time-scale of $\sim$ 1s Stringer (1987)). (3) What maintains the temperature depression in the snake region?

In this section we will review present theories dealing with questions (1) and (2) above. The third question has not been addressed in the literature or technical reports.

Snake formation

The theory of Weller *et al.* concerning snake formation is as follows. The injection of a fuel pellet into the discharge is accompanied by a large temperature drop as the pellet ablates and releases cold particles into the plasma. As $\eta \sim T_e^{-3/2}$, this initial temperature drop causes a decrease in the toroidal current density which is believed to create a magnetic island (Weller *et al.* 1987). The magnetic island with its local axis of symmetry following the $q = 1$ or $q = 3/2$ flux surface around the torus confines a fraction ($\sim 1\%$) of the plasma ablated from the pellet. Weller *et al.* have calculated that the observed temperature depression may be sufficient to maintain the magnetic island structure observed, but they note that as the measurements are uncertain, no firm conclusion can be drawn.

From this theory it is easy to see why snakes are formed on rational-q flux surfaces. Only on these surfaces can the snake form a *closed* helical rope circling the torus. On flux surfaces with irrational q values, the plasma from the ablated pellet will rapidly spread across the flux surface forming an annulus, preventing the formation of a magnetic island.

Snake lifetime

A theoretical estimate for the mass confinement time of a typical snake in JET has been made by Stringer (1987). Stringer based his calculations on neoclassical effects. He deduced a typical confinement time of 0.63s on assuming particle losses to be caused by toroidal drifts (the Ware pinch does not depend on number density *gradients* and is not the leading neoclssical term in snakes). This value is somewhat lower than the observed decay rates. More importantly, this mechanism will always produce a mass flux down the snake density gradient. Stringer concludes from the differences in the calculated and observed decay rates that an inward particle flux towards the snake axis, balancing the outward diffusion, is implied. But he did not suggest a mechanism.

The details of Stringer's calculation will not be presented, but neoclassical effects will be considered quantitatively when we apply Woods' transport theory to snakes.

4.2 A Model for Snakes

In this section we will attempt to develop a model sufficiently detailed to retain the essential characteristics of snakes, but simple enough to allow results to be derived with an analytical analysis.

4.2.1 Snake Variables and Geometry

The plasma variables that we need to model in the snake region are the toroidal current j_φ, the magnetic field $\boldsymbol{B}$ and the electron temperature T_e. The first sim-

plification that we will make is to assume that the background plasma variables in the snake region are constant across the snake cross-section. By 'background' plasma variable we mean the value that a variable would have if the snake was not present; we shall denote such variables with the subscript b. The assumption that background variables are constant can be justified on the grounds that the radial extent of the snake, l_r, is only a small fraction of the minor radius; in JET $a \simeq 1.2$m and typically $l_r = 17$cm.

We shall further assume that as a first approximation T_e, j_φ and B_φ are constant across the snake cross-section. It is observed that T_e in the snake is reduced from the background temperature by less than 10%, and to a first approximation this change may be ignored. Since $j_\varphi \simeq \eta_{||} E_\varphi \sim T_e^{-3/2} E_\varphi$, we can assume that T_e =constant implies j_φ =constant (the changes in current required to maintain the magnetic island structure can be ignored to first order).

As a last simplification, we shall perform the final model analysis in slab geometry. This assumption is perhaps the most difficult to justify. Of necessity, we must neglect the difference between l_θ and l_r and assume symmetry along and about the snake axis. This is necessary because Woods' theory of heat transport in toroidal confinement systems requires axisymmetry about the minor and major axes. However, by going a step further and neglecting the radial variation in terms like $(1/r_s)\partial(r_s n_e)/\partial r_s$, where r_s is the distance measured from the snake axis, we hope that we can remove unnecessary complication from the problem without losing its essential features. The simplification seems to be a reasonable one as a first attempt to understand snakes.

In the first part of the analysis we shall express the transport equations in a cylindrical coordinate system local to the snake (see Figure 4.3). Once transport equations appropriate for snakes have been determined in the local cylindrical coordinate system, we shall transform them to slab geometry. We do this to clarify the analysis. By adopting this approach we can distinguish between approximations that can be made because of real physical effects in snakes, and approximations that arise because of our choice of slab geometry.

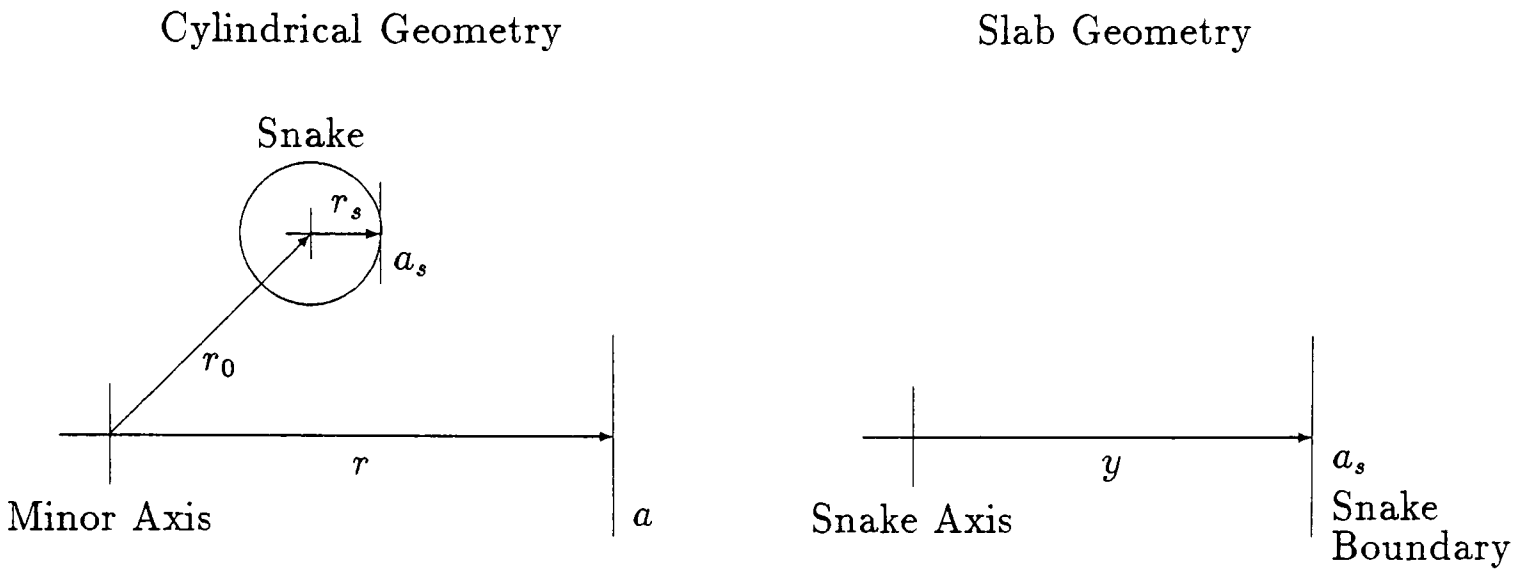

Figure 4.3: The snake coordinate systems used

As shown in Figure 4.3, we will use r_s to denote the radial variable in the cylindrical coordinate system local to the snake, and y to denote the distance from the snake axis in slab geometry.

We shall write down transport equations which include terms from both Woods' theory and neoclassical effects to begin with, and then demonstrate that the neoclassical terms can be neglected by estimating the magnitudes of both effects in snakes.

The Mass Flux

We begin by assuming that we can express the radial mass flux as the sum of two terms,

$$n_e v_r = n_e v_r^w + n_e v_r^{nc}, \tag{4.1}$$

where v_r^w is the radial fluid velocity due to second-order classical effects, and includes the terms derived by Woods, and v_r^{nc} is the neo-classical radial velocity. Summing $n_e v_r^w$ and $n_e v_r^{nc}$ can be justified on the grounds that they have different physical causes, which are both present in toroidal discharges.

An expression for v_r^w in a snake can be derived from equation (3.77). It was shown in Chapter 3 that the dominant term in (3.77) for the case of the RFP

is the term involving the divergence of the pressure tensor. This is also the case for the tokamak where Woods (1987) has shown that viscosity is the dominant particle loss mechanism. Retaining only the viscous term in (3.77), we obtain

$$v_r^w = \frac{1}{\rho_e \omega_{ce}} \nabla \cdot \boldsymbol{p}_e \cdot (\boldsymbol{b} \times \hat{\boldsymbol{r}}_s), \tag{4.2}$$

where $\hat{\boldsymbol{r}}_s$ is a unit vector in the direction of $\boldsymbol{r}_s$.

Only the $\nabla \cdot \boldsymbol{\pi}_{2e}$ term of $\nabla \cdot \boldsymbol{p}_e = \nabla \cdot (p_e \mathbf{1} + \boldsymbol{\pi}_{1e} + \boldsymbol{\pi}_{2e})$ contributes to v_r^w. This is because $\nabla \cdot (p_e \mathbf{1} + \boldsymbol{\pi}_{1e})$ has a radial component only, so $\nabla \cdot (p_e \mathbf{1} + \boldsymbol{\pi}_{1e}) \cdot (\boldsymbol{b} \times \hat{\boldsymbol{r}}_s) = 0$.

For the case of snakes in a tokamak we can make the approximations $b_\theta = 0$ and $b_\varphi = 1$, which, when substituted into the equation (2.37) for $\boldsymbol{\pi}_{2e}$ and (4.2), yield

$$v_r^w = \frac{0.73 m_e}{2 n_e e^4 B_\varphi^2} \frac{1}{r_s^2} \frac{\partial}{\partial r_s} \left\{ r_s^2 p_e \tau_e \left[\frac{\partial}{\partial r_s} \left(\frac{j_\varphi}{n_e} \right) \right]^2 \right\}. \tag{4.3}$$

To obtain (4.3) we have used the approximation $v_{e\varphi} \simeq -j_\varphi / e n_e$, where $v_{e\varphi}$ is the toroidal component of the electron fluid velocity.

Equation (4.3) can be simplified by taking j_φ and T_e to be constant in the snake region and by expressing $\nabla \cdot \boldsymbol{\pi}_{2e}$ in slab geometry, which amounts to neglecting the r_s^2 dependence. Noting that $p_e \tau_e \propto n_e$, we obtain

$$v_r^w = \frac{0.73 m_e}{2 n_e e^4 B_\varphi^2} p_e \tau_e j_\varphi^2 \left\{ \left[\left(\frac{1}{n_e} \right)' \right]^2 \right\}', \qquad (' \equiv \partial / \partial y), \tag{4.4}$$

where here, and in the sequel until indicated otherwise, $' \equiv \partial / \partial y$. We will change this notation when we scale the mass and heat transport equations later in this chapter.

The appropriate theory to use for v_r^{nc} depends on the neo-classical collisional parameter $\nu = qR/(\epsilon^{3/2} C \tau_D)$ (cf. section 1.5.2). In snakes in JET, $\nu \sim 0.2$ (Stringer 1987) and both electrons and ions are in the banana regime. Thus the correct expression to use for v_r^{nc} is that given by Rosenbluth, Hazeltine and Hinton (1972), which may be written as, substituting $T_i = T_e$ into (1.94) and omitting the $E_{||}$ term,

$$v_r^{nc} = -\frac{2.24 q^2 r_{Le}^2}{\epsilon^{\frac{3}{2}} \tau_e n_e} n_e', \tag{4.5}$$

where $\epsilon = r/R$. The factor $\epsilon^{3/2}$ appears in (4.5) because of particle trapping effects. Although we are working in a coordinate system local to the snake, particle trapping in this region is determined by variations in the magnetic field as the snake spirals around the torus. Thus the fraction of particles trapped in the snake will be determined by the value of the tokamak radial variable r rather than the snake variable r_s (see Figure 4.3). This point concerning coordinate systems arises again when we consider the electron thermal diffusivity in snakes.

To enable a comparison of $n_e v_r^w$ and $n_e v_r^{nc}$, we shall write (4.4) and (4.5) in the standard form for a mass diffusion equation, namely $n_e v_r = -\mathcal{D} n_e'$, where $\mathcal{D}$ is a mass diffusivity. Expressing equation (4.4) in this form we obtain

$$n_e v_r^w = -\mathcal{D}^w n_e', \tag{4.6}$$

where

$$\mathcal{D}^w \equiv \frac{0.73 m_e}{e^4 B_\varphi^2} p_e \tau_e j_\varphi^2 \frac{2}{n_e^3}\left[2\frac{(n_e')^2}{n_e^2} - \frac{n_e''}{n_e}\right] \tag{4.7}$$

is the mass diffusivity due to second-order classical effects. Similarly, equation (4.5) may be expressed as

$$n_e v_r^{nc} = -\mathcal{D}^{nc} n_e', \tag{4.8}$$

where

$$\mathcal{D} \equiv \frac{2.24 q^2 r_{Le}^2}{\epsilon^{3/2}\tau_e} \tag{4.9}$$

is the neo-classical mass diffusivity. We can determine the importance of $n_e v_r^{nc}$ relative to $n_e v_r^w$ by calculating the ratio $\mathcal{D}^w/\mathcal{D}^{nc}$. To simplify the expression somewhat, we will define $\alpha \equiv 2(n_e')^2/n_e^2 - n_e''/n_e$. It follows directly from (4.7) and (4.9) that

$$\frac{\mathcal{D}^w}{\mathcal{D}^{nc}} = \frac{1.46}{2.24}\frac{m_e}{e^4 B_\varphi^2}\frac{p_e \tau_e^2 j_\varphi^2}{q^2 r_{Le}^2}\frac{1}{n_e^3}\alpha. \tag{4.10}$$

With the help of (1.73) evaluated for electrons and (1.10) we can eliminate τ_e and r_{Le} in (4.10) to obtain

$$\frac{\mathcal{D}^w}{\mathcal{D}^{nc}} = 1.5 \times 10^{-4}\frac{\tilde{T}_e}{n_{19}^4}\frac{\tilde{j_\varphi}^2 \epsilon^{3/2}}{q^2(Z^* \ln\Lambda)^2}\frac{1}{\alpha}, \tag{4.11}$$

where $\tilde{T}_e = kT_e/e$ (units of ev), $n_{19} = n_e/10^{19}$ and $\tilde{j_\varphi} = j_\varphi/10^6$ (units of MAm^{-2}). Typical snake parameters in JET are $\tilde{T}_e = 1.2 \times 10^3 \mathrm{eV}$, $n_{19} = 5$, $I_\varphi = 3.3\mathrm{MA}$ and $a_s = 0.1m$, where a_s is the (average) radius of the snake (Stringer 1987). We can calculate j_φ from I_φ by assuming a current profile of the form $j_\varphi = j_{\varphi 0}(1-r^2/a^2)^{\alpha_j}$ where $j_{\varphi 0}$ is the current density on the discharge axis and $\alpha_j \sim 3.75$ (see Woods 1987 p.446). By the definition of I_φ, we deduce that $j_{\varphi 0} = (\alpha_j + 1)I_\varphi/(\pi a^2)$. As the snake is usually found on the $q = 1$ magnetic surface at $r \sim 50\mathrm{cm}$, we find that $\tilde{j_\varphi} \sim 1.7\mathrm{MAm}^{-2}$ and $\epsilon = r/R_0 \sim 0.17$. Substituting the values for $\tilde{T}_e$, n_{19}, $\tilde{j_\varphi}$ and ϵ into (4.10) we obtain, for $Z^* = 1$,

$$\frac{\mathcal{D}^w}{\mathcal{D}^{nc}} \sim 0.3\alpha. \tag{4.12}$$

We cannot make a precise estimate of α without detailed information about the number density profile in the snake region. In fact we will have cause to seek a steady-state solution to the mass equation which results in $\alpha = 0$. But we argue that, in general, $\alpha \sim 1/a_s^2$. We arrive at this estimate by noting that the length scale for changes in the number density profile within the snake, i.e. $(n_e'/n_e)^{-1}$, is the snake radius, and that $\alpha \sim (n_e')^2/n_e^2$ (neglecting the n_e''/n_e term).

Making the substitution $a_s \sim 0.1\mathrm{m}$ we find $\mathcal{D}^w/\mathcal{D}^{nc} \sim 30$. We conclude from this that the neo-classical mass flux may be neglected in snakes, as a first approximation at least.

The conservation of mass equation written for the electron fluid in slab geometry is

$$\frac{\partial n_e}{\partial t} + (n_e v_r)' = S_e, \tag{4.13}$$

where S_e is the electron mass source term in snakes. As we are neglecting $n_e v_r^{nc}$, (4.13) can be written

$$\frac{\partial n_e}{\partial t} + \left(n_e V_r^w\right)' = S_e, \tag{4.14}$$

where v_r^w is given by (4.4). We shall adopt (4.14) as the equation governing the radial flow of mass in snakes.

The Heat Flux

Rather than follow the method outlined above of comparing neo-classical and second-order classical effects for the mass flux, we shall accept Woods' conclusion that in tokamaks second-order effects determine the heat flux and assume this to be true for snakes.

We adopt Woods' expression for χ_e calculated from (2.11) for the tokamak, namely

$$\chi_e = \frac{5m_eC_e^2\tau^*}{12e^2n_eB_\varphi^2}\left\{\mu_0 j_\varphi \frac{2}{r^2}\int_0^r \{j_\varphi(r^*) - j_\varphi(r)\}\, r^* dr^* - rn_e\frac{\partial}{\partial r}\left(\frac{\partial p_t/\partial r}{rn_e}\right)\right\}, \quad (4.15)$$

where $p_t = k(n_eT_e + n_iT_i)$ is the total plasma pressure and $\tau^* = 2rq/C_e$. Equation (4.15) is modified for snakes as follows. The term in { }'s on the right-hand side of (4.15) arises from a term involving the deviator of the velocity gradient tensor $\overset{\circ}{\nabla}\boldsymbol{v}$ (cf. (2.11)). As $\overset{\circ}{\nabla}\boldsymbol{v}$ within the snake is determined by the variation in electron density across the snake radius, the tokamak variable r in this term should be replaced by the snake variable r_s (see Figure 4.3). The argument for τ^*, however, is different. Since this time is related to particle trapping effects (see section 2.2), we replace r with r_0, the distance from the snake axis to the minor axis of the discharge.

Making these substitutions, we obtain for the electron thermal diffusivity within the snake

$$\chi_e = \frac{5m_er_0qC_e}{6e^2n_eB_\varphi^2}\left\{\mu_0 j_\varphi \frac{2}{r_s^2}\int_0^{r_s} \{j_\varphi(r_s^*) - j_\varphi(r_s)\}\, r_s^* dr_s^* - r_sn_e\frac{\partial}{\partial r_s}\left(\frac{\partial p_t/\partial r_s}{r_sn_e}\right)\right\}, \quad (4.16)$$

The integral term on the right-hand side of (4.16) involves the term $j_\varphi(r_s^*) - j_\varphi(r_s) \simeq 0$, and can be neglected as a first approximation. It is true that later we shall introduce variations in the temperature, $T_e(r_s) = T_b + \Delta T_e(r_s)$ say, to drive the heat flux and since $j_\varphi \sim T_e^{-3/2}$, it may seem inconsistent to ignore variations in j_φ. However, the integral in χ_e appears as order ΔT_e while the pressure term has order unity. As $|\Delta T_e| \sim 0.1$, the approximation is justified. Neglecting the integral term in (4.16) and rewriting the pressure term in slab geometry, we

obtain

$$\chi_e = -\frac{5m_e r_s q C_e}{6e^2 B_\varphi^2} 2kT_e \left(\frac{n_e'}{n_e}\right)'. \tag{4.17}$$

To obtain (4.17), we have neglected terms involving ΔT_e from p_t'. From the definition of χ_e, $q_e = -(3/2)kn_e\chi_e\nabla T_e$ which, by (4.17), may be written as

$$q_{er} = -\frac{5m_e r_s q C_e}{4e^2 B_\varphi^2} 2k^2 n_e T_e \left(\frac{n_e'}{n_e}\right)' T_e'. \tag{4.18}$$

Equation (4.18) describes the radial flow of heat in the snake. In section 4.4 we will demonstrate that in steady-state snakes, (4.18) gives a radial outflow of heat, up the temperature gradient, sufficient to maintain a temperature depression in snakes.

Equations (4.14) and (4.18) may be more conveniently dealt with if they are expressed in terms of normalised, scaled variables.

The Scaled Transport Equations

To scale the transport equations, we introduce the dimensionless variable

$$x \equiv \frac{y}{a_s}, \tag{4.19}$$

where a_s is the snake radius. We shall also use the scaled and normalised functions defined by

$$\mathcal{N}(x) \equiv \frac{n_e(y)}{n_b}, \tag{4.20}$$

$$\mathcal{T}(x) \equiv T_e(y)/T_b, \tag{4.21}$$

where n_b and T_b are the electron number density and electron temperature of the plasma at the snake boundary. Typical values for n_b and T_b are listed Table 4.1 as background density and background temperature respectively. Equation (4.4) for v_r^w may be rewritten, using equations (4.19) through (4.21), as

$$v_r^w = \frac{2K_m}{a_s^3 n_b^3} \frac{1}{\mathcal{N}} \left\{ \left[\left(\frac{1}{\mathcal{N}} \right)' \right]^2 \right\}', \qquad ' \equiv \partial/\partial x. \tag{4.22}$$

where here, and for the remainder of this chapter, $' \equiv \partial/\partial x$, and a constant K_m associated with the mass flux is defined by

$$K_m \equiv \frac{0.73 m_e}{2e^4 B_\varphi^2} p_e \tau_e j_\varphi^2. \tag{4.23}$$

Substituting (4.20) into (4.14), we obtain for the scaled conservation of mass equation

$$\frac{\partial \mathcal{N}}{\partial t} + \frac{1}{a_s}(\mathcal{N} v_r^w)' = 0. \tag{4.24}$$

To obtain (4.24) we have set $S_e = 0$ in (4.14). As we are interested in the characteristics of snakes at times subsequent to the ablation of the fuel pellet, the only sources of mass within the snake are the ionization of impurities and neutral gas recycling. We assume that, as snakes lie toward the inner region of the discharge, we can neglect these mass sources. Defining the function

$$\varphi_m \equiv \frac{K_m}{a_s^4 n_b^3}, \tag{4.25}$$

we may rewrite (4.24) as

$$\frac{\partial \mathcal{N}}{\partial t} + \varphi_m \left\{ \left[\left(\frac{1}{\mathcal{N}} \right)' \right]^2 \right\}'' = 0. \tag{4.26}$$

The heat flux equation (4.18) is scaled with the help of (4.19), (4.20) and (4.21). We obtain

$$q_{er} = -\varphi_H \mathcal{N} \left(\frac{\mathcal{N}'}{\mathcal{N}} \right)' \mathcal{T} \mathcal{T}', \tag{4.27}$$

where the constant φ_H is defined by

$$\varphi_H \equiv \frac{5}{2} \frac{m_e r_s q C_e}{e^2 B_\varphi^2} \frac{n_b (k T_b)^2}{a_s^3}. \tag{4.28}$$

4.3 The Stability of Snakes

In this section we will use equation (4.22) as the basis of an explanation for the unexpectedly long snake decay time, τ_{sp}. We will begin by demonstrating that it is possible to obtain a mass flow up the number density gradient. As was pointed out in section 4.1.1, this is an essential property of any mass flux mechanism proposed to explain the stability of snakes. Next, we will find and examine the stability properties of a steady-state solution to equation (4.24).

An Inward Mass Flux

The possibility of an inward mass flux follows directly from (4.22). Expanding the derivative term, we have

$$v_r^w = \frac{2K_m}{a_s^3 n_b^3}\frac{\mathcal{N}'}{\mathcal{N}^4}\left\{\frac{\mathcal{N}''}{\mathcal{N}} - 2\frac{(\mathcal{N}')^2}{\mathcal{N}}\right\}, \qquad (K_m > 0). \tag{4.29}$$

Since $\mathcal{N}$ and $(\mathcal{N}')^2$ are positive, the direction of v_r^w depends on the sign of $\mathcal{N}'$ and the sign and magnitude of $\mathcal{N}''$. We have that

$$v_r^w < 0 \text{ if } \begin{cases} \mathcal{N}' > 0, & \text{and } \mathcal{N}'' - 2(\mathcal{N}')^2/\mathcal{N} < 0 \\ \mathcal{N}' < 0, & \text{and } \mathcal{N}'' - 2(\mathcal{N}')^2/\mathcal{N} > 0 \end{cases} \tag{4.30}$$

Thus it is the shape of the number density profile that determines the sign of v_r^w. The electron density in snakes is observed to be greater than the background density, and so $\mathcal{N}' < 0$. For $v_r^w < 0$ in snakes we require, from (4.30), $\mathcal{N}'' > 2(\mathcal{N}')^2/\mathcal{N}$.

4.3.1 The Steady-State Number Density Profile.

We made the observation in section 4.1.1 that the snake decay time is long compared with predictions based on neo-classical theory. As we are supposing the mass flux in snakes to be driven by second-order classical viscosity, an even more powerful term, we conclude that (4.26) must have a non-trivial steady-state solution. Setting $\partial\mathcal{N}/\partial t = 0$ in (4.26), we require a solution of

$$\left\{\left[\left(\frac{1}{\mathcal{N}}\right)'\right]^2\right\}'' = 0. \tag{4.31}$$

Integration of (4.31) yields

$$\mathcal{N}_0 = \frac{\Delta\mathcal{N} + 1}{x\Delta\mathcal{N} + 1}, \qquad 0 \le x \le 1, \tag{4.32}$$

where $\Delta\mathcal{N} \equiv \Delta n_e/n_b$ is the ratio of the density increment on the snake axis above the background density to the background density. To obtain (4.32) we have used the boundary conditions $n_e(a_s) = n_b$, $n_e(0) = \Delta n_e + n_b$ and $[n_e v_r^w]_{r_s=0} = 0$. The third condition arises from the fact that there is no mass source on the snake axis. The region of validity of (4.32) is determined by the extent of the snake.

The magnetic island confinement system exists only as far as $x = 1$. For $x > 1$ we cannot assume symmetry about the snake axis and (4.32) is no longer valid.

There is a further limitation on the validity of (4.32) which needs to be discussed. To obtain (4.26), of which (4.32) is a steady-state solution, we assumed that neoclassical mass flux was dominated by the second-order mass flux due to viscosity. However, (4.32) ensures that the flow due to viscosity is zero. To solve the complete steady-state problem consistently, we would have to retain the neo-classical term in (4.1) and include its effect in (4.26). Instead of solving this problem, we note that the effect of $n_e v_r^{nc}$ is weak ($\mathcal{D}^{nc}/\mathcal{D}^{w} \sim 0.03$). Consequently we expect the steady-state solution that would be obtained by solving (4.14) consistently to be a small perturbation of (4.32).

4.3.2 The Stability of the Steady-State Number Density Profile

While equation (4.32) for $\mathcal{N}_0$ is a steady-state solution to the mass flux equation (4.26), it is not immediately obvious that it is stable to perturbations in number density. We can demonstrate the stability of $\mathcal{N}_0$ by performing a linearised perturbation analysis. The calculations can be simplified by introducing the transformation

$$\phi \equiv \frac{1}{\mathcal{N}}. \tag{4.33}$$

Substituting ϕ into (4.25). We obtain

$$\frac{\partial \phi}{\partial t} = \varphi_m \phi^2 \Big[(\phi')^2\Big]''. \tag{4.34}$$

where φ_m is given by (4.25). We now expand ϕ as

$$\phi = \phi_0 + \epsilon\phi_1, \tag{4.35}$$

where $\phi_0 \equiv 1/\mathcal{N}_0$ corresponds to the steady-state number density profile, $\epsilon << 1$ is a small, dimensionless constant and ϕ_1 is a function of order unity. Substituting (4.35) into (4.34), we obtain

$$\frac{\partial \phi}{\partial t} = \epsilon \frac{\partial \phi_1}{\partial t} = \varphi_m(\phi_0 + \epsilon\phi_1)^2 \Big\{ [(\phi_0')^2]'' + 2\epsilon\{\phi_1'''\phi_0' + 2\phi_1''\phi_0'' + \phi_1'\phi_0'''\} + \epsilon^2[(\phi_1')^2]'' \Big\}, \tag{4.36}$$

We note that, by the definition of ϕ_0, $\left[(\phi_0')^2\right]'' = 0$. Furthermore $\partial\phi_0/\partial t = -(1/\mathcal{N}_0^2)(\partial\mathcal{N}_0/\partial t) = 0$, and from (4.32) for $\mathcal{N}_0$ we see that $\phi_0'' = \phi_0'''' = 0$. Retaining the non-zero terms in (4.36) we have, correct to $0(\epsilon)$,

$$\frac{\partial\phi_1}{\partial t} = 2\varphi_w\phi_0^2\phi_0'\phi_1'''. \tag{4.37}$$

Consider a short-wavelength perturbation about some point x_0 within the snake. Substituting $\phi_1 = e^{i(kx-\omega t)}$ into equation (4.37) we find

$$-i\omega = 2\varphi_w\phi_0(x_0)\phi_0'(x_0)(ik)^3. \tag{4.38}$$

We choose k to be a real constant, corresponding to a fixed-wavelength perturbation. From (4.38) we see that ω is also real, and perturbations in ϕ_0 neither grow nor decay. The stability of ϕ_0 implies the stability $\mathcal{N}_0$. This can be demonstrated by noting that, if $\mathcal{N} = \mathcal{N}_0 + \epsilon\mathcal{N}_1$,

$$\begin{aligned}\frac{1}{\mathcal{N}} &\simeq \frac{1}{\mathcal{N}_0}(1-\epsilon\frac{\mathcal{N}_1}{\mathcal{N}_0}) \\ &= \frac{1}{\mathcal{N}_0} - \epsilon\frac{\mathcal{N}_1}{\mathcal{N}_0^2} \\ &= \phi_0 + \epsilon\phi_1, \qquad \phi_1 = -\mathcal{N}_1/\mathcal{N}_0^2. \end{aligned} \tag{4.39}$$

From (4.39) we see that perturbations in ϕ_0 and $\mathcal{N}_0$ are related by $\phi_1 = -\mathcal{N}_1/\mathcal{N}_0^2$ and hence

$$\frac{\partial\mathcal{N}_1}{\partial t} = -\mathcal{N}_0^2\frac{\partial\phi_1}{\partial t}. \tag{4.40}$$

It follows that the stability of ϕ_1 implies the stability of $\mathcal{N}_1$.

The above stability analysis is not rigorous, and is restricted to short-wavelength perturbations. However, the result is encouraging; snakes appear to be stable, at least for the regime of perturbations investigated.

4.4 The Temperature Depression in Snakes

In this section we shall present an explanation for one of the most intriguing characteristics of snakes, which is the observation of a temperature depression within the snake. The direct evidence of a reduction of the temperature in snakes

becomes uncertain about 100ms after a snake's formation. After this time, ΔT_e decreases to a value less than the 100eV resolution of the measuring equipment. However, the persistence of snakes implies the existence of some mechanism which decreases the current density within the snake and maintains the magnetic island structure. We shall accept this as evidence of a continued temperature depression within the snake.

Some mechanism able to drive heat up a temperature gradient must be invoked to explain a temperature depression in snakes. One example of such a mechanism, although not the mechanism we shall pursue, is the thermo-electric effect. We shall consider Woods' second-order radial heat flux as an explanation for the unusual energy balance which seems to occur in snakes.

4.4.1 Energy Balance in Snakes

The basis of the calculations which follow is that snakes are in a state of thermal equilibrium, the ohmic dissipation in the snake being balanced by the conduction of heat up the temperature gradient. Assuming this is to be so *a priori*, we will deduce necessary conditions for the balance to be maintained. These conditions can then be compared with experiment as a check on the theory.

We begin with the electron energy equation written in slab geometry, namely

$$\frac{\partial}{\partial t}(\tfrac{3}{2}p_e) + \frac{\partial}{\partial y}(\tfrac{5}{2}p_e v_r + q_{er}) = j_\varphi E_\varphi - v_r p_i', \tag{4.41}$$

where $p_e = kn_eT_e$ and we have neglected radiation losses and the transfer of energy from the electron to the ion fluid. As we are assuming that the mass flux in snakes is zero, we can drop the terms involving v_r from (4.41) to obtain

$$\frac{\partial}{\partial t}(\tfrac{3}{2}p_e) + \frac{\partial}{\partial y}(q_{er}) = j_\varphi E_\varphi. \tag{4.42}$$

Integrating (4.42) over the snake radius and rearranging terms, we obtain

$$\frac{\partial \ln W_e}{\partial t} + \frac{1}{\tau_{sE}} = \frac{1}{\tau_{sE}^{\times}}, \tag{4.43}$$

where

$$W_e \equiv \int_0^{a_s} \tfrac{3}{2} p_e \, dy, \tag{4.44}$$

$$\tau_{sE} \equiv \frac{W_e}{[q_{er}]_{y=a_s}}, \tag{4.45}$$

$$\tau_{sE}^{*} \equiv \frac{W_e}{\int_0^{a_s} j_\varphi E_\varphi \, dy}. \tag{4.46}$$

In (4.43) τ_{sE} is the snake electron energy confinement time and τ_{sE}^{*} is the corresponding energy replacement time. We shall assume that the energy confinement and replacement times in snakes are dominated by conduction and dissipation in the electron fluid.

For steady-state conditions to prevail, it is necessary that $\tau_{sE} = \tau_{sE}^{*}$, and the following calculations are concerned with determining these times.

4.4.2 The Energy Replacement Time

To obtain an estimate of τ_{se} we need a model for the variation of n_e, T_e, j_φ and E_φ in the snake. The scaled number density profile can be assumed to be given by equation (4.32) for $\mathcal{N}_0$. We shall change our notation slightly, and write (4.32) as

$$\mathcal{N} = \frac{1+\alpha}{x+\alpha}, \qquad \alpha \equiv \frac{1}{\Delta \mathcal{N}}, \tag{4.47}$$

where $\Delta n \equiv \Delta n_e / n_b$.

We shall adopt a simple linear model for variations in T_e, and assume the scaled temperature $\mathcal{T} \equiv T_e(y)/T_b$, and T_b is the background electron temperature, to be

$$\mathcal{T} = 1 + \zeta(1-x), \qquad \zeta \equiv \Delta \mathcal{T}, \tag{4.48}$$

where $\Delta \mathcal{T} \equiv \Delta T_e / T_b$ and $x \equiv y/a_s$. We note here that $\Delta T_e < 0$ and hence $\zeta < 0$.

A profile for j_φ can be determined from E_φ, which we assume to be constant, the constitutive relation

$$\eta_{||} j_\varphi = E_\varphi, \tag{4.49}$$

and equation (4.48) for $\mathcal{T}$. An expression for $\eta_{||}$ sufficiently accurate for our purposes is

$$\eta_{||} = \frac{m_e}{2e^2 n_e \tau_e}, \tag{4.50}$$

where $n_e\tau_e = 2.75 \times 10^5 T_e^{3/2}/(Z^* \ln\Lambda)$. Rewriting (4.50) in terms of scaled profiles, we obtain

$$\eta_{||} = \eta_b \mathcal{T}^{-3/2}, \qquad \eta_b = \frac{64.5 Z^* \ln\Lambda}{T_b^{3/2}}. \tag{4.51}$$

It follows from (4.51), (4.49) and E_φ =constant that

$$j_\varphi = j_b \mathcal{T}^{3/2}, \tag{4.52}$$

where the background current density j_b is the current density in the plasma surrounding the snake. We can calculate j_b from the toroidal current I_φ and a model for the variation in j_φ across the radius of the entire discharge. We shall follow Woods, and assume a profile of the form $j_\varphi = j_{\varphi 0}(1-(r/a)^2)^{\alpha_j}$, where r is the radial variable of the torus, a is the minor radius of JET and typically $\alpha_j = 3.8$ (Woods 1987 p.446). It follows from $I_\varphi = 2\pi \int_0^a j_\varphi r\, dr$ that $j_{\varphi 0} = (1+\alpha_j) I_\varphi/(\pi a^2)$, and hence

$$j_b = \frac{(1+\alpha_j) I_\varphi}{\pi a^2}(1-(r_0/a)^2)^{\alpha_j}, \tag{4.53}$$

where $a = 0.12$m is the (average) minor radius of JET.

We can now calculate the ohmic dissipation in the snake. With the help of (4.52), (4.51) and (4.49), we obtain

$$\int_0^{a_s} j_\varphi E_\varphi\, dy = a_s j_b^2 \eta_b F_\Omega, \tag{4.54}$$

where

$$\begin{aligned} F_\Omega &= \int_0^1 \mathcal{T}^{3/2}\, dx \\ &= -\frac{2}{5\zeta}\Big[1-(1+\zeta)^{5/2}\Big]. \end{aligned} \tag{4.55}$$

Values of F_Ω are listed in Table 4.2. Typically $|\zeta| \leq 0.1$, and to a good approximation $F_\Omega = 1$. Thus we are justified in neglecting the variations in current density across the snake radius.

ζ	-0.05	-0.1	-0.15	-0.2
F_Ω	0.963	0.926	0.890	0.855

Table 4.2: The function $F_\Omega(\zeta)$

		α		
		0.5	1.0	2.0
	-0.05	1.60	1.35	1.18
ζ	-0.1	1.55	1.31	1.15
	-0.2	1.45	1.23	1.09

Table 4.3: The function $F_W(\alpha, \zeta)$

Performing a similar analysis for W_e, given by (4.44), we obtain

$$W_e = \tfrac{3}{2} k n_b T_b a_s F_W, \tag{4.56}$$

where

$$\begin{aligned} F_W &= \int_0^1 \mathcal{N}\mathcal{T}\, dx \\ &= (1+\alpha)\Big[\{1+\zeta(1+\alpha)\}\ln|1+\frac{1}{\alpha}| - \zeta\Big]. \end{aligned} \tag{4.57}$$

In Table 4.3, we see that allowing for variations in T_e introduces only a minor correction into the expression for W_e. Accordingly, we shall use the approximation

$$F_W \simeq (1+\alpha)\ln|1+\frac{1}{\alpha}| \tag{4.58}$$

when calculating W_e.

Substituting (4.56) and (4.54) into equation (4.46) for τ_{sE}^*, we obtain

$$\tau_{sE}^* = \frac{3}{2}\frac{n_b T_b}{j_b^2 \eta_b}\frac{F_W}{F_\Omega}. \tag{4.59}$$

Parameters typical of snakes in JET are (Weller *et al.* 1987) $n_b = 5 \times 10^{19}\mathrm{m}^{-3}$, $\tilde{T}_b = 1.2 \times 10^3\mathrm{eV}$, $I_\varphi = 3.3MA$, $B_\varphi = 2.5T$, and, assuming that snakes are located on the $q = 1$ magnetic surface, $r_0 = 0.5\mathrm{m}$. We shall adopt a value of $Z^* = 5$ and $\alpha_j = 3.8$ as being typical of JET discharges. For these parameters (4.53) and (4.51) yield $j_b = 1.7 \times 10^6\mathrm{Am}^{-2}$ and $\eta_b = 1.0 \times 10^{-7}\Omega\mathrm{m}^{-1}$. Thus, from (4.59)

and taking $\alpha \simeq 1.0$, $\tau_{sE}^{*} \simeq 65$ms. This is the time-scale on which we expect changes in the energy content of the snake to occur, provided τ_{sE}^{*} and τ_{sE} are not closely balanced.

Approximately 100ms after snake formation, $\Delta T_e/T_b$ in the snake is observed to reduce from its initial value to less than 0.1 (Weller *et al.* 1987). This observation provides some experimental confirmation of our estimate for τ_{sE}^{*}.

4.4.3 The Energy Confinement Time

In order to calculate τ_{sE}, we must estimate the heat flux at the snake boundary. As we are assuming steady-state conditions we may employ the averaging procedure developed by Woods (see section 3.4). Integrating the steady-state form of (4.42), we have that

$$\int_0^y q'_{er}\, dy^* = [q_{er}]_0^y = \int_0^y j_\varphi E_\varphi\, dy^*. \tag{4.60}$$

Integration of (4.60) yields

$$\int_0^{a_s} q_{er}\, dy = \int_0^{a_s} dy \int_0^y j_\varphi E_\varphi\, dy^*, \tag{4.61}$$

To obtain (4.61) we have used $q_{er}(0) = 0$. Dividing (4.60) evaluated at $r = a_s$ by (4.61) and solving for $[q_{er}]_0^{a_s}$, we obtain

$$[q_{er}]_0^{a_s} = \frac{1}{a_s A_\epsilon} \int_0^{a_s} q_{er}\, dy, \tag{4.62}$$

where the dimensionless ratio A_ϵ is defined by

$$A_\epsilon \equiv \frac{\dfrac{1}{a_s}\displaystyle\int_0^{a_s} dy \int_0^y j_\varphi E_\varphi\, dy^*}{\displaystyle\int_0^{a_s} j_\varphi E_\varphi\, dy}. \tag{4.63}$$

It was shown in section 4.4.2 that, to a good approximation, $j_\varphi E_\varphi$ =constant. In this case we obtain $A_\epsilon = 1/2$.

The integral in (4.62) can be evaluated with the help of equation (4.27). We find that

$$\int_0^{a_s} q_{er}\, dy = a_s \varphi_H F_Q, \tag{4.64}$$

		α		
		0.5	1.0	2.0
	-0.05	0.128	0.036	0.010
ζ	-0.1	0.247	0.070	0.020
	-0.2	0.453	0.130	0.037

Table 4.4: The function $F_Q(\alpha, \zeta)$

where φ_H is given by (4.28) and the profile shape factor F_Q is defined by

$$\begin{aligned} F_Q &\equiv \int_0^1 \mathcal{N}\Big(\frac{\mathcal{N}'}{\mathcal{N}}\Big)' \mathcal{T}\mathcal{T}'\, dx \\ &= -\zeta(1+\alpha)\Big\{\zeta\Big[\frac{1}{1+\alpha} - \frac{1}{\alpha}\Big] + \tfrac{1}{2}(1+\zeta+\zeta\alpha)\Big[\frac{1}{\alpha^2} - \frac{1}{(1+\alpha)^2}\Big]\Big\}. \end{aligned} \tag{4.65}$$

Values for $F_Q(\alpha, \zeta)$ can be found in Table 4.4. It follows from (4.45), (4.56) and (4.62) that

$$\tau_{sE} = \frac{3}{4}\frac{a_s^4}{kT_b}\frac{F_W}{F_Q}\frac{1}{K}, \tag{4.66}$$

where

$$K \equiv \frac{5}{2}\frac{m_e r_s q C_e}{e^2 B_\varphi^2} \tag{4.67}$$

is a constant associated with the heat flux (cf. (4.28)) and $q = r_0 B_\varphi / R B_\theta$. Substituting the parameters adopted in section 4.4.2 as being typical of snakes in JET, we obtain $\tau_{sE} \simeq 30$ms. To obtain this estimate we took $\alpha = 1$, $\zeta = 0.1$ and $a_s = 0.11$m. This estimate for τ_{sE} is a factor of 2 smaller than our estimate of τ_{sE}^*. This is not altogether surprising, given that $\tau_{sE} \propto a_s^4$. For steady-state conditions to prevail, we must have $\tau_{sE} = \tau_{sE}^*$, or from (4.66) and (4.59)

$$\tfrac{3}{4} a_s^4 \frac{1}{K k T_b}\frac{F_W}{F_Q} = \tfrac{3}{2}\frac{n_b k T_b}{j_b^2 \eta_b}\frac{F_W}{F_\Omega}. \tag{4.68}$$

Substituting expressions for F_Q and F_Ω, and retaining terms $O(\zeta)$ we obtain

$$a_s^4 = \frac{K n_b (k T_b)^2}{j_b^2 \eta_b}\zeta(1+\alpha)\Big[\frac{1}{(1+\alpha)^2} - \frac{1}{\alpha^2}\Big]. \tag{4.69}$$

We lack sufficient data to make a thorough test of (4.69). The best we can do here is to note that with typical snake parameters and the values $\alpha = 1.0$, $\zeta = -0.1$, (4.69) yields the estimate $a_s = 13$cm. This estimate is in good agreement with

the values of l_r and l_θ listed in Table 4.1. However, we cannot place too much emphasis on this result as the high power of a_s appearing in (4.69) makes it insensitive to changes in the other variables appearing in this equation.

Appendix A

The Equilibrium Poloidal Magnetic Field in Toriodal Machines

We wish to establish the result

$$B_\theta(r,\theta) = B_{\theta 0}(r)/(1 - \Lambda\epsilon\cos\theta), \tag{A.1}$$

$$\Lambda = \beta_p - \beta_{p0} + l_i/2 - 1, \tag{A.2}$$

$$B_\varphi(r,\theta) = B_{\varphi 0}(r)/(1 + \epsilon\cos\theta), \tag{A.3}$$

where

$$\beta_p(r) = \frac{4\mu_0}{r^2 B_{\theta 0}(r)} \int_0^r p_0(r^*) r^* \, dr^*, \tag{A.4}$$

$$\beta_{p0}(r) = \frac{2\mu_0 p_0(r)}{B_{\theta 0}^2(r)}, \tag{A.5}$$

$$l_i(r) = \frac{2\mu_0}{r^2 B_{\theta 0}(r)} \int_0^r B_{\theta 0}^2(r^*) r^* \, dr^*, \tag{A.6}$$

and the subscript "0" denotes values applying to the cylindrical limit, $\epsilon = 0$. The theory leading to (A.1) for the case $r = a$ where $\beta_{p0} = 0$ is given in Wesson (1987, pp.70-74). We shall outline the argument, omitting most of the algebraic details.

The starting point is the Grad-Shafranov equilibrium equation (Shafranov 1966) for the poloidal magnetic flux function ψ:

$$R\frac{\partial}{\partial R}\left(\frac{1}{R}\frac{\partial\psi}{\partial R}\right) + \frac{\partial^2\psi}{\partial Z^2} = -\mu_0 R^2 \frac{dp}{d\psi} - F\frac{dF}{d\psi}, \tag{A.7}$$

where $F = RB_\varphi$, and like p, is a function of ψ only. Equation (A.7) is written in terms of the cylindrical coordinates shown in Figure 1.1. When expressed in terms of the local coordinates r and θ (also shown in Figure 1.1), (A.7) becomes

$$\begin{aligned}\left(\frac{1}{r}\frac{\partial}{\partial r}r\frac{\partial}{\partial r}+\frac{1}{r^2}\frac{\partial^2}{\partial\theta^2}\right)\psi &- \frac{1}{R_0+r\cos\theta}\left(\cos\theta\frac{\partial}{\partial r}-\frac{\sin\theta}{r}\frac{\partial}{\partial\theta}\right)\psi \\ &= -\mu_0(R_0+r\cos\theta)^2p'(\psi)-F(\psi)F'(\psi). \quad \text{(A.8)}\end{aligned}$$

where here, and in the sequel, $' \equiv \partial/\partial\psi$.

The next step is to introduce the expansion $\psi(r,\theta) = \psi_0(r) + \psi_1(r,\theta)$, where ψ_1 is a small $O(\epsilon)$ correction to the cylindrical limit to allow for toroidal effects. It follows from (A.8) that ψ_0 and ψ_1 satisfy

$$\frac{1}{r}\frac{d}{dr}\left(r\frac{d\psi_0}{dr}\right) = -\mu_0R_0^2p'(\psi_0)-F(\psi_0)F'(\psi_0), \quad \text{(A.9)}$$

and

$$\begin{aligned}\left(\frac{1}{r}\frac{\partial}{\partial r}r\frac{\partial}{\partial r}+\frac{1}{r^2}\frac{\partial^2}{\partial\theta^2}\right)\psi_1 &- \frac{\cos\theta}{R_0}\frac{d\phi_0}{dr} \\ &= -\frac{d}{dr}\left\{\mu_0R_0^2p'(\psi_0)+F(\psi_0)F'(\psi_0)\right\}\frac{dr}{d\psi_0}\psi_1 - 2\mu_0R_0r\cos\theta\,p'(\psi_0). \quad \text{(A.10)}\end{aligned}$$

When the solutions ψ_0 and ψ_1 are obtained, the poloidal magnetic field follows from

$$B_{\theta 0} = \frac{1}{R_0}\frac{d\psi_0}{dr}, \qquad B_\theta = \frac{1}{R}\frac{\partial}{\partial r}(\psi_0+\psi_1). \quad \text{(A.11)}$$

Now we assume that the magnetic surfaces have circular cross-section, but that they are not concentric. Suppose that toroidicity results in the displacement of the flux surface ψ =constant a distance $\Delta(r)$ towards the major axis from the position it would have in the cylindrical limit. Then

$$\psi = \psi_0+\psi_1 = \psi_0 - \Delta(r)\frac{\partial\psi_0}{\partial R} = \psi_0 - \Delta(r)\cos\theta\frac{d\psi_0}{dr}. \quad \text{(A.12)}$$

Substituting this into (A.10) and using (A.11), we obtain the differential equation

$$\frac{d}{dr}\left(rB_{\theta 0}^2\frac{d\Delta}{dr}\right) = \frac{r}{R_0}\left(2\mu_0r\frac{dp_0}{dr}-B_{\theta 0}^2\right). \quad \text{(A.13)}$$

From (A.11) and (A.12)

$$B_\theta(r) = B_{\theta 0}(r)\left(1-(\epsilon+\frac{d\Delta}{dr}\cos\theta)\right). \quad \text{(A.14)}$$

Solving (A.13) for $d\Delta/dr$, we obtain

$$rB_{\theta 0}^2 \frac{d\Delta}{dr} = \frac{2\mu_0}{R_0} \int_0^r \left[r_1^{\times} \frac{dp_0}{dr} - \frac{B_{\theta 0}^2}{2\mu_0} r_1 \right] dr_1. \tag{A.15}$$

Integrating the pressure term in (A.15) by parts, we obtain

$$\begin{aligned} \int_0^r r_1^2 \frac{dp_0}{dr}\, dr_1 &= \left[r_1^2 p_0 \right]_0^r - \int_0^r 2r_1 p_0\, dr_1 \\ &= r^2 p_0 - 2\int_0^r 2r_1 p_0\, dr_1. \end{aligned} \tag{A.16}$$

Substitution of (A.16) into (A.15) and then into (A.14) yields (A.1) as required. This result is in agreement with that obtained by Shafranov (1966). In the same review, Shafranov derives (A.3) for $B_\varphi(r,\theta)$.

References

Alper, B. *et al.* (1986). Proc. 11th International Conference on Plasma Physics and Controlled Nuclear Fusion Research, IAEA-CN-47/D-II-I, Kyoto.

An, Z. G., Diamond, P. H. *et al.* (1986). Proc. 11th International Conference on Plasma Physics and Controlled Nuclear Fusion Research, IAEA-CN-47/D-V-8, Kyoto.

Artzimovich, L. A. (1965) *Elementary plasma physics*, Blaisdell Publishing Company, New York.

Aydemir, A. Y. and Barnes, D. C. (1984). *Physics Review Letters*, **52**, 930.

Aydemir, A. Y. *et al.* (1985). *Physics of Fluids*, **28**, 898.

Bennett, W. H. (1934). *Physical Review*, **45**, 890.

Bevir, M. K. and Gimblett, C. G. (1985)*Physics Fluids*, **28** 1826.

Bevir, M. K. and Grey, J. W. (1981). Los Alamos Report LA-8944-LC Los Alamos National Laboratory, Los Alamos, New Mexico).

Bickerton (1958). *Proceedings Physical Society*, **72**, 618.

Bodin, H. A. B. (1984). Proc. International Conference on Plasma Physics, Lausanne.

Burnett, D. (1935) *Proceedings London Mathematical Society*, **40** 382.

—(1987). Proc. Conference on Physics of Mirrors, Reverse Field Pinches, and Compact Tori, ISPP, Varenna.

—and Newton, A. A. (1980). *Nuclear Fusion*, **20**, 1255.

Boyd, T. J. M. and Sanderson, J. J. (1969) *Plasma dynamics*, Thomas Nelson

and Sons, Ltd., London.

Braginskii, S. I. (1965). *Reviews of Plasma Physics*, Vol. 1 (ed. M. A. Leontovich), 205-311, Consultants Bureau, New York.

Carolan, P. G. *et al.* (1987). Proc. Conference on Physics of Mirrors, Reverse Field Pinches, and Compact Tori, ISPP Varenna.

—*et al.* (1987). Proc. 14th EPS Conference, Madrid.

Chapman, S. and Cowling, T. G. (1952, 1970). *The Mathematical theory of non-uniform gases* Cambridge University Press.

Chen, F. F. (1984). *Introduction to plasma physics and controlled fusion.* Plenum Press, New York.

Connor, J. W. and Taylor, J. B. (1984). *Physics of Fluids*, **27**, 2676.

Edwards, A. W. *et al.* (1987). Private Communication.

Galeev, A. A. and Sagdeev, R. Z. (1979). *Reviews of Plasma Physics*, Vol. 7 (ed. M. A. Leontovich), 257, Consultants Bureau, New York.

Gimblett, C. G. and Watkins, M. L. (1976). Proc. of the 3rd Topical Conference, Abingdon.

Grad, H. (1949). *Comm. pure appl. Maths.* **2** 331-407.

Haas, F. A. and Thyagaraja, A. (1986). *Plasma Physics and Controlled Fusion*, **28**, 1093.

Hender, T. C. and Robinson, D. C. (1982). *9th International Conference on Plasma Physics and Controlled Nuclear Fusion*, Vol. 3, 417, IAEA, Vienna.

Hinton, F. L. and Oberman, C. (1969). *Nuclear Fusion.* **9** 319.

Hinton, F. L. and Hazeltime, R. D. (1976). *Reviews of Modern Physics* **48** 239.

Hugill, J. (1983). *Nuclear Fusion*, **23**(3), 331-73.

Innocente, P. and Martini, S. (1987). Proc. Conference on Physics of Mirrors, Reverse Field Pinches, and Compact Tori, ISPP Varenna.

Jacobson, A. R. (1984). *Physics of Fluids*, **27**, 7.

Kadomtsev, B. B. and Pogutse, O. P. (1967). *Soviet Physics JETP*, **24**, 172.

Kruskal, M. and Schwarzschild, M. (1954). *Proceedings Royal Society* A223 348.

La Haye, R. J. *et al.* (1986). *Nuclear Fusion* **26** (3) 255.

Laval, G. *et al.* (1971). *Plasma Physics and Controlled Nuclear* Vienna II 507.

Liewer, P. C. (1985). *Nuclear Fusion*, **25**(5), 543.

Miyamoto, K. (1976). *Plasma physics for nuclear fusion.* MIT Press, Cambridge, Mass.

Moffatt, H. K. (1978). *Magnetic field generation in electrically conducting Fluids*, Cambridge University Press.

Moses, R. W. (1984). Proc. International Conference on Plasma Physics, Lausanne.

Ortolani, S. (1987). Proc. Conference on Physics of Mirrors, Reverse Field Pinches, and Compact Tori, ISPP Varenna.

—and Valisa, M. (1984). Proc. International Conference on Plasma Physics, Lausanne.

Pfirsch, D. and Schlüter, A. (1962). Max-Planck-Institut Report MP1/PA/7/62.

Reiman, A. (1981). *Physics of Fluids*, **24**(5), 956.

Robinson, D. C. (1987). "Toroidal Pinches", presented at *Rosenbluth Symposium*, Austin, Texas.

—and Todd, T.N. *The Influence of a Helical Field on a Reverse Field Pinch*, mimeo.

Rosenbluth, M. N., Hazeltine, R. D. and Hinton, F. L. (1972). *Physics of Fluids*, **15**, 116.

Rusbridge, M. G. (1977). *Plasma Physics*, **19**, 499.

—(1980). *Plasma Physics*, **22**, 331.

Shafranov, V. D. (1965). *Reviews of plasma physics*, Vol. 2 (ed. M. A. Leontovich), 103-150, Consultants Bureau, New York.

—(1957). *Journal Nuclear Energy* II **5** 86.

Spitzer, L. and Härm, R. (1953). *Physical Review* **89** 977.

Stringer, T. E. (1987). Private Communication.

Taylor, J.B. (1974). *Physical Review Letters*, **33**, 1139.

—(1986). *Review of Modern Physics*, **58**, 741.

Turner, L. and Christiansen, J. P. (1981). *Physics of Fluids*, **24**(5), 893.

Ware, A. A. (1970). *Physical Review Letters* **25** 15.

Weller, A. *et al.* (1987). *Physical Review Letters*, **59**(20), 2303.

Wesson, T. A. (1987). *Tokamaks*, Oxford University Press.

Woods, L. C. (1983). *Journal of Plasma Physics*, **29**, 143.

—(1987). *Principles of magnetoplasma dynamics*, Oxford University Press.

Woltjer, L. (1958). *Proc. National Academy of Science*, **44**, 489.

Wurden *et al.* (1987) Proc. Conference on Physics of Mirrors, Reverse Field Pinches, and Compact Tori, ISPP Varenna.